8-2012

Physical Modeling of Suction Caissons Loaded in Two Orthogonal Directions for Efficient Mooring of Offshore Wind Platforms

Jade Chung

PHYSICAL MODELING OF SUCTION CAISSONS LOADED IN TWO ORTHOGONAL DIRECTIONS FOR EFFICIENT MOORING OF OFFSHORE WIND PLATFORMS

By

Jade Chung

B. Eng. Dalhousie University, 2007

A THESIS

Submitted in Partial Fulfillment of the

Requirements for the Degree of

Masters of Science

in Civil Engineering

The Graduate School

The University of Maine

August, 2012

Advisory Committee:

Melissa Landon Maynard, Assistant Professor of Civil Engineering, Advisor

Thomas C Sandford, Associate Professor of Civil Engineering

William G. Davids, Professor of Civil Engineering

Joseph T. Kelley, Professor of Earth Sciences

THESIS ACCEPTANCE STATEMENT

On behalf of the Graduate Committee for Jade Chung, I affirm that this manuscript is the final and accepted thesis. Signatures of all committee members are on file with the Graduate School at the University of Maine, 42 Stodder Hall, Orono, Maine.

Melissa Landon Maynard, Ph.D.

August 2012

08/03/2012

LIBRARY RIGHTS STATEMENT

In presenting this thesis in partial fulfillment of the requirements for an advanced degree at The University of Maine, I agree that the Library shall make it freely available for inspection. I further agree that permission for "fair use" copying of this thesis for scholarly purposes may be granted by the Librarian. It is understood that any copying or publication of this thesis for financial gain shall not be allowed without my written permission.

Signature: 

Date: AUGUST 3, 2012

PHYSICAL MODELING OF SUCTION CAISSONS LOADED IN TWO ORTHOGONAL DIRECTIONS FOR EFFICIENT MOORING OF OFFSHORE WIND PLATFORMS

By Jade Chung

Thesis Advisor: Dr. Melissa Landon Maynard

An Abstract of the Thesis Presented
in Partial Fulfillment of theRequirements for the
Degree of Masters of Science
in Civil Engineering
August 2012

Over the past decade a number of Federal and State policies and programs have promoted the development of the wind energy industry, including the establishment of offshore wind. A strategy by the Department of Energy set objectives of reducing cost and reducing time to deployment through specific deliverables such as innovative anchor and mooring design for floating offshore systems and hardware design concepts including turbine array grids. This research program proposes and investigates use of suction caissons as combined anchors to resist line loads from multiple platforms as an efficient solution for anchoring a network of wind turbine platforms.

Suction caissons are a ‘mature’ anchor technology in the offshore oil and gas industry, yet there is minimal experience with application for offshore wind platforms. Established design methods, standards and recommended practices from the oil and gas industry, serve as a starting point for further adaptation. Considerations of the differences in conditions (e.g. loads, risk, failure and serviceability tolerances) between the two applications, is important for developing efficient anchor design suited to offshore wind platforms. A physical modelling program was

developed to investigate the behaviour of caissons subjected to orthogonal cyclic and post-cyclic monotonic line loads, compared to the behaviour of single line loaded caissons.

Modeling was performed in a geotechnical centrifuge in order to simulate in-situ stress profile at model scale, as stresses are critical to soil and foundation behavior. Load tests were performed on a model suction caisson anchor installed by jacking into normally consolidated kaolin clay (in-flight). Baseline tests were performed with single line loading for comparison to the multi-line loading tests. Line loads were applied in orthogonal directions for the multi-line load tests. The effect of varying cyclic mean load and cyclic load amplitude was also investigated. Comparison of test results was based on line displacement, applied line load, caisson rotation and internal pore pressure at the underside of the caisson cap.

Centrifuge test results appear to indicate that the line load-displacement response during monotonic loading is similar for the multi-line and the single line loaded suction caisson anchors. The post-cyclic peak monotonic line load resistance provided by the caisson loaded in multiple directions was greater than the resistance provided by the caisson loaded in a single direction (accounting for the total resultant load applied). For all selected load cases, the accumulated permanent displacements during the cyclic loading did not result in a displacement (serviceability) failure of the suction caisson nor contribute significantly to the displacement correlating to the peak line load resistance of the caisson.

Test results indicate that the resistance capacity of a given caisson is not reduced by applying line loads in multiple directions, when considering the resistance to the total resultant load. Test observations appear to support conceptualizations of a modified “zone of influence” (active/passive earth pressure wedges) due to the changing load orientation from resolving multiple out of phase line loads.

DEDICATION

To my loving and supportive husband

Michael Jean

To my father whose work ethic and dedication inspires me

See-Wing Chung

To the loving memory of my late mother

Yew-Teck Chung

ACKNOWLEDGEMENTS

I would like to thank the Department of Energy for sponsoring this research through the DeepCwind Consortium program.

I would like to express my sincere gratitude to Dr. Melissa Landon Maynard, for accepting me into this research program and for serving as my advisor throughout my graduate studies. Her dedication to research and development endeavours is nothing short of inspirational, and her many hours of guidance and review work has helped me tremendously throughout this program. I am also thankful for the assistance that I received from Dr. William Davids, Dr. Tom Sandford and Dr. Joe Kelley during my research and studies.

I would like to thank all of the staff at the Center for Offshore Foundations at the University of Western Australia. I am particularly appreciative of Dr. Christophe Gaudin, for co-ordinating the centrifuge program, without his expert help this research program would not have been possible. Many thanks also to: Don Herley and Manuel Palacios, for the extended hours of work on the centrifuge operations and the endless patience they had with my unfortunate inexperience; Philip Hortin, Shane De Catania and John Breen for all the instrumentation, electronics, digital systems and general support they provided; Dave Jones for the machinery work and being sympathetic to last minute requests.

I am so thankful for the many blessings that I have received from the Lord, including this unique research opportunity, and amazing support from my family and colleagues.

TABLE OF CONTENTS

LIST OF TABLES

LIST OF FIGURES

LIST OF ABBREVIATIONS

API	American Petroleum Institute
BOEMRE	Bureau of Ocean Energy Management Regulation, and Enforcement
COFS	Center for Offshore Foundation Systems
DNV	Det Norske Veritas
DOI	US Department of the Interior
EWEA	European Wind Energy Association
EERE	Office of Energy Efficiency and Renewable Energy
FEM	Finite element method
GL	Germanischer Lloyd
G_s	Specific gravity
HMLA	High mean low amplitude
H-V	Horizontal - vertical
IEC	International Electrotechnical Commission
IMarEST	Institute of Marine Engineering Science and Technology
ISO	International Standards Organization
LEM	Limiting equilibrium method
LL	Liquid Limit
LMLA	Low mean low amplitude
LMHA	Low mean high amplitude
OWSInD	Offshore Wind Innovation and Demonstration
PI	Plasticity Index
PL	Plastic Limit
PLA	Plastic limit analysis
PPT	Pore pressure transducer

STOMPI	Sub terrainean oil-impregnated multi-Pressure instrument
TLP	Tension leg platform
USDOE	US Department of Energy
VLA	Vertically loaded drag anchor

LIST OF SYMBOLS

c_v	Coefficient of vertical consolidation
c_h	Coefficient of horizontal consolidation
d	penetrometer diameter
D	Diameter of caisson
D_{eq}	Equivalent diameter of caisson
G_{sec}	Secant shear modulus
L	Length of caisson
l	Length of load line
M	Slope of line load-displacement curve
M_{in}	Initial slope of line load-displacement curve (line loads less than mean cyclic load)
M_{pc1}	First post-cyclic monotonic line load-displacement curve slope
M_{pc2}	Second post-cyclic monotonic line load-displacement curve slope
N	Gravitational multiplier
N_c	Bearing capacity factor
n	Number of cycles
n_{50}	Number of cycles to 50% of total displacement (taken at 540 cycles)
N_{ball}	Ball penetrometer bearing factor
P-δ	Line load-displacement (relationship)
P_{amp}	Magnitude of the cyclic load amplitude (mean to peak), specific to the test being referenced
P_{in}	Initial load reached during line tensioning preceding cyclic loading
$P_{re,amp}$	Resultant cyclic load amplitude, specific to test being referenced
$P_{cy,max}$	Maximum load during cyclic loading ($P_{mean} + P_{amp}$)
P_{mean}	Mean load magnitude applied during cyclic loading, specific to test being referenced

$P_{mn,peak}$	Reference peak monotonic resistance (corrected for % installation pore pressure dissipation)
$P_{re,peak}$	Resultant peak monotonic resistance
P_{peak}	Peak monotonic load resistance (failure load) individual to the test being referenced
S1	Soil model/sample no. 1
S2	Soil model/sample no. 2
s_u	Undrained shear strength
$s_{u,ave}$	Average undrained shear strength
T_{90}	Dimensionless time factor (pore pressure dissipation)
u	Internal pore pressure measured at caisson cap
u_{hs}	Hydrostatic pore pressure at level of caisson cap
v	Penetration rate
z	Depth below soil surface
α	Side shear parameter
α_{int}	Internal shear parameter
δ	Line displacement
δ_{in}	Permanent cyclic displacement prior to initiation of cyclic loading
δ_{cyc}	Permanent cyclic displacement
δ_{peak}	Displacement at peak load resistance (failure)
δ_x	Caisson displacement in y-direction
δ_y	Caisson displacement in y-direction
δ_z	Caisson displacement in y-direction
γ'	Submerged unit weight
γ_{cy}	Cyclic shear strain
γ_{ave}	Average shear strain

$\varkappa_{cyc}$	Angular rotation of caisson in L1 plane due to cyclic loading
$\varkappa_{in}$	Angular rotation of caisson in L1 plane due to initial monotonic load (to mean load)
ω_{sweep}	Angle (interior) bound by range of orientation of resultant load vector during cyclic loading
ω_{peak}	Largest angle (interior) bound by orientation of resultant load at failure and resultant load vector during cyclic loading
ψ_{cyc}	Angular rotation of caisson in L2 or L plane due to cyclic loading
ψ_{in}	Angular rotation of caisson in L2 or L plane due to initial monotonic load (to mean load)
θ	Angle of the load line with respect to the horizontal

1. INTRODUCTION

In order for deepwater floating wind farms to progress from theoretical and demonstrational installations to viable industrial energy production, economical improvements are required. Better cost efficiency in wind energy is achieved through improved production capacity and technology advances. Increased production capacity is continuing steadily through increasing size of turbines and expansion of installations to locations with better wind resources. This drive towards greater capacity has fuelled the progression of wind technologies from on land installations (1100 – 1930), to shallow water installations (1990-continued) to increasingly deeper waters. The idea of a large floating wind turbine for electricity generation was introduced in 1972 by Dr. W.E Heronemus, a professor at MIT. This concept was first realised in a 2008 pilot project by Blue H Technologies BV: an 80kW turbine on a TLP-type platform deployed off the coast of Italy in 108m of water (Utsunomiya and Nishida 2009). The first full scale (2.3MW) floating wind turbine was deployed off the coast of Norway in 2009 as Statoil's Hywind project. (Bilgili et al. 2011)

1.1. Federal Wind Energy Legislation and Federal Programs

Over the past six years a number of federal programs were instituted to promote development of offshore wind energy industry. In particular, the Energy Policy Act of 2005 (H.R.6 – 109th Congress 2005) designated responsibility for conducting a program of research, development, demonstration and commercial application for offshore wind energy to the Secretary of the Department of the Interior. The 2006 Advanced Energy Initiative (National Economic Council 2006) identified critical areas of focus for development of the wind industry, including improvement of efficiency and lowering of costs of conventional wind turbine technology.

Born out of these federal policies, various goals, plans and strategies for offshore wind energy development were conceptualized by other federal bodies. Beginning in 2002, the Office

of Energy Efficiency and Renewable Energy (EERE) published multi-year (5-year) wind energy program plans with a top priority of "increasing the viability and deployment of renewable energy technologies" (EERE 2002). A collaborative effort between the U.S. Department of Energy, Black and Veatch engineering and consulting and the American Wind Energy Association has set a target at 20% energy production by wind resources by 2030 (EERE 2008). In 2011, the EERE published the National Offshore Wind Strategy, establishing the Offshore Wind Innovation and Demonstration (OSWInD) initiative which had two critical objectives: reducing cost and reducing timeline to deployment. The OSWInD goal is 54GW installed capacity by 2030 with the key inclusion of a cost goal at $0.07/kWh, with an interim goal of 10 GW installed capacity by 2020 at a cost of $0.10/kWh (EERE 2011).

In order to meet these development goals, program initiatives have evaluated the greatest challenges to offshore wind energy development and determined critical focus areas. The OSWInD (EERE 2011) program identified 3 focus areas: Market Barrier Removal, Technological development, and Advanced Technology Demonstration, of which the latter two focus areas specified key deliverables involving improved, efficient design of deep water offshore anchorage systems. Objective of the Technological Development focus area is to reduce risk in the short term and continue to develop technologies for the long term through establishing appropriate design codes, standards and performance models. Key deliverables contributing to the objective included "innovative anchor and mooring designs for floating offshore systems to lower cost and risk" and "grid architecture and hardware design concepts including turbine array grid." One of the key deliverables of the Advanced Technology Demonstration focus area is the "support of innovative engineering activities such as for foundations." An analogous initiative to OSWInD for projects located farther from shoreline on the outer continental shelf is the DOI's Smart from the Start initiative (EERE 2010). In March 2012, the federal government announced an additional 6-year, $180 million funding initiative for the installation of four offshore wind energy prototypes to be distributed geographically throughout U.S. waters (USDOE 2012).

1.2. Maine State Programs

A key driving factor for alternative energy development in Maine is high percentage of residential homes (79%) relying on oil for heating (Maine State Planning Office 2007). Maine intends to reduce reliance on fossil fuels and to contribute to the renewable energy goals of the Northeast U.S (Ocean Energy Task Force 2009). Offshore wind energy development is one of the proposed methods of working towards this goal. With the support of the state legislature, in January 2010, the Maine Ocean Energy Task Force proposed to construct a 5 GW network of floating offshore wind turbines as part of the state's electrification strategy (University of Maine and James Sewall Company 2011).

1.3. Locating Offshore Energy Developments

Deepwater offshore wind energy development has garnered substantial support from these wind energy initiatives due to the potential efficiencies unique to large offshore developments. Deepwater offshore locations provide the best wind resource for consistent high capacity generation as the average winds are stronger and the greater distance from onshore topographic features results in reduced wind turbulence (EERE 2007). Better wind resources and development of increasingly efficient large turbines for offshore applications results in dramatic reduction in cost of energy (EERE 2011). Offshore development of wind energy also allows for generation sites in close proximity to high load centers, and to coastal zones where electricity costs are typically higher (EERE 2007).

Definition of 'deepwater' is individual to the industry in context, based on the relative economy of fixed or floating platform designs. Whereas fixed platform foundation designs are economical for the oil and gas industry to water depths exceeding 100 m, deepwater floating platforms are employed only for water depths greater than this. For the wind energy industry, fixed platform foundations systems become uneconomical in water depths exceeding 60 m, thus deepwater floating platforms with mooring systems are more suitable (Figure 1.1).

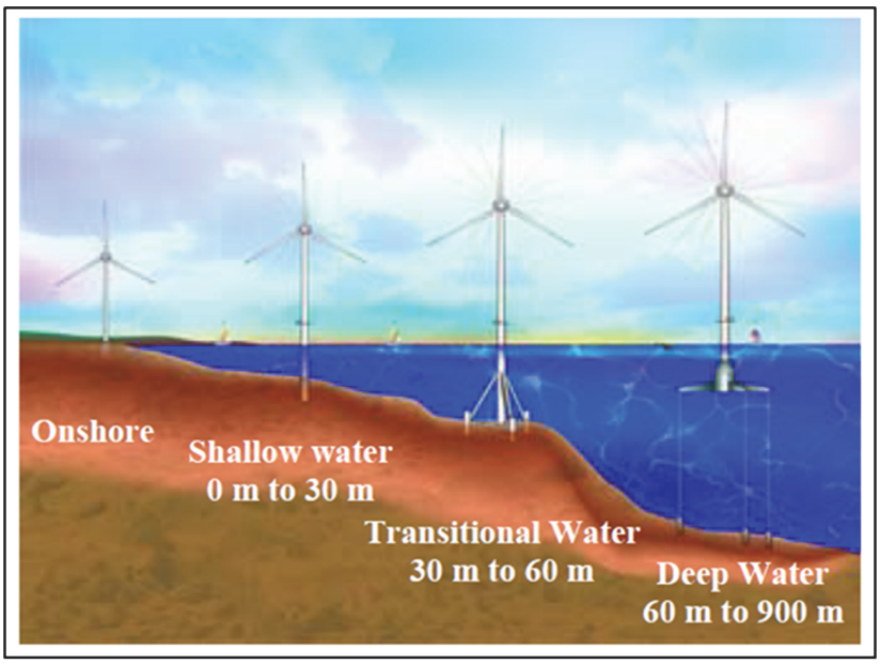

Figure 1.1. Water depth classifications for offshore wind energy (from Musial and Butterfield 2004).

1.4. Wind Energy Developments in Maine

According to wind resource studies (Schwartz et al. 2009; Musial and Ram 2010) New England has some of the highest offshore wind energy capacities of all US waters as indicated in Figure 1.2. New England Offshore wind energy potential has been rated at: 100.2 GW in 0-30m water depth, 136.2 GW in 30-60m water depth and 250.4 GW in water depths greater than 60 m (Musial and Ram 2010). 1GW installed capacity typically equates to 3.4 million MWh/year (Dolan and Heath 2010).

To this end, the State of Maine has designated three Ocean Energy Demonstration sites in Maine waters, all located between one and two miles offshore south of Monhegan Island. The purpose of these sites is to enable deployment of offshore energy demonstration installations. These sites were selected based on the following key criteria: wind resource (>8 m/s), bathymetry (water depth > 60 m), minimal conflict with existing marine obstructions, dredge dumps,

shipping channels and unexplored ordinances, and proximity to existing undersea cables or locations pre-permitted for undersea cables (Maine State Department of Conservation 2009).

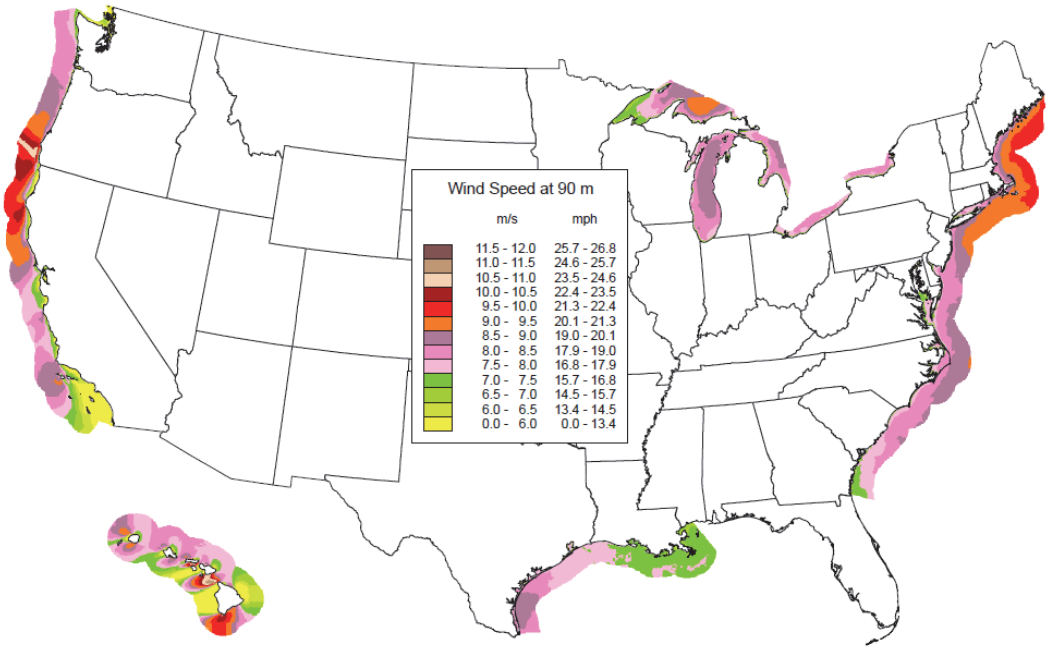

Figure 1.2. USA offshore wind resource potential at 90 m (from Schwartz et al. 2010).

UMaine-led DeepCwind Consortium (DeepCwind), funded by the DOE, is continuing to develop offshore wind technologies with the intention of supporting the various state and federal technological and economic wind energy goals (University of Maine and James Sewall Company 2009). The objective of DeepCwind is to develop floating technology to compete economically with other forms of energy ($/kWh) without subsidies by 2020 and beyond. DeepCwind is progressing towards these goals through work in various tasks including:

- Micrositing, Geophysical Investigations and Geotechnical Engineering;
- Study of Environmental and Ecological Impacts;
- Permitting and Policy;
- Floating Turbines Design and Lab Testing;
- Metocean Monitoring;

- Education and Outreach; and
- Program Operations, Fabrication and Deployment.

This research on suction caissons for anchorage of floating wind platforms is a component of the geotechnical engineering in Task 1, contributing to the overall goal of DeepCwind as an investigation of economical foundation design.

1.5. Wind Energy Economics

Cost effectiveness is one of the greatest challenges to the establishment of offshore wind industry. Presently efficiency benefits of large offshore wind energy developments are offset by higher costs associated with offshore installations and operations (EERE 2007). The levelized generation cost for fossil fuel sources is $70-95/MWh, whereas for offshore wind the levelized generation cost is $100-120/MWh (Esteban et al. 2010). The present installed capital cost of offshore wind is estimated at $4250/kW. The cost is greater than for onshore installations due to: perceived risk, increased challenges of at-sea operations, complexity of turbine foundations, balance-of-system infrastructure, higher interconnection and installation costs, limited manufacturing supply, and also contribution of one-time costs for establishment of the offshore industry (designated installation vessels, necessary port/harbour upgrades, new/modified manufacturing facilities, and workforce training) (EERE 2011; Musial and Ram 2010; Wiser and Molinger 2007). The perceived risk contributes 50% of the installed capital cost as developers, financers and insurers continue to be hesitant to invest in offshore wind development projects (EERE 2011). Additionally, offshore wind turbine costs rise with increasing depths and distances (Green and Vasilakos 2011 Table 2 from EEA). The cost of turbines for onshore installations are 75% of the total project cost, whereas similar turbines installed offshore would comprise only 33% of the total offshore cost due to higher cost of operations at sea (Esteban et al. 2011).

In order to meet the 54 GW goal, a 50% reduction to the present capital cost is required (EERE 2011). One of the critical activities for cost reduction in the short term is to reduce

perceived risk of developers, financers and insurers by better understanding the design regime through technology demonstrations, performance models, and establishment of design codes and standards for offshore systems including foundation/anchorage systems (EERE 2011). For long term cost reductions, development of innovative inexpensive foundation designs is required (EERE 2011).

This research program contributes towards cost reduction objectives through performing key activities and deliverables identified in the various plans, strategies and initiatives. A combined anchor design is proposed in this program to lower cost associated with installations and provide foundation design to support a grid array of turbines. Scale modelling (centrifuge testing) of the proposed anchor design is conducted as a demonstration of the performance of the proposed technology. The results of the anchor testing program are assessed with reference to existing design standards and recommended practices, providing further understanding of the anchor performance relative to the design regime specific to offshore wind energy platforms.

1.6. Selection of Anchor Type

A number of anchor types have been developed or modified for application with offshore oil and gas floating platforms including: gravity anchors, fluke anchors, vertically loaded drag anchors (VLA), anchor piles, suction caissons, suction embedded plate anchors and dynamically penetrating anchors. Concise summaries of the history and application of various anchor types are provided in Andersen (2008). Selection of an anchor type for a given project is typically dependent on water depth, geology, mooring system geometry, design load, cost and availability of materials and equipment. Because of the relatively homogeneous subsurface conditions in the two regions of greatest offshore oil and gas development (North Sea – Figure 1.2; Gulf of Mexico – Figure 1.3) geology may not have been the most restrictive factor in the selection of appropriate anchor type.

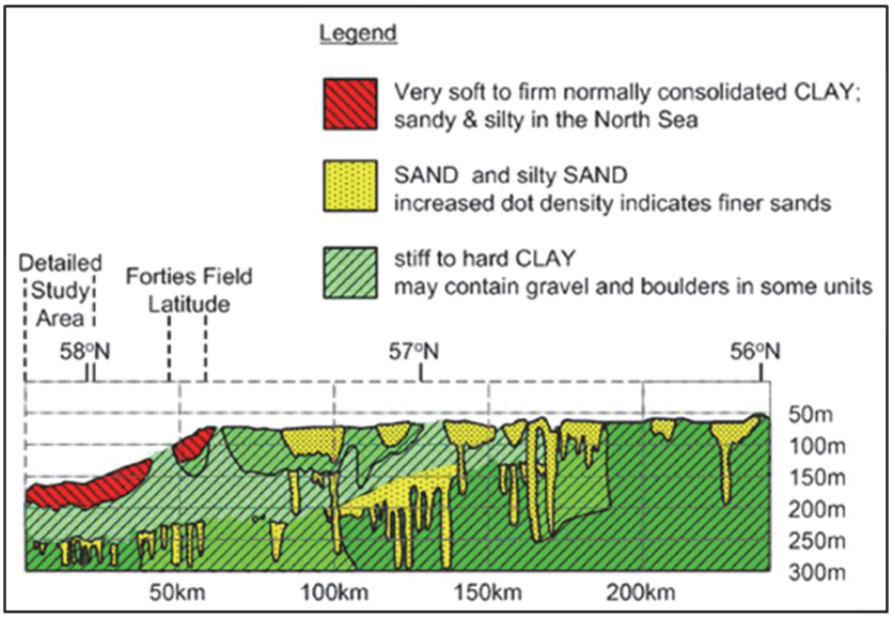

Figure 1.3. Typical N-S stratigraphy cross-section of North Sea near South Fladden (from Schneider and Senders 2010).

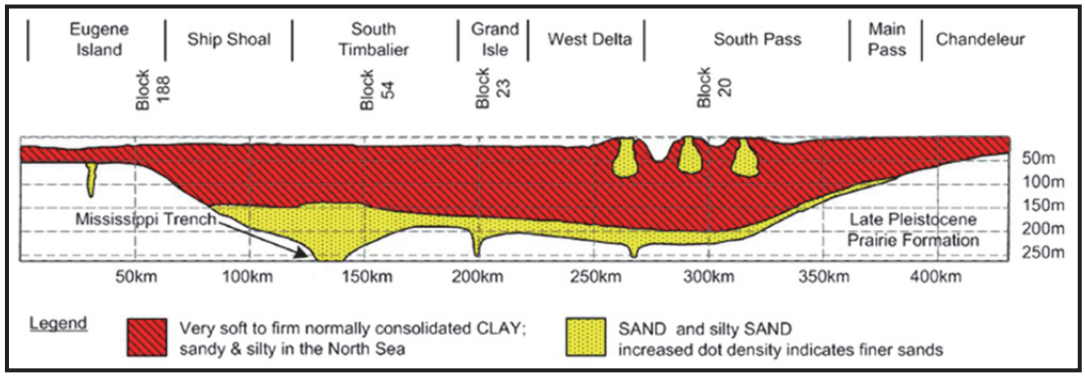

Figure 1.4. Typical E-W stratigraphy cross-section of northern Gulf of Mexico (from Schneider and Senders 2010).

This research program is targeted towards development of foundation systems for conditions at the proposed test sites off Monhegan Island. Geology is a major factor in the selection of anchor type for this location. Depth to bedrock is inconsistent within test sites, with overburden thicknesses varying between 0 m (bedrock outcrops) to 35 m over horizontal distances of 30 m to 100 m, as shown in Figure 1.5. Due to the irregular distribution of bedrock outcrops and variation in depth of overburden over the limited area of a given platform site,

selected anchor type would require a relatively small installation footprint and capability for precise installation. Cost of installations and materials is another prime consideration as economy is a key objective for offshore wind platform development.

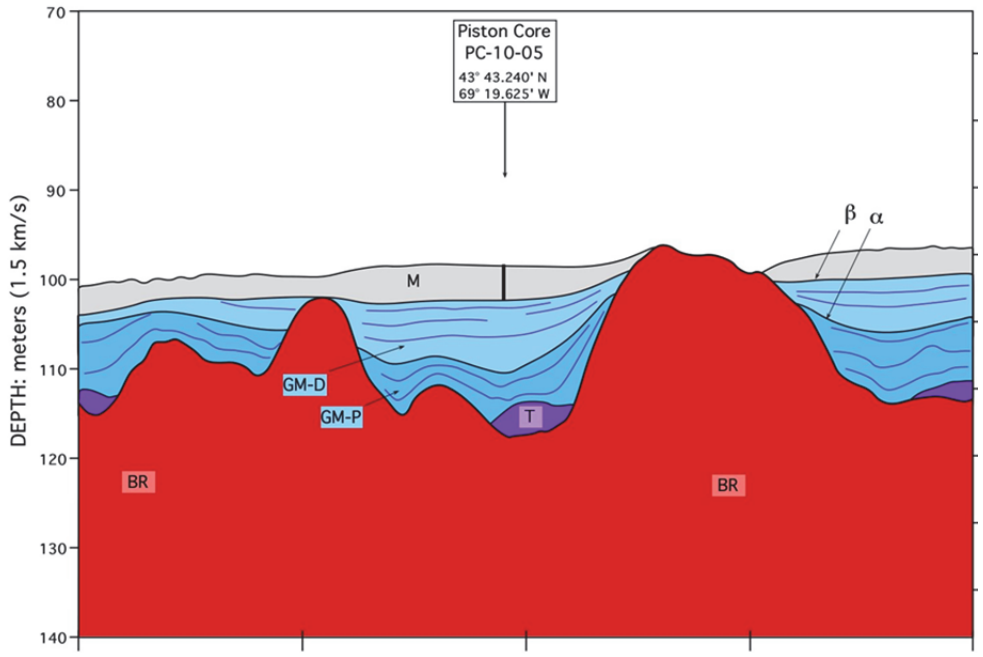

Figure 1.5. Stratigraphy cross-section at UMaine Deepwater Offshore Wind Test Site (from Belknap et al. 2011).

Suction caisson anchor was selected to meet these criteria. The installation footprint of a suction caisson anchor is small, and the caisson anchor can be installed at a precise location. Suction caisson anchors are suitable for budgeted foundation cost due to the relatively minimal installation and construction equipment requirements (e.g., a single anchor handling vessel, a pump, and a remotely operated vehicle for top cap closure) provided experts and equipment can be readily mobilized to the development site. Additionally, the symmetry of a suction caisson anchor is an important characteristic to support key design component of the proposed anchor design concept.

1.7. Anchorage Design Concept

The proposed anchor design concept integrates anchor components for multiple platforms such that a single anchor provides resistance to loads applied from more than one platform. The intent of this proposed design is to increase efficiency of the foundation system required for grid array of platforms required for an offshore wind farm. Huang and Aggidis (2008) first proposed the combined anchor concept for application with wave energy converters, however the basic premise of optimization of number foundation elements is appropriate for numerous offshore applications requiring foundation for array of installations.

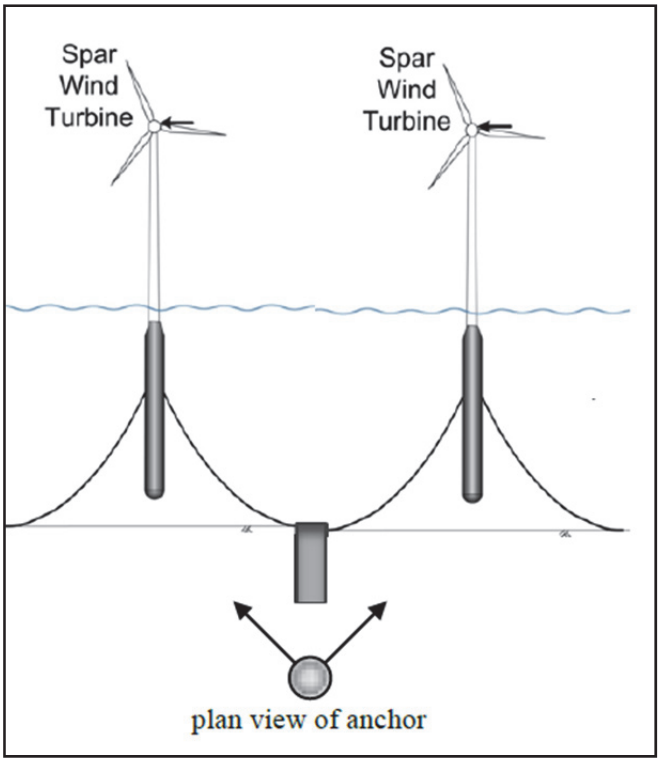

Figure 1.6. Schematic of integrated anchor component for multiple platforms (from Melissa Landon Maynard, personal correspondence, 2012)

1.8. Research Objectives

The objective of this research program is to investigate the performance and behaviour of suction caisson anchors subjected to orthogonal cyclic loads, with application to anchorage of

floating wind turbine platforms. This investigation was performed using model scale testing in a geotechnical centrifuge in order to effectively represent the variation of soil stresses with depth, which is integral to behavior and performance of suction caisson anchor performance. Analysis of the caisson anchor design was performed based on the load-displacement behavior and peak monotonic load resistance measured in centrifuge model scale tests in comparison to baseline tests on single line loaded caisson anchors, predicted capacities and results of similar tests in literature.

The test program is designed to highlight the following caisson anchorage aspects:

1. Post-cyclic (multi-directional) monotonic load resistance/behavior
2. Effect of out-of-phase cyclic multi-directional loads on caisson resistance and deformation
3. Effect of cyclic load amplitude on post-cyclic monotonic load resistance/behavior
4. Effect of cyclic mean load on post-cyclic monotonic load resistance/behavior
5. Pore pressure response to multi-directional cyclic loading at various mean loads and load amplitudes
6. Displacement accumulation as affected by multi-directional cyclic loading at various mean loads and load amplitudes.

1.9. Thesis Structure

This thesis is organized into six chapters. A brief description of each chapter follows: Chapter 2 provides a literature review of the topics pertinent to the development of suction caissons for resisting two orthogonal loads. Recent development and progress of suction caissons along with applications of suction caissons for deepwater offshore anchors are summarized. Current standards for evaluating suction caisson strength are identified. Background theory on cyclic shear strength and deformation is summarized in addition to an overview of recent research and proposed theory on these topics. Model scale considerations regarding physical modeling in a

geotechnical centrifuge are discussed. Chapter 3 describes the centrifuge testing program including conceptual development of the orthogonal loading test program, a detailed description of the equipment and setup and explanation of the procedures followed for the tests. Chapter 4 presents the results of the centrifuge testing program and an in-depth analysis of the results. The actual results versus the anticipated behaviour and the results of previous research are discussed. Potential reasons and accounts for unexpected test results are offered. Chapter 5 interprets outcomes of the study and presents applications and further development opportunities. Chapter 6 concludes and summarizes research performed.

2. BACKGROUND

2.1. Suction Caissons

Suction caissons are open ended, hollow steel cylinders sections installed as foundation components in marine soils. There are a number of different terms used in the offshore industry that refer to similar foundation structures using comparable installation procedures including: suction piles, suction anchors, and suction bucket or bucket foundations. Although strict differentiation between these foundation and anchorage elements is blurred by colloquial usage of the terminology, general distinctions are provided by Tjelta (2001).

Suction caissons are similar to traditional pipe piles in function and application, but differ in pile geometry and installation method. Suction caissons tend to have length to diameter aspect ratios smaller than six, which is less than the aspect ratio of traditional pipe piles. The smaller aspect ratios of suction caissons tends to be reflected by short, rigid pile behaviour rather than flexible behaviour typical of the more slender driven piles. As implied by the name, suction caissons are installed by applying suction to the internal caisson cavity creating a pressure differential with the external environment. The resulting net downward force on the outside of the caisson causes the caisson to penetrate the soil.

2.1.1. Suction Caisson History

50 years have passed since initial proposal of the suction-installed pile concept (Goodman 1961). Suction caissons were first used as temporary mooring anchors for catenary mooring lines of storage tankers at Gorm field (North Sea) in 1980 (Senpere and Auvergne 1982). However, it was the developments in skirted foundation usage that formed the basis for investigation of suction caissons as foundation components for permanent installations. Suction installed skirted foundations were first proposed for BP's Forties field in the North Sea, in 1970s, although the final design reverted back to steel jacket structures. The feasibility of skirted foundations in soft clay soils was proven in a field test for Gulfaks C (North Sea) conducted in

1985, as a full scale model of the performance of rigidly connected suction installed foundations for steel pile jacket structures in the offshore oil and gas industry (Tjelta et al. 1986). Acceptance of suction installed skirted foundations grew and was used for numerous offshore installations including Europipe 16/11 E riser platform and Sleipner T CO_2 treatment platform (Tjelta 1994, 1995). Longer skirt lengths were increasingly proposed for designs, such as for the Troll 'A' Platform, moving development towards components resembling piles or caissons. The first application of suction caissons in 'permanent' structures was as TLP anchors was in 1993, at the Snorre Field (oil and gas) in the North Sea (Fines 1991; Andersen et al. 1993). Since then, numerous field, laboratory, centrifuge and numerical modelling programs have been performed to investigate the capacity and behavior of suction caissons to refine design methods.

Structural behaviour and performance of suction caissons used in conjunction with wind turbines and wind energy platforms studies have recently been investigated through field installations, and physical and numerical modelling. The majority of wind energy – specific work performed has been for rigidly connected foundation- structure systems for shallow water (<30 m) conditions. Studies on response of suction caissons to monotonic, cyclic and fatigue load progressions anticipated for monopile and tripod wind turbine structures (Houlsby et al. 2005; Byrne and Houlsby 2006; Achmus et al. 2009), and numerical analyses including finite element modelling focusing on effects of lateral (wind) loads on large diameter piles and suction caissons (Abdel Rahman 2007; Ibsen 2008) have contributed towards proposed design procedures for suction caissons for monopile and tripod wind structures. The first field installations of suction caissons for offshore wind turbines fixed to the seafloor were: an experimental 3.0 MW turbine in 2003 at the Frederikshavn test field near Denmark (Ibsen and Brincker 2005); a tripod frame structure for the 6 MW industrial scale wind turbine installation near Weiringermeer, Holland in 2003, which was a joint venture between Delft University of Technology, ECN, NEG-Micon Holland and Ballast Neham (Zaaijer 2002,2003); and a full scale industrial 5.0 MW suction-installed monopile turbine at the Horns Rev 2 field near Denmark by DONGEnergy as a

prototype for industrial sized installations. Recently, suction caissons have been proposed as a foundation option for the proposed 504 MW Galloper Wind Farm near Suffolk, UK (Royal Haskoning 2011).

Dramatic increase in suction caisson use over the past two decades is partially due to the contributions from model scale testing and theoretical and numerical analysis. Results from parameterization and comparison studies have particularly benefitted suction caisson design methods. In conjunction with the two major suction caisson prototype installation types, two distinct branches of centrifuge testing of suction caissons have evolved: flexible mooring line anchorage and rigidly connected foundation structures. Theoretical methods of estimating resistance capacity (§2.1.3) for both branches of caisson application were calibrated and verified using the results from various centrifuge tests, and numerical modeling methods. A brief description of recent centrifuge testing for these two branches of suction caisson application follows.

2.1.2. Suction Caisson Anchors for Mooring Systems

One of the pioneering centrifuge programs on suction caissons was conducted by Fulsang & Steensen-Bach (1991) which involved a model caissons with aspect ratio of two (L/D = 2) loaded vertically by a cable attached to the top cap. A comparison was made between the results of tests at 1 g and 40 g to investigate the role of suction on uplift resistance. These tests revealed reverse end bearing capacity failure in clays at the base of the caisson. A tensile failure mechanism was observed for the test at 1 g, revealing that model scale tests at 1 g may not replicate actual behavior.

The development and confirmation of analytical models for suction caisson resistance capacity estimates has been a major focus. Based on a centrifuge study of vertical uplift capacity of suction caissons in normally consolidated kaolin clay, Clukey & Morrison (1993) observed the external skin friction to be equal to about 80% of cone penetrometer tested (CPT) undrained shear

strength (s_u) and the internal skin friction to be about 45% of CPT s_u. Allersma et al. (1999) and Kirstein et al. (1999) extended these studies to investigate mobilization of horizontal bearing capacity and suction resistance against inclined loads, conducting centrifuge tests on caissons with L/D = 1.66 loaded from various inclined angles and attachment depths along the side of the caisson. Results from these tests (Allersma et al. 1999; Kirstein et al. 1999) indicate the API RP 2A (API 1995) recommended method (empirical) for horizontal bearing of suction caisson design, as a function of caisson diameter, soil unit weight and internal friction, tend to result in conservative estimates of load resistance. Further comparisons between centrifuge modeling and other analytical methods of estimating uplift resistance such as PLA method and FE analysis using ABAQUS were performed for suction caissons with L/D = 4.7 to 4.9 subjected to vertical, horizontal, and 33° incline line loading applied a distance of 2/3 caisson depth below the top of caisson (Clukey et al. 2004). Results of centrifuge modelling indicated that PLA tended to over predict capacity to a maximum error of 9%, and the FE model tended to agree more closely with centrifuge modelling results.

A study on three key components of caisson resistance to vertical tensile loads (i.e. internal side shear, external side shear, and inverse bearing capacity) was conducted by Jeanjean et al. (2006). A double-walled caisson having an L/D = 6 was used to isolate the internal and external friction components. The testing was performed in near-normally consolidated kaolin clay at 37.5g. It was observed that the internal friction is lower than external friction regardless of whether the caisson was installed by jacking or by suction, and internal friction peaks at a greater displacement than external friction due to mobilized end bearing, This is somewhat contrary to a common design assumption that inverse bearing capacity could be mobilized only through maintenance of internal/external pressure gradient. Other test results indicated that caissons with a sealed top cap provided 140% of the capacity provided by open-top suction caissons. Results supported assumptions that installation method has minimal effect on resulting capacity. Results also suggested that current API (2006) design recommendations adapted from traditional pile

design are not applicable for suction side shear as they substantially overestimate the external side shear parameter α.

Cyclic loading is an important consideration for all offshore design, and has accordingly been investigated by centrifuge testing of suction caissons. Clukey et al. (1995) conducted centrifuge modeling of multi-staged cyclic loads (sequential 'packages', with 1 – 5 Hz, and $P_{amp}/P_{mn,peak}$ applied at the top cap of a suction caisson model with L/D = 2 at 100g. Loads were applied at angles varying angles (+/-6° from vertical). Analysis of centrifuge modeling results provided data for definition of a relationship between 'equivalent number of cycles' and 'cycles to failure' plots for the suction caisson in kaolin clay (Figure 2.1). Results indicate that caisson response is dependent on the combination of static offset, cyclic load level and load angle. Post-cyclic monotonic load resistance is increased (by an average 5-35%), when excess pore pressure was allowed to dissipate prior to monotonic load to failure. Allersma (2000) performed centrifuge modeling of cyclic and long term vertical uplift loading applied at the top cap of a suction caisson (L/D = 1.16) installed in sand and clay. It was observed that if maximum cyclic load ($P_{cy,max}$) is less than 85% of the static peak monotonic load ($P_{mn,peak}$), over 5000 cycles were required to fail the caisson. Displacements due to sustained loads were significant if sustained load magnitude was between 90-100% $P_{mn,peak}$. If sustained loads were less than 80% $P_{mn,peak}$ minimal displacement resulted.

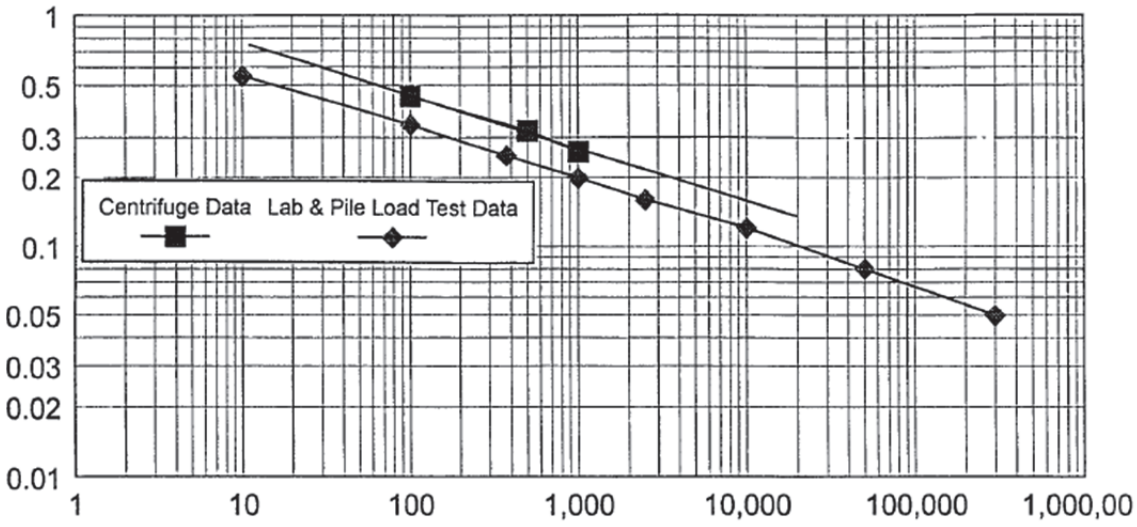

Figure 2.1. Vertical uplift failure curve for L/D = 2 suction caisson in kaolin clay (from Clukey et al. 1995).

Definition of required (and limiting) installation forces is important for effective caisson installation and appropriate selection of installation equipment. For given site conditions (water depth, subsurface stratigraphy, soil strength, etc.) and a selected caisson size there is a minimum installation force required to penetrate the caisson to design depth. There is also a maximum suction force that may be applied prior to (undesirable) initiation of cavitation and soil heave inside the caisson.

Verification and calibration of analytical methods defining caisson installation forces has been the focus of a number of testing programs. Bang (2001) performed centrifuge modeling and laboratory scale modeling of suction caisson installation in conjunction with field testing of 5m steel piles with various diameters (L/D = 10, 5, 3.33, 2; Cho et al 2002) to verify and calibrate a proposed analytical method for determining installation forces as a function of mobilized skin friction / cohesion and bearing resistance. Analysis of installation stresses applied to laboratory, centrifuge and field models indicate good agreement on mobilized skin friction parameter calculated from all three test types.

Efficiency of design has been another major focus for centrifuge studies of suction caissons, especially as economy is one of the key reasons for the move to suction caissons.

Studies by Allersma et al. (1999) and Kirstein (1999) revealed that for horizontal or near-horizontally loaded caissons, the optimum load attachment point was a distance of 0.4-0.6L up from tip of caisson, and capacity was reduced with increasing load angle (from horizontal). Lee et al. (2003) present a modified concept of suction caissons to take advantage of the greater soil strength at depth. A cylindrical section is installed to depth by interlocking to the base of a traditional caisson. The system is installed in the traditional manner, however the upper caisson is then removed leaving the cylindrical section embedded at depth. This type of anchoring system is referred to as embedded suction anchors (Figure 2.2). Based on centrifuge modelling of embedded suction anchor in kaolin clay, with L/D = 1.7 and three vertical flanges with length / width = 5 arranged symmetrically about the circumference of the anchor, subjected to inclined load at various pad eye positions optimum pad eye position was found to be at approximately 0.45L from caisson tip .

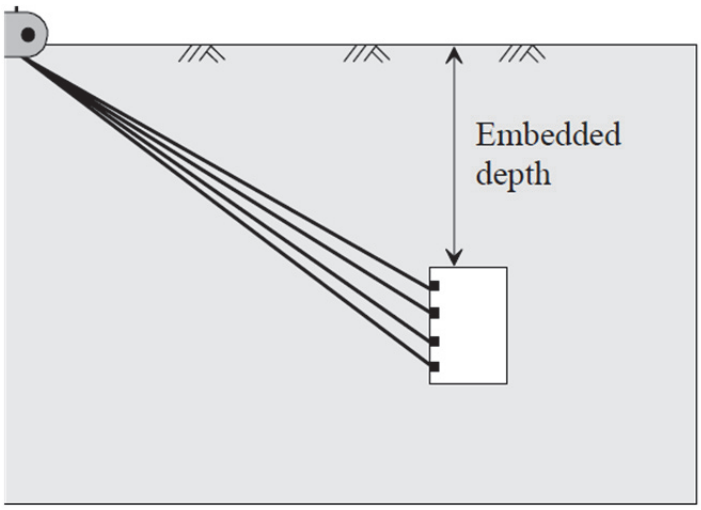

Figure 2.2. Embedded suction anchor concept
(From Lee et al. 2003).

Although the general form, design, installation and analysis of suction caissons has been well established through the oil and gas experience and associated research, there continues to be potential for improvements in cost-efficient design, particularly suited for the emerging offshore renewable energy industry. Because the growth of offshore alternative energy is highly dependent on reduction of costs (as previously noted), as achieved in the short term by establishment of

standards and deployment of prototypes, and in the long term by development of economical foundation technologies, this research program aims to physically model an economical foundation option, to evaluate existing design standards relative to test results. and to provide basis for further exploration of economical anchor design.

2.1.3. Design of Suction Caisson Anchors

Important topics to consider for the engineering analysis and design of suction caisson anchors include installation, design (critical) load conditions, pad eye position, load resistance mechanism, and dynamic load effects. Prescriptive methods have been developed for the offshore oil and gas industry to address these topics, however modifications may be appropriate for application with offshore wind platforms as differences in critical load conditions network/system layout exist.

The Bureau of Ocean Energy Management, Regulation, and Enforcement (BOEMRE 2010) provides guidelines on appropriate design standards to be applied for offshore wind energy installations, indicating that various American, European and International standards may be applied, with preference given to the American standards or those which are most conservative. However, not all established offshore geotechnical and foundation design standards and recommended practices are relevant specifically to design of suction caisson anchors. None of the foundation design standards or recommended practices are specific to application with offshore wind energy platforms. A summary of the more commonly cited design standards and recommended practices is provided in Table 2.1.

Lessons learned and developments made by offshore oil and gas are beneficial to offshore wind development. However, it is essential the similarities and differences are understood. Environmental loads are different in shallow waters than in deep waters. One important difference is increased effect of boundary layer(s) or influence of discrete layers due to reduced water column height over which the conditions may be averaged. Difference in physical

conditions between deepwater oil and gas and deepwater wind energy sites may limit which of those anchor types developed for oil and gas are applicable for alternative energy sites.

Table 2.1. Summary of standards and recommended practices for offshore foundation design.

Regulatory Organization	Standard No. (Year)	Foundation Design Recommendations
American Petroleum Institute (API)	API RP 2A WSD (2005)	• foundations for fixed platforms including: driven piles, drilled piles, belled piles and shallow footings
American Petroleum Institute (API)	API RP 2SK	• anchor systems for floating platforms including: suction pile anchors • recommended methods for suction pile anchor design: Finite Element Method, Limiting Equilibrium Method, Plastic Limit Analysis and Beam-Column Method
Det Norske Veritas (DNV)	DNV RP E303 DNV SP	• suction pile anchor design for floating platforms • recommended methods for suction pile anchor design: Finite Element Method (and other numerical methods) and Limiting Equilibrium Method.
Germanischer Lloyd (GL)	Guideline for the Certification of Offshore Wind Turbines	• references API RP 2A LRFD (API 1993) – foundations for fixed structures • additional guidance on piles in layered soils and pile resistance to lateral loads
International Standards Organization (ISO)	ISO 19901-4 (2003)	• shallow foundations for fixed platforms
International Electrotechnical Commission (IEC)	IEC 61400-3 (2009)	• reference Germanischer Lloyd, Det Norske Veritas and International Standards Organization

Critical design condition is also different for wind turbines. Based on initial models, cyclic wave loads tend to dominate the critical design loads for floating wind turbines. For existing fixed structure offshore wind, the critical design condition is usually the fatigue loading of over 1 billion smaller amplitude load cycles; whereas the design condition for offshore oil and gas platforms are storm conditions with 100 to 1000 load cycles (Schneider and Senders 2010).

Dynamic loading of the wind turbine mooring system is a critical consideration and one of the more challenging components of floating platform design. A combination of turbine and mooring system dynamics interactively define natural harmonics of the system. It is important

that combined turbine/mooring system is designed so natural frequencies of the system are dissimilar to environmental load frequencies to avoid substantial amplification of load and displacements. Anchor design requires consideration of all applied loads, including any load amplification that might occur from turbine/mooring/environmental interaction.

2.1.4. Suction Caisson Installation

Installation of a suction caisson is performed partially by penetration of the caisson into the seabed by caisson self-weight/free fall and completed by the application of underpressure (suction) by pumping water from the space formed between the inside top of the caisson and the seafloor. Pressure differential created between the outside of the caisson and the inside of the caisson provides the underpressure required for penetration of the caisson to the design depth, which is where the caisson top cap is flush with the sea bed following installation. Installation is more efficient compared to conventional pile driving, and full installation is achieved within hours using a single anchor handling vessel, remotely operated vehicle, and a pump (Colliat 2002). Precise anchor location is another benefit of the suction caisson installation, in comparison to drag or drop anchor methods.

Self-weight penetration and required underpressure are important considerations for the installation design of a suction caisson. During installation, penetration resistance is provided by the side shear along the caisson wall and the bearing capacity at the caisson tip. Depth of self-weight penetration and the subsequent suction force requirement are calculated by estimating the friction factor and bearing resistance characteristics of the soil. Andersen et al. (2005) details the theoretical derivation and resulting equations for estimating the self-weight penetration depth and required suction pressure for installation. There is also a maximum allowable underpressure as limited by internal soil heave and cavitation. Details for calculating the maximum allowable underpressure is provided in Randolph and Gourvenec (2011).

2.1.5. Applied Loads on Suction Caissons

Sources of load on a floating platform include: permanent structural loads, environmental loads, and coupled dynamic loads. Each of the load types may consist of static, sustained, or cyclic components. Structural loads are static loads, defined by the physical properties of the floating platform and mooring system. Environmental loads contribute both sustained and cyclic loads as controlled by the metocean conditions onsite (Chakrabarti 2005; Clukey et al. 1995; El-Gharbawy and Olson 1999).

Cyclic environmental loads typically include wave impact, impulse and run-up loads. Current and wind load are considered as sustained environmental loads. Based on the offshore oil and gas experience, cyclic loads substantially contribute to the total load on an offshore structure. For a TLP system, the cyclic load magnitude is 40% of the sustained loading on the anchors for TLP systems (Narasimha Rao et al. 1997). Design environmental loads parameters are often statistically determined, based on conditions corresponding to spectral average wave period, significant wave height, etc.

Coupled dynamic loads on a moored floating platform are the most challenging to define. It requires consideration of interactions between the wind inflow, aerodynamics, elasticity, and controls of the wind turbine, along with the incident waves, sea current, hydrodynamics, and platform and mooring dynamics of the floater (Jonkman 2007). These aero-servo-hydro-elastic loads and responses are extremely variable with the physical design, the environmental conditions and the interactions between them. Load magnitudes and cyclic load frequencies resulting from these dynamic interactions are important for foundation (anchor) design.

2.1.6. Mooring Systems and Load Transfer

The angle of loading on a suction caisson is controlled by mooring line configuration. Catenary, taut-line or tension mooring configurations, may be used in conjunction with suction

caisson anchors resulting in load angles from near-horizontal to vertical. In all cases, the loads will be applied as a tensile force in the mooring line between the floating body and the point of pad-eye connection at the caisson. For tension leg platforms (TLP), the majority of the load applied to the caisson is vertical, where the mooring line is attached to the top of the caisson. Taut line systems transfer both lateral and vertical loads to the caisson at the pad-eye location. Catenary mooring lines apply considerable lateral loads, and vertical load components are limited. The dynamic characteristics of the loading are dependent not only on the mooring configuration but also on the mooring line material, which may be steel chain, steel cable or synthetic cable.

2.1.7. Load Resistance Estimation Methods

Load resistance of an anchor is dependent on the orientation of the applied load. Predominantly vertical loads (resulting from tension leg and steep taut line configurations) are resisted by a combination of side friction on the surface area of the caisson and 'inverse' bearing at the base of the caisson (Randolph 2002; Thorel et al. 2005; Luke et al. 2003, 2005; Jeanjean 2006). Predominantly horizontal loads imposed by catenary and low-incline taut lines are resisted by a combination of passive earth pressure, soil flow, and base shear (Andersen et al. 1999; Dahlberg et al. 2006; DNV 2005). These resistance mechanisms are simplifications, as true resistance modes are individual to each case depending on soil stratigraphy, characteristics, and strength as well as foundation and mooring geometry and soil-pile interaction.

Estimation of vertical load resistance can be simplified to three basic resistance mechanisms depending on the hydraulic conditions at the top and base of the caisson as illustrated in Figure 2.3 (Randolph 2002; Thorel et al. 2005; Luke et al. 2003, 2005). Resistance is provided by weight of anchor (and ballast), shear on external surface, and the components described in Table 2.2. The external shear taken as the product of the undrained shear strength (s_u) and interface strength factor or side resistance factor (α). The majority of investigational

results support the "fully sealed" mode (c) failure mechanism. However, it is anticipated that the actual failure mechanism for sealed top-cap caissons for long-term and cyclic vertical loads is likely a hybrid of failure modes (b) and (c) (Randolph and House 2002).

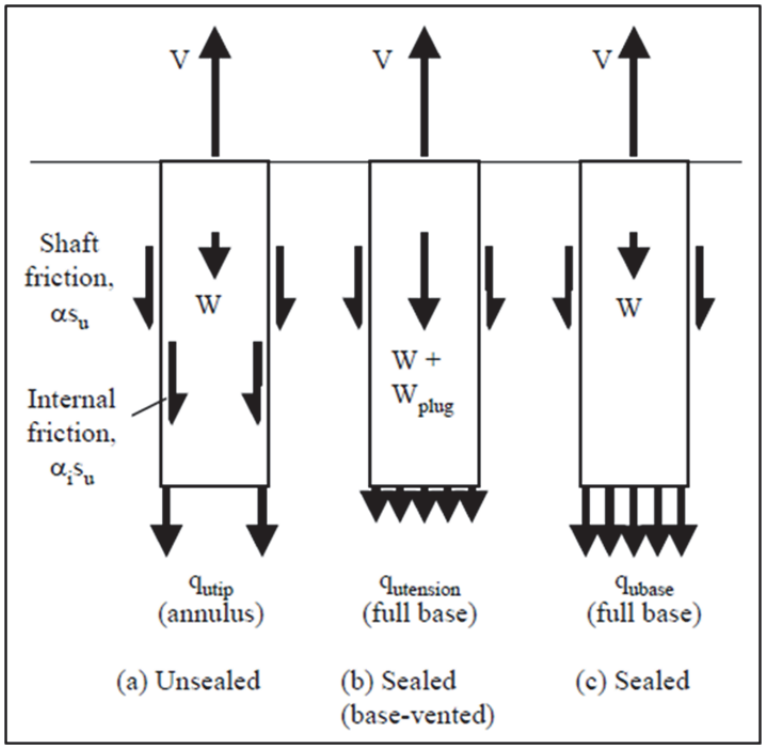

Figure 2.3. Resistance mechanisms of suction caissons against vertical load (from Randolph and House 2002).

Table 2.2. Soil – structure failure modes of vertically loaded suction caissons.

Failure Mode	Description
(a)	Shearing resistance on internal surface and end bearing resistance on tip of pile only (unsealed cap)
(b)	Weight of soil plug and tensile capacity at base of plug (sealed cap – hydraulic flow at base precluding suction)
(c)	Reverse end bearing for the full caisson cross sectional area (fully sealed)

The soil failure mechanism for a caisson subjected to inclined load is more complex and dependent on the specific caisson and loading geometry and soil properties. Methods for

evaluating failure mechanisms and load resistance capacities are classified as: theoretical, semi-empirical, and numerical models, in particular finite element models (FEM). Theoretical methods are based on various soil-structure interactions that occur in different depth intervals along the length of the caisson. Two common theoretical methods are Limiting Equilibrium Method (LEM) and Plastic Limit Analysis (PLA). The LEM (Andersen and Jostad 1999, 2002, 2004) incorporates the different zones of soil-structure behaviour as a piece-wise solution. PLA (Murff and Hamilton 1993; Aubeny and Murff 2005) estimates the combined effects of the various zones in a simplified model. Semi-empirical methods for estimating resistance capacity, such as the p-y and beam-column methods, have evolved from methods developed for driven piles. These semi-empirical methods are typically the simplest to apply, but generally are the least representative of actual caisson behaviour. Important differences between typical piles and suction caissons not reflected in the semi-empirical methods is the effect of caisson stiffness (due to lower L/D aspect ratio) on lateral load response and the significant contribution of (reverse) end bearing to caisson capacity (Eltaher et al. 2003). Numerical modelling has the greatest potential for defining the most likely failure mechanism, provided that sufficient and accurate soil strength and property profiles and load/mooring line properties are known.

In the LEM, load resistance is provided by different reaction mechanisms in each of 3 zones along the anchor (Figure 2.4). In the upper zone, the soil reaction force is comprised of active and passive earth pressure. In the lower zone, horizontal and vertical reaction forces are provided by horizontal soil flow around the anchor. At the tip of the suction caisson, inverse bearing capacity reacts against applied loads. LEM provides the ultimate capacity for suction caisson anchors with the following assumptions: normally consolidated clay, taut, semi-taut and catenary mooring system configurations translational-only failure, load application (pad-eye) position at the “optimal depth”, and zero net overturning moment at the projected center of the caisson tip.. Limiting Equilibrium method and calculation procedures are presented in the DNV recommended practice as a convenient and accessible method justified by a study comparing

results from the LEM and 3-D finite element model construction and analysis (Andersen et al. 2005). It was also found in the study that the Horizontal-Vertical resistance coupling is adequately addressed using the plane LEM.

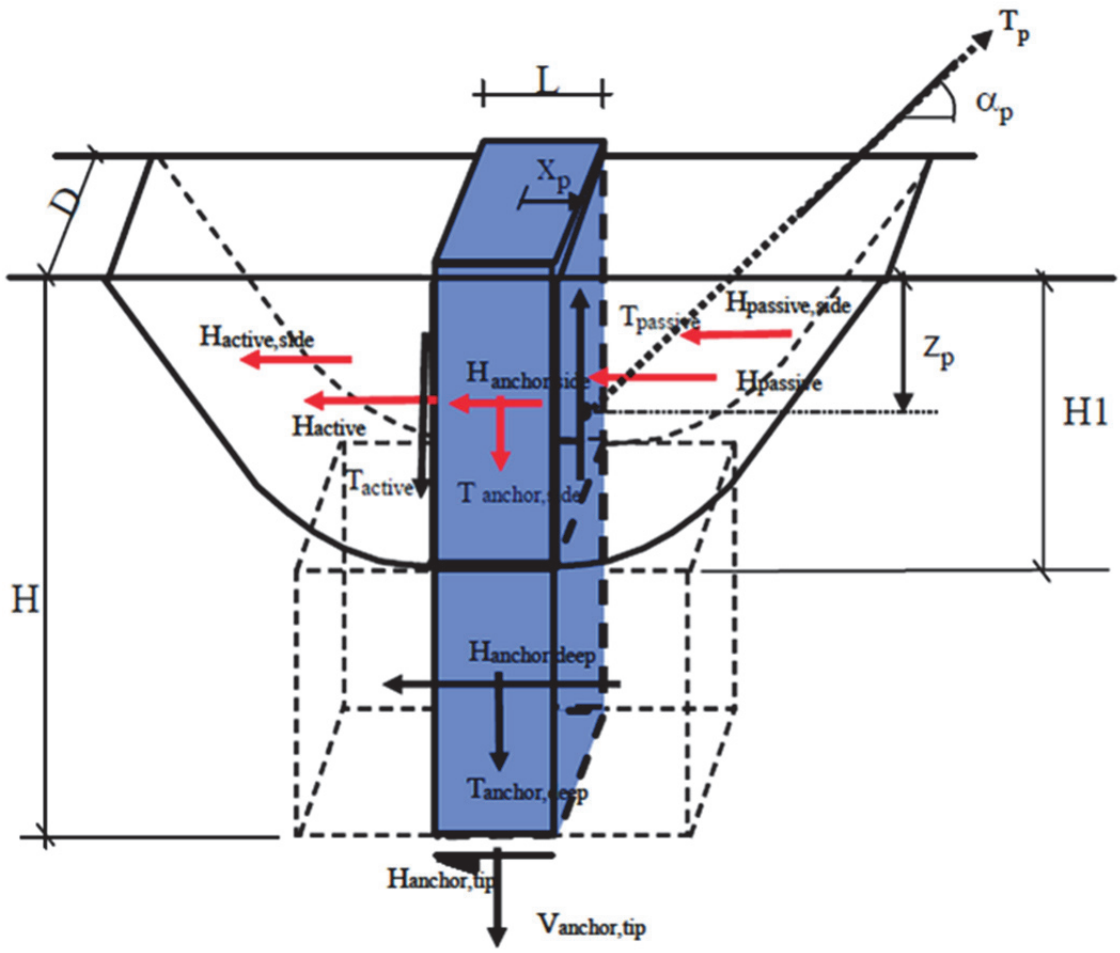

Figure 2.4. Idealized resistance mechanism for Limiting Equilibrium Method (from Det Norske Veritas 2005).

Plastic limit analysis (PLA) for suction caisson capacity was initially developed based on an upper bound plastic limit analysis model of internal energy dissipation along the failure surfaces of the material that result from applied external loads. The initial model and analysis proposed by Murff and Hamilton (1993) consists of 3 zones that are similar to the geometry of the prescribed mechanism for the LEM (Figure 2.4). The model applies generalized yield conditions based on the applied stresses and resultant strains along the soil-caisson interface,

allowing computation of the peak capacity. The initial 3-zone PLA model as developed by Murff and Hamilton (1993) projects a surface failure wedge along the upper zone, plane-strain soil flow through the lower zone around the suction anchor, and a spherical failure at the tip of the suction anchor, as detailed in Figure 2.5a. The simplified 2-zone PLA model proposed by Aubeny and Murff (2005) reduces the upper surface failure and lower flow zone to a single mechanism characterized by the depth to center of caisson rotation. The hemispherical slip surface at the tip of the suction anchor is retained in the simplified model (Figure 2.5b). This models the kinematic collapse mechanism through which the rate of internal energy dissipation is calculated and equated to the rate of work by the external applied load. Integration of rate of work over the failure surface provides the suction caisson capacity.

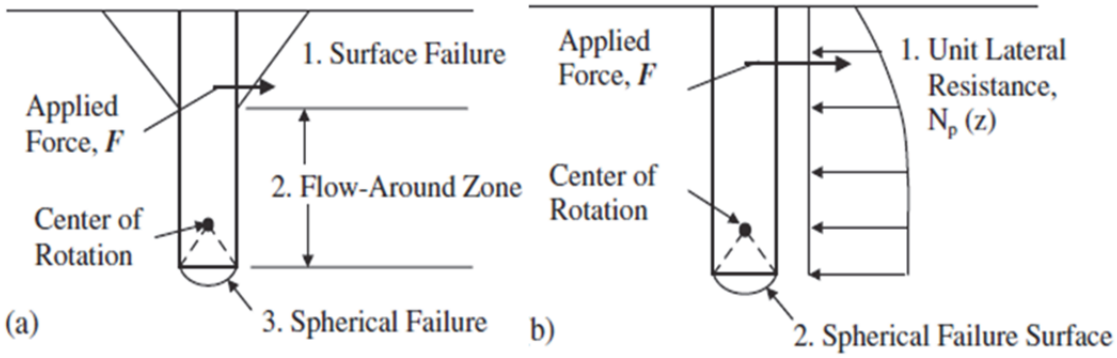

Figure 2.5. Idealized and simplified suction caisson resistance mechanism for PLA (Aubeny et al. 2003).

General FEM programs, such as ABAQUS and DIANA are increasing in popularity for investigation of suction caisson behaviour and capacity. Finite element analysis allows identification of the critical failure mode and the associated loads, moments, deformations and rotations. User inputs include the soil strength profile, Young's modulus and Poisson's ratio for the soil, and roughness parameters and adhesion coefficients at soil-caisson interfaces. Applying Von-Mises failure criterion, either a displacement or a load controlled analysis can be performed to develop displacement-load and rotation-moment relationships to define the ultimate capacity for the specified model parameters.

Load resistances estimated using different methods may be discrepant due to the various simplifications and assumptions integrated into each method. The most accurate determination of load resistance would be obtained by conducting a field trial of a full-scale suction caisson installation. This would also be the most expensive and provide the least transferrable information for locations with varied subsurface conditions. Numerical modelling (including FEM) would likely provide the next most accurate estimation of load resistance due to the comprehensive inclusion of subsurface and structural parameters in the analysis. LEM and PLA methods are likely the least accurate due to the various simplifications and assumptions inherent to both methods. However, the LEM and PLA methods are the most accessible and therefore, the simplest for industry use.

2.1.8. Effect of Cyclic Loading on Peak Resistance

Not only does cyclic loading contribute a major proportion of the total loading on a caisson, but the time variance of loading may affect immediate and delayed soil-structure interactions. Vertical capacity is potentially affected by changes in: soil-anchor skin friction adhesion, internal-external pressure differential, and undrained shear strength. In comparison to the sustained load case, adhesion may be reduced during cyclic loading due to the constant stress and strain of the soil-caisson interface and by limitation of thixotropic strength increase. Reduction of the pressure differential could result in modification of the resistance mechanism, reducing contribution of inverse bearing capacity. The effect of cyclic loading on undrained shear strength is stress and strain dependent, thus the ultimate load resistance is also dependent on the cyclic stress and resultant strain. Lateral capacity is similarly affected by cyclic loading, where plastic flow around a caisson is dependent on the adhesion parameter and the conceptual passive/active earth pressures and base shear resistance are controlled by undrained shear strength.

2.1.9. Undrained Cyclic Loading of Suction Caisson Anchors

Resistance to cyclic loading is of interest due to the cyclic nature of environmental (e.g., wave loads, impulse wave loads, and tide loads) and coupled dynamic loading of floating structures. Adequate suction caisson design requires identification of appropriate design foundation soil shear strength. Laboratory studies, including triaxial, direct simple shear and triaxial torsional shear devices, were conducted to obtain better understanding of the mechanics of soil resistance to cyclic shear by closely monitoring pore pressure and strain responses. Direct application of the various laboratory test mechanisms relative to suction pile-soil interactions can be visualised as shown in Figure 2.6 (Andersen 2009).

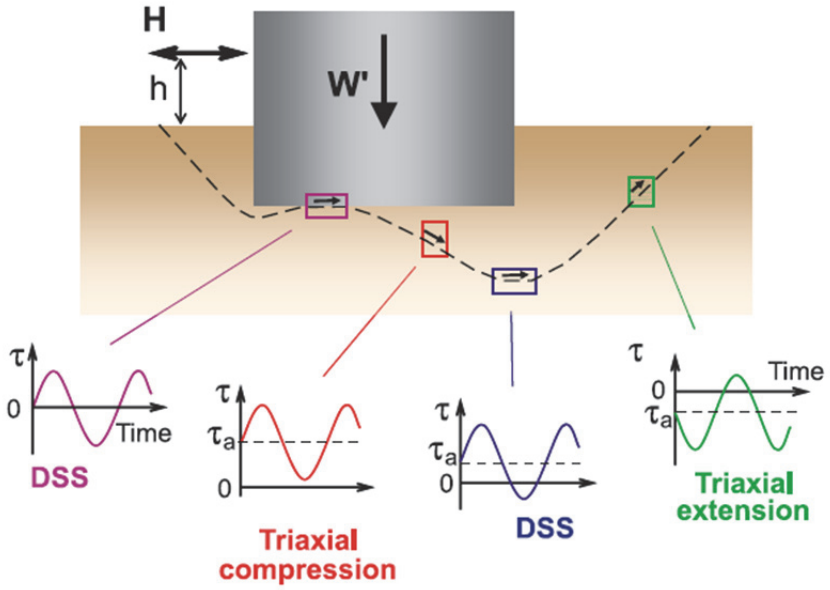

Figure 2.6. Relationship between laboratory s_u tests and suction caisson failure surface (from Andersen 2009).

2.1.10. Pore Pressure Development During Cyclic Loading

Consideration of long-term loading effects on soil shear strength such as pore pressure generation, fatigue, degradation and consolidation are also important for design. Early address of cyclic undrained shear strength by Larew and Leonards (1962), has been followed by numerous theoretical, laboratory, model and field studies conducted in the past five decades. During cyclic loading, the stress path is modified from the monotonic condition; the applied total stresses

increase and decrease and the pore pressure fluctuates and/or accumulates in response. In the τ-σ space, cyclic shear loading is represented by stress path loops as the applied shear stress is varied and the accumulated pore pressure from each subsequent cycle decreases the effective shear strength incrementally as shown in Figure 2.7 (Poulos 1988). As the cyclic loading continues, the loops approach the failure envelope progressively with continued increase of pore pressure.

With the continuation of cyclic shear loading, either:

- the loading will be sufficient to cause failure (identified by continued strain of the soil without an increase in applied stress) or
- the loading will be insufficient to cause failure as an equilibrium condition is attained between the applied shear stress and the pore pressure response.

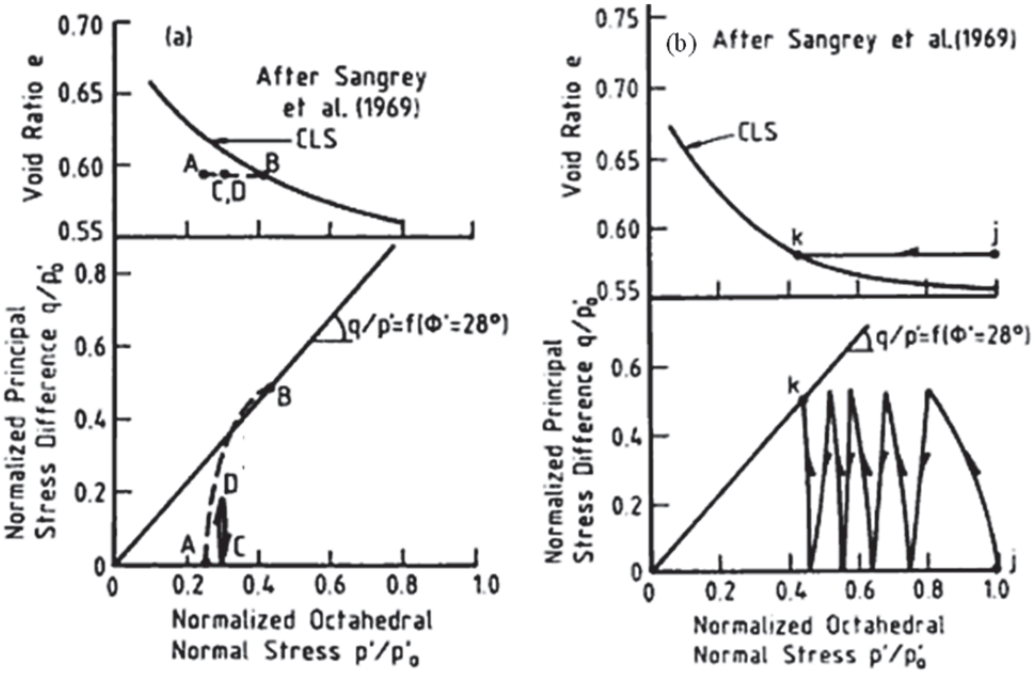

Figure 2.7. Void ratio and stress path progression during cyclic loading (a) below critical stability threshold (CLS) (b) above CLS (after Poulos 1988).

Through a 50-year design life of an offshore foundation, the number of load cycles applied is on the order of 150 000 000, therefore consideration of cyclic loading is important for appropriate suction caisson design. There is a characteristic critical level of repeated stress (also

referred to as: critical level of stability (CLS), critical stability threshold) for a particular soil and stress history that separates two distinct pore pressure and strength responses. If the applied cyclic shear stress is below the critical stability threshold, an unlimited number of load cycles may be resisted as the pore pressure accumulation occurs at decreasing rates until equilibrium between pore pressure increase and excess pore pressure dissipation is achieved (Sangrey 1969; Zergoun 1974). In this case, equilibrium condition is attained prior to the stress path reaching the failure line (Figure 2.7 a) and loading cycles continue without further strain increases as no further permanent pore pressures are accumulated (Andersen, 1976). When the applied cyclic stress is greater than the critical stability threshold, repeated loading will cause the pore pressure to increase continually, reducing the effective stress progressively until soil failure occurs (Larew and Leonards 1962; Sangrey et al. 1969; Ansal and Erken 1989). A study on two-way cyclic loading of both over consolidated and normally consolidated clay using a laboratory triaxial device reveals that both magnitude and rate of the positive pore pressure accumulation is greater for higher amplitude cyclic shear stress (Matsui et al. 1980).

Critical stability threshold is clay dependent and has been reported to be between 0.18 to 0.90 of the ultimate monotonic undrained shear strength (Lefebvre and LeBoeuf 1989). Although there is significant scatter in reported data, the value of the critical stability threshold tends to increase with increasing plasticity (El Hosri et al. 1984; Zhu and Law 1988; Erken and Ansal, 1994). Stress history and structure also tend to affect critical stability threshold. cyclic loading of overconsolidated clays tends to cause an initial decrease pore pressures followed by pore pressure increase with increasing number of load cycles. The greater the overconsolidation ratio (OCR) the more substantial initial decrease of pore pressure is observed and the lesser the overall increase of positive excess pore pressure accumulated over a large number of cycles (Matsui et al. 1980). Pore pressure response to loading is an indicator of the critical load level. Upon reaching the critical load level, pore pressure continues to increase even if the load magnitude was decreased during continued cycling (Sangrey et al. 1969).

2.1.11. Stress-strain Behaviour During Cyclic Loading

For a certain soil and stress history, there is a threshold cyclic shear stress level where equilibrium is achieved between applied cyclic stress and both pore pressure and strain response (Sangrey et al. 1969; Larew and Leonards 1962; Chaney and Fang 1986). Below this threshold, continued application of cyclic stress does not cause progression towards failure. Above this threshold, plastic, non-recoverable deformations progressively accumulate along with a continual decrease in secant shear modulus (Theirs and Seed 1968). There is an analogous critical cyclic shear strain level, which only if exceeded, results in excessive generation of pore pressure, strain softening and rapid progression toward failure (Erken and Can Ulker 2007). The critical cyclic strain level has been found as approximately 0.5% for undisturbed fine grained soils (Erken and Can Ulker 2007).

During cyclic loading, strain is composed of two components: creep and cyclic strain. Creep is strain associated with mean load, cyclic strain may be attributed either elastic compression, consolidation, or both. During initial stage of cyclic loading, prior to pore pressure equalization) the deformation is attributed to elastic compression under the total applied loads (average+cyclic); as the number of applied cycles increases, achievement of equilibrium/dissipation of excess pore pressures results in consolidation deformation (Ponniah and Finlay 1988).

An investigation by Hyde et al. (1976) compares strain resulting from secondary compression (creep) and deformation induced by repeated load cycles. It is postulated that due to the similarities between the effects of a constant maintained load and a constant average load, the average secant shear modulus (G_{sec}) during non-failure cyclic loading can be estimated to be the same as for a constant load equal to the mean cyclic load magnitude. In both cases, logarithm of strain rate is a linear function of the logarithm of time using similar decay rates for both sustained and repeated loading on soils with the same stress history.

There does not appear to be a consensus in literature on the variables controlling reduction of shear modulus due to cyclic loading. Numerous variables have been cited to control the degradation of shear modulus including: ratio of cyclic stress amplitude to undrained shear strength (Andersen 1976); accumulated strain (Zergoun and Vaid 1994), cyclic strain amplitude (Andersen 1976) although even at low values of cyclic strain shear modulus is reduced (Matsui et al.1992; Castro and Christian 1976; Koutsofta 1978; Matsui and Abe 1981); degradation index (ratio of $G_{sec,\ n=i}$ to $G_{sec,\ n=1}$) and number of applied cycles (Figure 2.8) (Vucetic 1988); cyclic load frequency and pore pressure generation (Yao and Nie 1994; Wang and Yao 1996; Zhou and Gong 2001); and ratio of applied (horizontal) cyclic shear stress to vertical effective consolidation stress (Boulanger and Idress 2007).

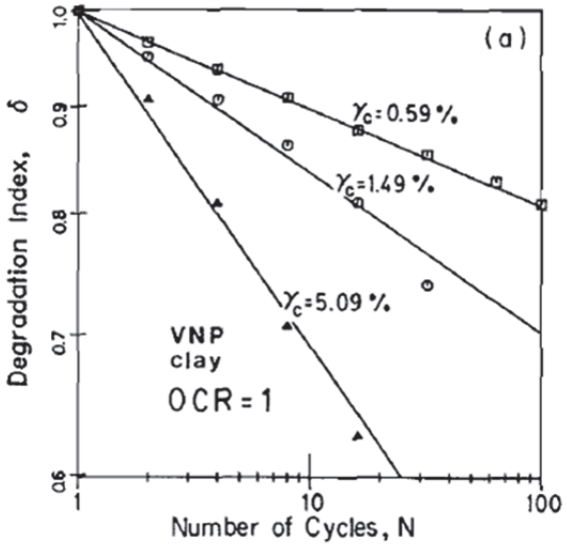

Figure 2.8. Degradation index varying with number of load cycles for Venezuelan North of Paria clay (from Vucetic 1988).

2.1.12. Short Term Cyclic Pre-loading Effects on Strength and Stress-strain Behaviour

Stress-strain behaviour of soils during post-cyclic monotonic loading is affected by cyclic preloading, however there is not a consensus in the literature on the post-cyclic monotonic behaviour of cohesive soils. A strain softening effect on post-cyclic monotonic stress-strain

behaviour due to cyclic preloading is reported for normally consolidated, overconsolidated and apparently overconsolidated clays based on cyclic consolidated undrained triaxial compression (Andersen 1988; Castro and Christian 1976; Koutsoftas 1978; Matsui et al. 1980). Other studies (Motherwell and Wright 1978; Andersen 1975) on normally consolidated marine clays report increased stiffness in post-cyclic monotonic stress-strain behaviour, based on cyclic consolidated undrained triaxial compression test results. The discrepancy may be attributed to the difference between strain-controlled and stress-controlled cyclic loading, where post-cyclic strain modulus tended to be decreased after strain-controlled cyclic loading and increased after stress-controlled loading (Jitno 1990)

There does not appear to be consensus in literature on the effect of cyclic preloading on monotonic undrained shear strength. However, a concept of cyclic loading threshold similar to the aforementioned CLS boundary for pore pressure response and cyclic shear strength is proposed. Based on a review of results obtained from various studies (Matlock and Holmquest 1976; Bogard and Matlock 1979; Grosh and Reese 1980; Poulos 1981), there is a threshold of cyclic loading below which undrained capacity is minimally affected and above which failure is induced (Briaud 1986) indicating a reduced capacity. Moreover, the result of cyclic loading reaching pore pressure equilibrium is to impose an apparent overconsolidated state in the soil immediately after cycling (Yasuhara et al. 1992), which tends to result in increased post-cyclic monotonic undrained shear strength (Dutt et al 1992). The short term post-cyclic undrained shear strength is a function of the level apparent overconsolidation, the excess pore pressure and the initial effective stress (Yasuhara 1995).

Other research reports reduction in short term post-cyclic undrained shear strengths (Thiers and Seed 1968; Andersen 1976; Lefebvre and LeBoeuf 1989; Andersen 2009). Although the original failure envelope of the soil is considered to remain the same (Lefebvre and LeBoeuf 1989), excess pore pressure accumulated during cyclic loading is cited to reduce effective stress (Andersen 1976) and decrease undrained shear strength. It was further reasoned that reduction of

post-cyclic monotonic undrained shear strength is additionally caused by the destruction of inter-particulate bonds and re-alignment of particles parallel to the direction of strain (Briaud and Felio 1986). Estimates for the reduction of undrained shear strength was related to strain accumulated during cyclic preloading (Figure 2.9) (Thiers and Seed 1968; Castro 1976).

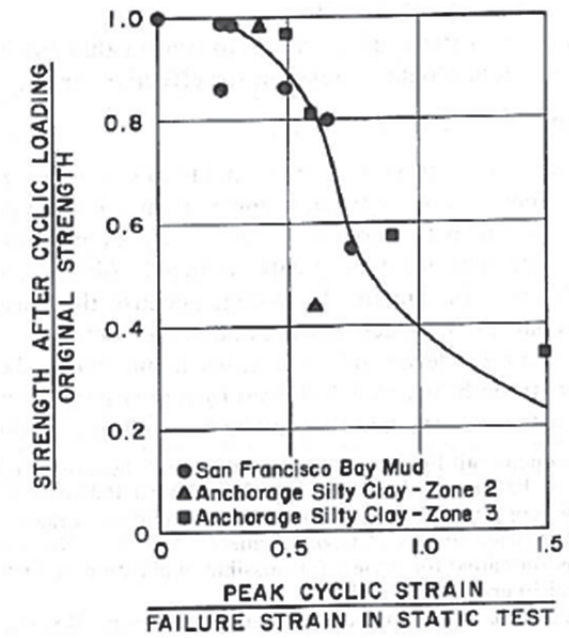

Figure 2.9. Degradation of undrained shear strength due to cyclic preloading (from Castro and Christian 1976).

It is important to note that the aforementioned effects of cyclic loading on monotonic undrained shear strength are based on ideal laboratory situations applying results from triaxial, direct simple shear and simple shear test programs. For application in physical foundation models, the undrained monotonic shear strength needs to be considered in conjunction with interaction with the structure.

2.1.13. Delayed Cyclic Pre-loading Effects on Monotonic Shear Strength

In the vast majority of cases, cyclic preloading results in initial stiffness increase and monotonic undrained soil strength increase after sufficient time has passed such that any excess pore pressures accumulated during cyclic loading have dissipated. This increase in post cyclic

monotonic undrained shear strength is attributed to the induced overconsolidation state and the reduced pore pressure generation in subsequent cyclic or monotonic undrained loading (Thiers and Seed 1968; Brown et al. 1977; Castro and Christian 1976; Andersen 1988; Matsui et al. 1977; Matsui et al. 1992; Koutsoftas 1978; Yasuhara1985; Matsui et al. 1992).

2.2. Centrifuge Background

A geotechnical centrifuge applies more realistic forces to a model scale soil sample model foundation through use of an inertial acceleration field greater than earth's gravity, achieved by high velocity rotation soil/foundation model system. The basic beam centrifuge setup consists of a soil sample/model box connected by a hinge to the rotational arm, centered about the drive motor and gear components (Figure 2.10). As the rotational arm and attached soil sample box are rotated, outward inertial force, proportional to the square of rotational velocity, is applied to the sample/model. This setup results in applied stresses that are a function of the self-weight and geometric properties of the soil and foundation models. This is important, as effective stresses in soil are critical to geotechnical design problems such as retaining walls, soil structure interaction, buried structures and excavations, foundations, dynamic loading of earth structures, environmental transport processes, and cold regions engineering, to list a few. Objectives of model scale tests include:

- Analyze a specific problem with result relating to a select prototype and project
- Gain better understanding of a general problem, covering a broader scope of application
- Study of stress changes and displacements applicable to a certain type of geotechnical project,
- Calibrate numerical models

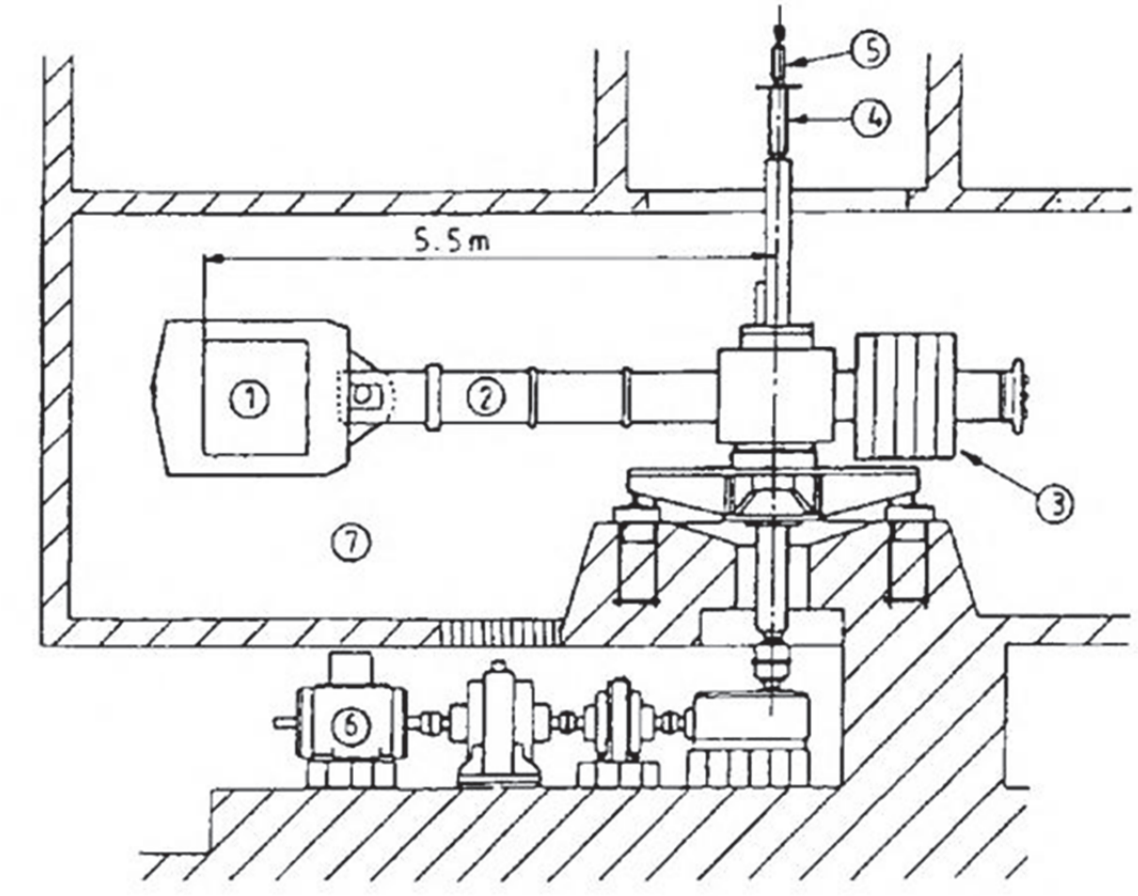

Figure 2.10. Schematic of beam centrifuge
(1: swinging soil model; 2: centrifuge beam; 3: counterweight; 4: slip-ring assembly; 5: rotary-joint assembly; 6: drive system; 7: aerodynamic enclosure) (from Wood 2004)

Geotechnical model scale testing using a centrifuge is most commonly conducted to gain insight into a generalized problem and identify the effects of various parameters on the model being evaluated. Centrifuge modeling successfully recreates equivalent effective stress conditions, which are integral to soil behavior. Reduced scale and the relatively low cost of centrifuge testing allow multiple tests to be performed in a relatively short time frame, ideal for parametric studies comparing varied designs. The accessibility to centrifuge facilities is also a major benefit; geotechnical centrifuges are available across the USA and worldwide. Unlike full scale testing, it doesn't require mobilization of heavy/specialized equipment to remote test sites and is not subject to the same restrictions as full-scale in-situ testing. The sources of greatest

controversy or criticism regarding centrifuge testing are scaling issues. However, if these scaling concerns are adequately identified and addressed, centrifuge modeling is as valid as any other method of geotechnical modeling.

2.2.1. Centrifuge Scaling Laws

Model testing is never a perfect scale replica of all prototype scale parameters. Approximations must be made and potential effects of any discrepancies must be estimated. Both physical parameters (i.e.: dimensions, densities, unit weights, etc.) and mechanical properties (i.e.: modulus, hydraulic conductivity, dissipation, etc.) need to be addressed regarding centrifuge scale modelling. Due to the design and mechanical operation of a centrifuge, there are also a number of inherent conditions affecting parameters important to geotechnical analysis including: non-uniform acceleration fields (acceleration is dependent on radius from rotational center), inability of the soil model to replicate geological history, and coriolis effect resulting from relative position of model test and the rotational centrifuge plane. Analysis of the effects of these conditions can be performed using dimensionless analysis and/or consideration of governing differential equations (Cao 2003). A summary of some of the key scale factors is summarized in Table 2.3 (Cao 2003) and explained in more detail in the following sections.

Table 2.3. Summary of key centrifuge scale factors (after Cao 2003).

Parameter modeled	**Scale Factor (Prototype: Model at 'N' G)**
Acceleration	1:N
Model dimension	N:1
Soil density	1:1
Soil unit weight	1:N
Stress	1:1
Strain	1:1
Force	N^2:1
Displacement	N:1
Void ratio	1:1
Time (Inertial events)	N:1
Time (Consolidation and diffusion)	N^2:1
Time (Viscous flow)	1:1

2.2.2. Linear Dimensions

A major benefit of centrifuge model testing is maintenance of stress profile at a reduced scale that corresponds well to the full scale prototype condition. Similitude at corresponding depths between model scale and prototype scale is created by coordinating model dimensions and rotational speed of the centrifuge. Where the gravitation force due to the rotational speed is 'N' times gravity, linear dimensions in the centrifuge model are scaled to 1/N of the prototype dimensions.

2.2.3. Varying G-levels Through Radius of Rotation

Inertial force created by centrifuge rotation is dependent on the angular velocity and the radius of rotation. Where the geotechnical model has a dimension (depth) in the plane of the rotation extending from the radial arm of the centrifuge, the radius of rotation varies through the depth of the model. The result of this is a variation of the applied inertial force through the depth of the sample. A comparison of the distribution of vertical stress for the 1 g prototype vs. the scaled vertical stress profile resulting from the radial effect of the centrifuge is shown in Figure 2.11. The maximum and minimum overstress due to the varying radius effect can be derived (Taylor 1995) to define the depth of similitude of prototype and model stress as 2/3 of the model depth. The effective radius, or radius at which the 'g-force' should be monitored is then 1/3 of the model depth. (Schofield 1980; Taylor 1995).

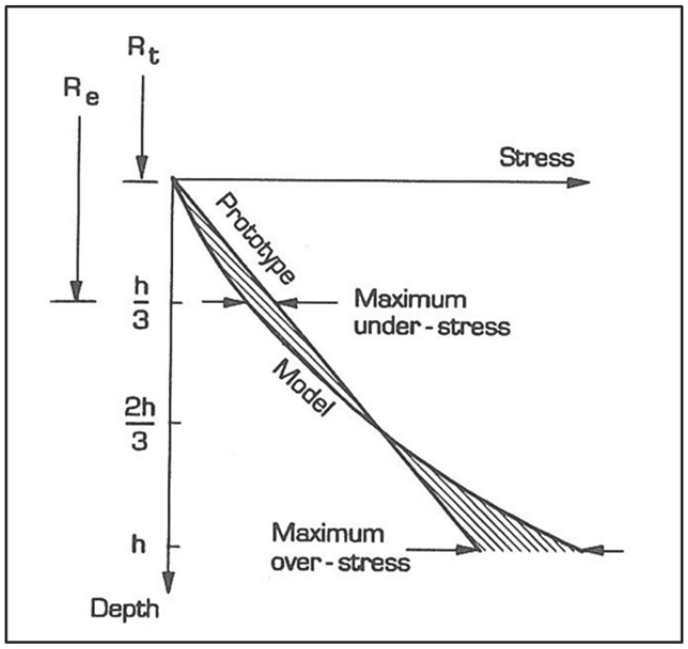

Figure 2.11. Vertical stress profile in prototype model and centrifuge model due to centrifuge radial effect (from Taylor 1995).

2.2.4. Rotational Acceleration Field

Two differences result from the rotational inertial field that cause deviations from the prototype condition of constant gravity. The first arises from the position of the model relative to the radial arm of rotation and the second results from the Coriolis effect. The creation of an accelerational field about a fixed axis results in lateral component of acceleration on model components that are offset from the radial arm within the plane of rotation. The magnitude of the lateral acceleration is dependent on the distance of offset, therefore the lateral component can be minimized by locating model events centrally within the soil model. The Coriolis acceleration is an apparent acceleration dependent on the relative motions of the object and the frame of reference. This apparent acceleration occurs if the motion and the frame reference are not both fixed to the same coordinate system. This apparent effect can be therefore be negated if the frame of reference is fixed to the plane in which object motion occurs.

2.2.5. Geological Processes / Soil History

Marine soils can have a complex geological history, especially at locations in proximity to the current coastline. The soils may have initially been deposited in the marine or land environment, followed by periods of submergence, emergence, glacial loading, scour, ice scour, desiccation, aging, other natural phenomena, or human activity, among many things. Exact replication of the geological processes to form the soil model would be extremely difficult, and for most centrifuge testing objectives, unnecessary. Most centrifuge investigations are intended to study generic problems or perform parametric studies and in most cases re-creation of select components of the geologic history such as consolidation state is sufficient in terms of soil strength and behavior and is reasonably achievable in the centrifuge.

2.2.6. Particle Size Effects

As shown in §3.2.1, the model to prototype scale for linear dimension due to the inertial acceleration at 'N' times gravity is 1:N. Due to this dimensional scaling, the particles in sample represent particles that would be 'N' time larger in the prototype condition. This may or may not be significant to the behavior of the model depending on the relative size of the model, particle, and pores. If the particle and pore sizes in the soil model are several orders of magnitude smaller than the size of the foundation/structure size being tested, the difference in behavior is minimal. However, it would not be appropriate to literally scale rupture surfaces that defined by particle size, directly defining prototype behavior from model scale observations. Results from a study by Ovesen (1979) indicate that where the diameter to grain size ratio is less than 15 significant deviations from expected behavior occur. Tatsuoka et al. (1991) suggest that a constant limiting ratio might be overly simplistic and a comparison of ratio of particle size to shear band width is more appropriate for estimation of particle size effect significance. Model of models testing may provide insight on effect of relative sizes of particles and foundations (Murff 1996; Taylor 1995),

but does not guarantee that extrapolation to prototype size will be exact. Depending on model to prototype scale, model of model tests may or may not be attainable in centrifuge testing.

2.2.7. Time Scales

For diffusion and consolidation events, Dimensional analysis of the consolidation equation indicates that time to consolidation varies with the square of the length of the drainage path. Since the scale of model to prototype drainage path is 1:N, the model to prototype scale for required time for consolidation is $1:N^2$. Due to the reduced time for diffusion, the loading rates required to maintain an undrained condition might need to be increased dramatically in coarser-grained soils, potentially leading to inertial effects in the model. A potential solution in the case of sands, where diffusion will occur extremely rapidly in the centrifuge, is to use silicon oil as the pore fluid instead of water.

The model to prototype time scale for dynamic processes is 1:N. Derivation of the displacement, velocity acceleration scales between a model and a prototype are presented in full by Taylor (1995). Whereas the model displacement is 1/N of the prototype displacement, and the model acceleration is n times the prototype acceleration, the velocity magnitude would be equivalent in the model and the prototype, resulting in a model time scale factor of 1/N of the prototype time for dynamic processes only.

2.3. Recent Developments/Research

Continued advance of oil and gas developments into greater sea depths and the growing interest in suction caisson usage has spurred further research on the performance refinements for suction caissons anchors for floating platforms. By 2003 there were 19 published cases of full scale, large scale, centrifuge, and laboratory tests on the topics of suction caisson installation, capacity and extraction (Andersen et al. 2005). Other studies have addressed optimal attachment point, crack formation between the caisson and soil, and strain behaviour for single line loaded suction caissons.

Suction caisson capacity against inclined loading has been investigated through a number of physical modelling studies. Initially, failure envelopes for shallow foundations and skirted foundations were defined through horizontal-vertical (H-V) resistance interaction diagrams (e.g. Figure 2.12). These diagrams have been modified and adapted for suction caissons (Bransby and Randolph 1998; Chen and Randolph 2007). An analytical definition of horizontal and inclined load resistance of suction caissons with respect to H-V resistance interaction was proposed (Cho and Bang 2002) and further developed for installation methods and loading angles based on results of seven centrifuge tests on the monotonic inclined load capacity of model caissons (Clukey et al. 2004). By 2005, a number of theoretical and semi-empirical methods were established for the analysis of installation, capacity and behaviour. Two major discrepancies remaining between capacity estimation methods were: α-values and reverse bearing capacity factor (N_c). Interface friction (α) values of 0.5 to 0.8, and N_c values between 13 and 21 were proposed based on laboratory (1G) model scale tests performed in normally consolidated kaolinite clay (Luke 2005). Calibrations and refinements of finite element models of suction caisson anchor resistance to inclined loads using centrifuge modelling results have been performed for specific offshore installations (Jeanjean et al. 2006). A summary of some of the centrifuge test results from Clukey et al. (2004), Jeanjean et al. (2006) is provided in Table 2.4.

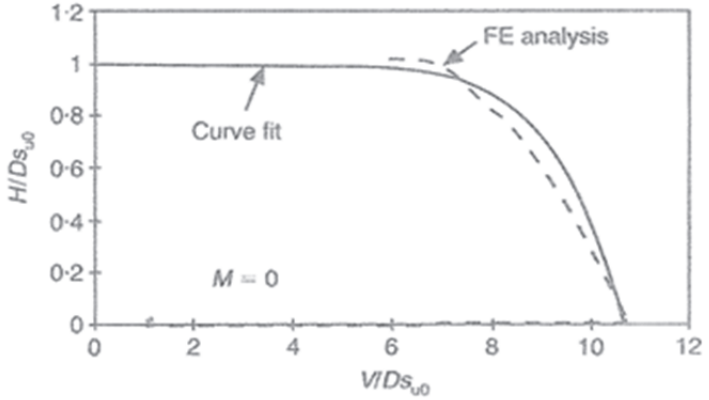

Figure 2.12. Horizontal - Vertical interaction diagram for shallow offshore foundation (from Bransby and Randolph 1998).

Table 2.4. Summary of suction caisson inclined load resistance tests in literature

Load Type	Test Name	L/D	L_i/L	θ (°)	Reference Monotonic			Cyclic Load Parameters					
					$s_{u,ave}$ (kPa)	$P_{mn,peak}$ /N	$d_{mn,peak}$/ D	No. Cycles	frequency (Hz)	P_{amp}/ $P_{calc,peak}$	P_{mean}/ $P_{calc,peak}$	$s_{u,ave}$ (kPa)	P_{peak}/N
Monotonic	Clukey et al. (2004),#3	4.7	0.67	40.0	18.4	9.57	-	-	-	-	-	-	-
	Clukey et al. (2004),#4	4.9	0.67	42.0	19.4	8.64	-	-	-	-	-	-	-
	Jeanjean et al. (2006) #1	2.3	0.33	43.5	38.0	8.71	0.1	-	-	-	-	-	-
	Jeanjean et al. (2006) #2	2.3	0.58	46.0	38.0	7.55	0.1	-	-	-	-	-	-
	Jeanjean et al. (2006) #3	2.1	0.18	40.0	34.0	5.90	0.1	-	-	-	-	-	-
	S1-T04-LM	2.0	0.60	47.0	4.6	7.36	1.392	-	-	-	-	-	-
Cyclic	Clukey et al. (1995) #1	2.3	0.00	90.0	57.5	9.09	n/a	500	5	0.14	0.22	57.46	9.57
								500	1	0.14	0.22		
								500	5	0.27	0.31		
								500	1	0.27	0.31		
	Clukey et al. (1995) #2	2.1	0.00	82.0	55.1	8.76	n/a	500	5	0.17	0.22	55.06	9.18
								500	1	0.17	0.22		
								500	5	0.30	0.31		
								500	1	0.30	0.31		
	Clukey et al. (1995) #2	2.0	0.00	88 to 92	43.1	8.82	n/a	500	5	0.20	0.30	43.09	11.94
								500	1	0.20	0.30		
								500	5	0.26	0.30		
								500	1	0.36	0.40		
	Chen and Randolph (2007) #B12cyc	4.0	0.00	90.0	16.9	17.28	n/a	50	0.5	0.22	0.22	17.70	12.43
								50	0.4	0.29	0.29		
								50	0.25	0.38	0.38		
	NOTES: S1-T03, S1-T05, S2-T13 - See Results and Test Details shown in Table 4.3 SYBOLS: L = caisson length; D = caisson diameter; L_i = depth to pad-eye; θ = load inclination; $s_{u,ave}$ = average shear strength over caisson length; $P_{mn,peak}$ = reference monotonic peak pullout resistance; $d_{mn,peak}$ = displacement at reference monotonic peak pullout resistance; P_{amp} = load amplitude; $P_{calc,peak}$ = calculated peak load resistance; $N = s_{u,ave} D L$; n/a = data not available												

Suction caisson response to cyclic loading has been another key area of research focus. Particular areas of interest are the relationship between cyclic load ratios and number of cycles to failure, and the effect of cyclic loading on load-displacement behaviors and ultimate load resistance. Initial centrifuge testing of cyclic loading on suction caissons in kaolinite clay indicated a 10-fold increase in number of cycles to failure with 44% decrease in applied cyclic load ratio (cyclic load / calculated load resistance) (Clukey et al. 1995). Furthermore, provided the applied cyclic load did not result in failure, the measured post-cyclic ultimate resistance was greater than the calculated ultimate resistance (Clukey et al. 1995). This non-degradation was confirmed in another centrifuge investigation of a suction caisson model subjected to cyclic loading, where post-cyclic peak monotonic load resistance of suction caissons was 120% of the monotonic undrained shear strength without cyclic preloading (Allersma 2004). However, results from other research are contradictory, indicating post-cyclic peak monotonic load capacity to be only 61 – 90% of the initial peak monotonic load capacity without cyclic pre loading (Andersen et al. 1993; El-Gharbawy and Olson 1999; Randolph and House 2002; Chen and Randolph 2007). The potential reduction of capacity is proposed to be a result of reduced α and N_c values due to cyclic loading, where suggested post cyclic values of $\alpha = 0.65 – 0.80$, and $N_c = 6.4$ to 9.0 (Chen and Randolph 2007). Select results of centrifuge tests of model suction caissons performed by Clukey and Morrison and (2005) and Chen and Randolph (2007) are shown in Table 2.4.

3. PHYSICAL MODELING PROGRAM

The focus of this research program is to investigate multi-line loading on suction caissons using physical modeling. Modeling was performed using a geotechnical centrifuge as it provides a more realistic soil model in terms of effective stresses for better replication of full scale prototype behavior. This chapter provides a brief summary of the main physical modeling concepts using geotechnical centrifuge, description of design and components of the modeling program, setup of the modeling program, predictions of performance and behavior of multi-line loaded caissons, and procedures used during the modeling.

There is minimal literature available on multi-directional loading of suction caissons, and therefore this research program is a novel development upon previous single-line modeling of suction caisson loading. This centrifuge program aims to investigate the performance of multi-directionally loaded suction caissons relative to performance of single-line loaded suction caissons with regard to application for anchoring of offshore wind platforms on the basis of:

- Stiffness of response during monotonic loading;
- Progression of lateral displacement during cyclic loading;
- Rotational and translational displacements during loading and at failure;
- Ultimate or peak (failure) resistance of a suction caisson;
- Pore pressure response during loading;
- Effect of P_{amp} on the above mentioned criteria;
- Effect of P_{mean} on the above mentioned criteria;

3.1. Testing Program Development

The behavior and resistance capacity of a suction caisson anchor subjected to orthogonal loads applied by taut line connections is investigated through a centrifuge modeling program. This investigation program progresses from a simple single line layout and with monotonic, then cyclic loading, continuing through various sequences of monotonic, sustained and cyclic

orthogonally applied loads. Single line monotonic (§3.1.1) and cyclic tests (§3.1.2) form the basis of comparison with literature and other tests. The first increase in load scheme complexity is sequential application and maintenance of load on orthogonal load lines, representative of failure condition during field installations of suction caissons. The following tests involve more complex load combinations, which are still simplifications of the operational conditions that are anticipated for orthogonally loaded suction caisson anchors. For the purposes of this initial research program, two general conditions were selected for comparison:

1. Sustained-cyclic loading: This is intended to model the case where the cyclic loading is predominantly applied on only one line. The effect of this cyclic loading on the peak monotonic inclined load resistance in the orthogonal (sustained) direction is of interest.
2. Cyclic-cyclic loading: This is intended to model the case where both lines are subject to cyclic loading. The effect of these cyclic loads on the peak monotonic inclined load resistance in only one of the two lines is of interest.

The amplitude of the cyclic load and mean load magnitudes are also varied between the tests with cyclic components to observe trends and relative performance. The focus of the following subsections is to present the developmental considerations for this centrifuge modelling program. Specific test setup and logistics are provided in §3.2 and §3.3.

3.1.1. Monotonic Single Line Tests

Monotonic single line tests are performed to compare with calculated design resistances (LEM from DNV 2005), results from published literature, and as baselines for other tests. The premise of the monotonic single line test is constant rate of displacement loading of a single line until failure is observed, which is designated as the peak monotonic inclined load resistance. This is the conventional definition of suction caisson ultimate capacity from recommended practice documents and published literature. Stress-strain behavior, peak line load resistance,

displacement at peak resistance, rotational displacement and pore pressure response from these single line monotonic tests are the baselines for comparison for the two-line tests. Two single line monotonic tests are proposed to investigate the effect of percent dissipation of excess pore pressure generated during installation on capacity and for comparison to subsequent tests in the test series. This was mainly considered as a means to investigate the effect of excess pore pressure on single line capacity and the potential to reduce the time waiting after installation to allow for more loading cycles. It is preferable to delay loading the caissons until all excess installation pore pressures have dissipated, however, due to equipment schedule limitations, extrapolations using results from two tests performed at different percentages of pore pressure installation was considered acceptable.

3.1.2. Cyclic Single Line Tests

Cyclic loading as experienced in the marine environment is highly random; however, loading is commonly simplified by using a sinusoidal load progression applied to the lines attached to the model caisson. Cyclic loading is accounted for in DNV RP-E303 (DNV 2005) for suction caisson design by using modified undrained shear strength values, based on results from laboratory tests such as cyclic triaxial and cyclic direct simple shear tests, to replace the standard undrained shear strength values in LEM, PLA or numerical analysis methods. Andersen (2009) provides design charts for cyclic undrained shear strength, based on cyclic direct simple shear (DSS) tests performed on Drammen clay (Figure 3.1). The laboratory defined cyclic undrained shear strength (DSS) charts report strengths corresponding to failure at defined number of cycles, it does not explicitly address other behaviors resulting from cyclic loading of suction caissons such as change in stiffness, pore pressure response and effect on subsequent monotonic loading.

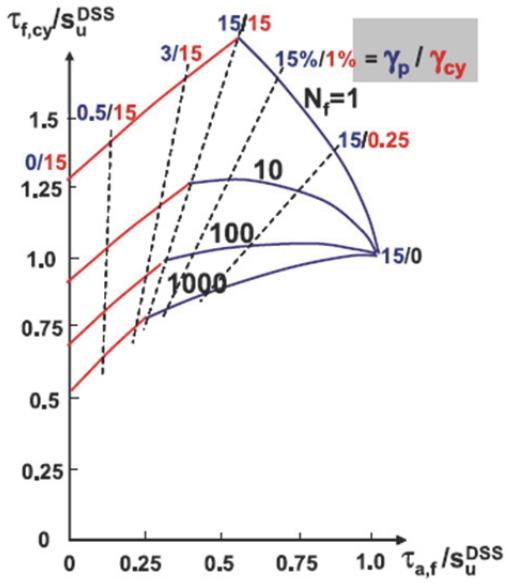

Figure 3.1. Cyclic undrained shear strength as related to average shear stress at failure, monotonic undrained shear strength and number of cycles to failure (from Andersen 2009).

The purpose of the cyclic tests was to observe the effects of cyclic load magnitude on ultimate capacity. Single line cyclic tests performed were monitored throughout the cyclic loading and subsequently loaded monotonically to failure to determine the effect of the cyclic pre-loading on the peak monotonic inclined load resistance of the caisson for comparison to the predicted capacities of conventional recommended practice and baseline single line monotonic test results.

Single line cyclic tests were performed with selected combinations of high and low mean line loads (P_{mean}) with high and low cyclic load amplitudes (P_{amp}) about P_{mean} as a simplification of the numerous cyclic conditions that might be expected in true offshore conditions. Load magnitudes and amplitudes selected were defined as a percentage of the peak monotonic single line load resistance ($P_{mn,peak}$). All cyclic tests performed were one-way cyclic only, due to the complexity of the following orthogonal line loading which, due to equipment limitations, would not allow for more representative two-way or partial two way cyclic loading to be performed. Consideration was given to the combination of the ratio of the mean load and cyclic amplitude to

the monotonic maximum resistance, i.e., $P_{mean}/P_{mn,peak}$ and $P_{amp}/P_{mn,peak}$, which was based on Andersen (2009). Andersen (2009) provides data relating analogous cyclic DSS parameters γ_{ave}/s_u (where average shear strain, γ_{ave}, is normalized by undrained shear strength, s_u) and γ_{cy}/s_u (where γ_{cy} is cyclic shear strain amplitude) to the number of cycles required to reach failure for direct simple shear (DSS) tests. While the failure mechanism in the DSS test is not the same as for a suction caisson, $s_{u\text{-}DSS}$, is the basis for suction caisson capacity estimation using recommended practices. Results from Andersen (2009) were extended to the selection of P_{mean} and P_{amp} values in this testing program. Using guidance from Figure 3.1, P_{mean} and P_{amp} values were selected so that failure would not be anticipated within the 60 minute cyclic load period (equivalent to 2.6 years at 150 g, as subsequently discussed). Research by Chen and Randolph (2007) was also considered in the selection of P_{mean} and P_{amp}. Chen and Randolph (2007) report that maximum one-way cyclic load resistance (against vertical uplift) is reached when the maximum cyclic load ($P_{cy,max} = P_{amp} + P_{mean}$) exceeds 72% $P_{mn,peak}$, for suction caissons with L/D = 4. Values of P_{mean} and P_{amp} selected for model suction testing are summarized in Table 3.1.

Table 3.1. Summary of cyclic load parameters in suction caisson load tests.

	TARGET LOAD	
LOAD COMBINATION TYPE	$\mathbf{P_{mean}}/ P_{peak}$	$\mathbf{P_{amp}}/ P_{peak}$
Low Mean Low Amplitude (LMLA)	0.35	0.15
Low Mean High Amplitude (LMHA)	0.35	0.25
High Mean Low Amplitude (HMLA)	0.55	0.15

It was anticipated that the failure of the suction caisson during cyclic loading will not be induced by any of the load combinations (P_{amp} and P_{mean}) selected, based on previous laboratory and physical modelling results (Andersen 2009). If cyclic failure is not induced, the critical level of repeated loading is not achieved, therefore a strain and pore pressure equilibrium condition is expected to occur similar to that occurring during triaxial and direct simple shear tests (Sangrey 1969; Zergoun 1974; Matsui et al. 1980; Lefebvre & LeBoeuf 1989). Therefore, the result of the

cyclic loading on caissons is anticipated to be similar to the results of cyclic triaxial tests where over consolidated conditions are created (Matsui et al. 1980; Yasuhara et al. 1992; Dutt et al. 1992), and strength at failure is increased in comparison to the monotonic test.

3.1.3. Multi-line Tests

Multi-line tests are the critical component of this testing program as multi-line loaded suction caissons are proposed here as an economical anchor solution for floating platforms. Performance evaluations of suction caissons loaded in two orthogonal directions are based on strength and deformation. Key issues to be addressed through these tests are:

1. Evaluation of the performance of multi-line loaded suction caissons in comparison to the performance of single line loaded suction caissons,
2. Investigation of load parameters that affect performance of the multi-line loaded suction caissons.

In this program, multi-line loading is represented by two orthogonal loads. Selection of two orthogonal load directions to model the multi-directional loading is based on the concept of force vector resolution (from basic statics and dynamics) in that any configuration of directional loading on a given caisson can be resolved into orthogonal components (Figure 3.2).

The LEM (DNV 2005) identifies certain regions of soil adjacent to the caisson which provide resistance against applied inclined loads (Figure 2.4), referred to herein as the ‘zone of influence’. This zone of influence is an idealization of the soil volume contributing to the caisson resistance to load, thus the conditions within this volume (strength, hydraulic conductivity, stiffness, etc.) are considered to control the caisson load resistance. The size of the zone of influence is determined by the size of the caisson and the soil parameters, while the *orientation of the zone of influence is determined by the direction of the line load*. Theoretically, if a caisson is loaded in a single, constant direction, the zone of influence extends from the caisson parallel to that direction (Figure 3.3a). Extending this concept and assuming a caisson is loaded sequentially

by two orthogonal lines where a load is first applied in one direction then released and then a load is applied and released in the orthogonal direction, two zones of influence would exist, each parallel to a respective loading direction and perpendicular to one another (Figure 3.3b). Therefore, sequential loading and unloading with multiple lines in multiple directions conceptually results in multiple zones of influence being invoked.

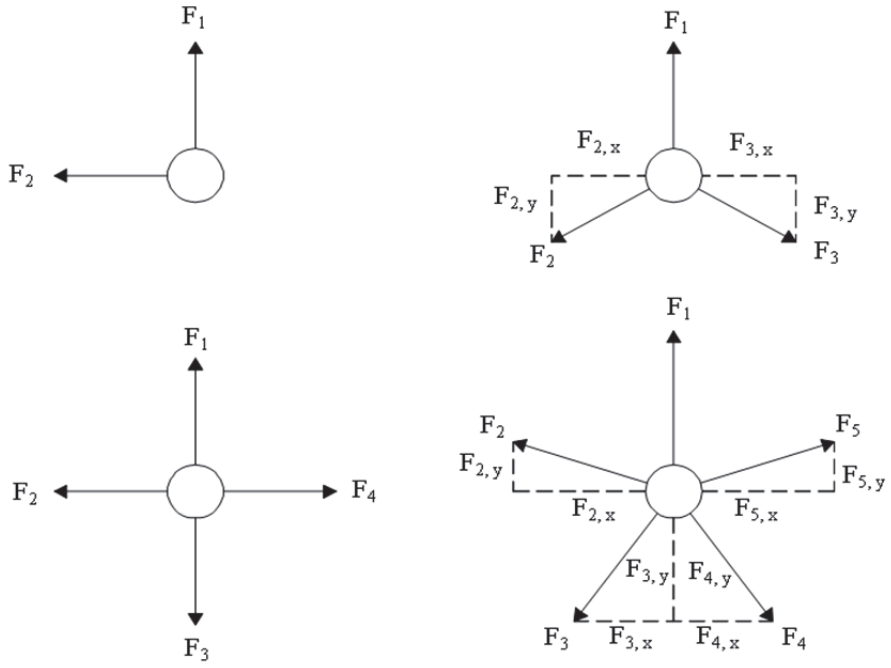

Figure 3.2. Schematic of multi-directional forces resolved to orthogonal x - y force vectors.

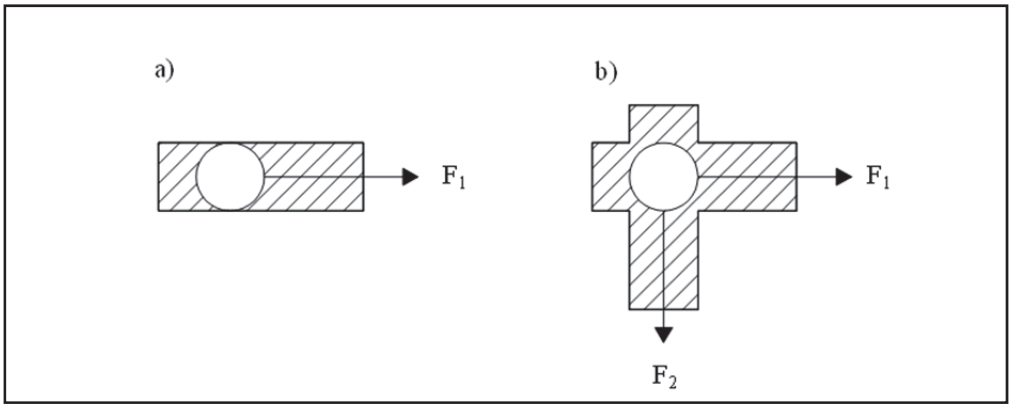

Figure 3.3. Zones of influence resulting from two load configurations.
a) single load; b) two orthogonal loads.

If, instead of sequential orthogonal loading the caisson was subjected to concurrent orthogonal loading, theoretically, the net effect (vector summation) of the two orthogonal loads would control the suction caisson response. Considering two instantaneously applied constant magnitude orthogonal loads, the zone of influence of the caisson would simply be equal to the soil volume contributing to the resistance mechanism for the resultant load (vector summation) of the two orthogonal loads. Similarly, if the orthogonal loads were each applied at equal rates (as a percentage of the final load per unit time) the direction of the resultant would be constant, invoking the same zone of influence as if both loads had been applied instantaneously.

However, instantaneous application or precisely equal rates of orthogonal loading are unrealistic for numerous reasons including out of phase loading, asymmetrical loading, and loadings with different frequencies. Consideration of orthogonal loads applied in more practical conditions (such as applying and sustaining load in one direction followed by applying and sustaining load in a second direction) reveals the *load resultant changing directions throughout the loading progression*. The effect of this is a progressively changing zone of influence, and a greater total volume of soil which has contributed to the resistance mechanism. The resulting effect of this enlarged zone of influence on the resistance capacity and behavior of the suction caisson is investigated through the orthogonal loading components of this program.

The point of application of the load resultant is the centroid of the circular caisson, and as the direction of the resultant load continues to vary throughout the cyclic loading progression, the resultant load vector can be visualized as 'sweeping' through a range of angular orientations (Figure 3.4). The range of angular orientations achieved by the resultant, of the two applied cyclic load progressions, is herein referred to as the *sweep angle* (ω_{sweep}). The importance of ω_{sweep} is the area / volume of soil participating within the zone of influence throughout the cycling of the orthogonal loads. A single cyclic line load (represented with a sweep angle = 0 °) would invoke a zone of influence consisting of a certain volume of soil. The resultant load vector of multiple cyclic line loads having a ω_{sweep} greater than zero could be envisioned to invoke a larger

'cumulative' zone of influence, as the orientation of the resultant load changes and the soil area volume participating in the zone of influence changes in response.

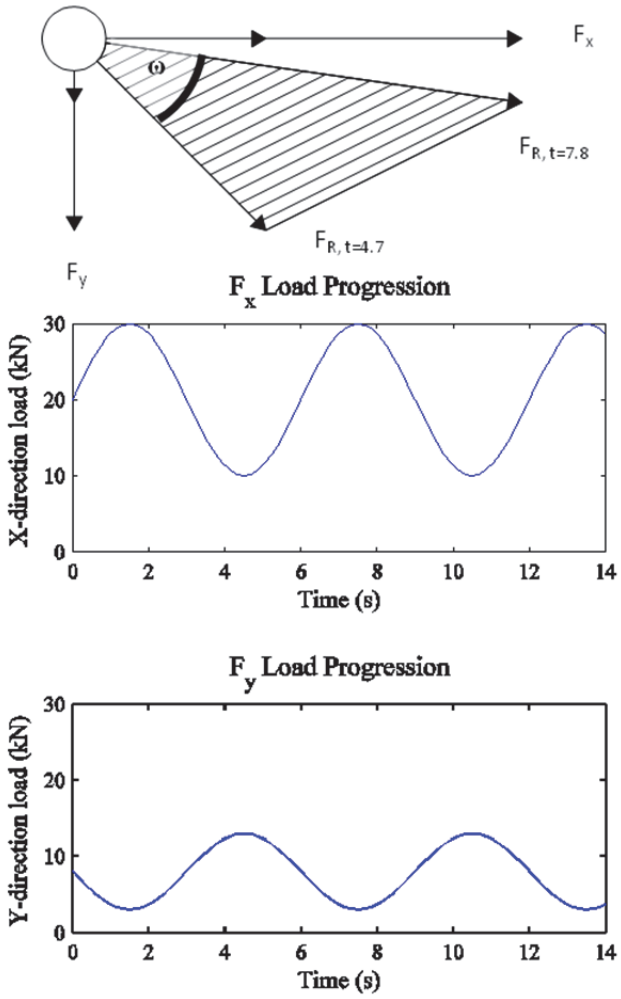

Figure 3.4. Resultant sweep angle (ω_{sweep}) and loads (P_{res}) due to combined effect of 180° phase offset sinusoidal wave loads.

Sweep angle of the resultant load vector is controlled by the ratio of the perpendicular loads. In terms of practical consideration of marine loading, the variation of perpendicular load ratios may be controlled by the varying the mean load and load amplitude of the applied cyclic loading. A limited number of load amplitude and mean load magnitudes and combinations were selected for these initial tests. The intended cyclic load parameter values for the multi-line cyclic tests are the same as for the single line cyclic tests and are provided in Table 3.1. A visualization

of the sweep angles resulting from selected load combinations of sustained, cyclic and monotonic loads in orthogonal directions with varied mean loads, load amplitudes and phase modulations is shown in Figure 3.5.

A codified test name was assigned to each test performed based on sample number, test number, line number(s) and associated load types. The values used in the test naming code are explained in Table 3.2. A summary of the intended tests and the manipulated variables is provided in Table 3.3.

Table 3.2. Explanation of test code naming.

Generic Test Code: S[X] – T[X] □[XX] – [XX] / L[XX] – [XX]		
Code	Explanation	
	Object	Variations
S[X]	Sample number	1, 2
T[X]	Test number	1 – n
L[XX]	Line number	Blank for single line, 1, 2
[XX]	Type of loading	S: sustained M: monotonic C: cyclic

Table 3.3. Summary of parameters tested in suction caisson load tests.

CAT.	Test Name	Test Parameters
Monotonic	S1-T01 -L-M	(equipment problems - results omitted)
	S1-T02 -L-M	baseline - partial consolidation
	S1-T04 -L-M	baseline - full consolidation
	S2-T12 -L1-S / L2-M	resultant sweep angle
Cyclic 1 LMLA	S1-T03 -L-C	low mean low amplitude cyclic preload
	S2-T06 -L1-C / L2-SM	sweep angle: sus low mean & low mean low amplitude
	S2-T08 -L1-C / L2-CM	sweep angle: off phase low mean low amplitude
Cyclic 2 LMHA	S1-T05 -L-C	low mean high amplitude cyclic preload
	S2-T07 -L1-C / L2-SM	sweep angle: sus low mean & low mean high amplitude
	S2-T09 -L1-C / L2-CM	sweep angle: off phase low mean high amplitude
Cyclic 3 HMLA	S2-T13 -L-C	high mean low amplitude cyclic preload
	S2-T11 -L1-C / L2-SM	sweep angle: sus high mean & low mean low amplitude
	S2-T10 -L1-C / L2-CM	sweep angle: off phase high mean low amplitude

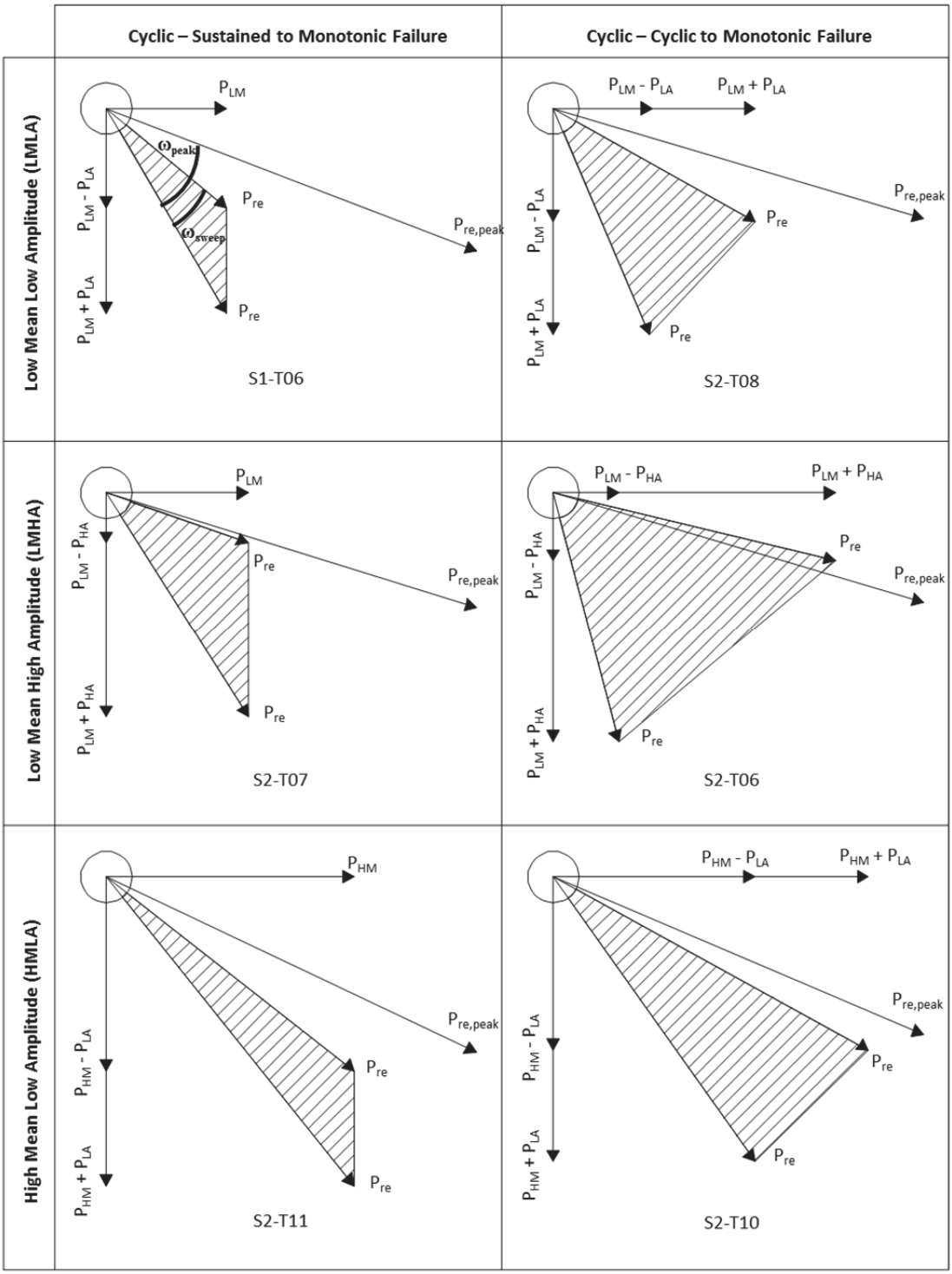

Figure 3.5. Sweep angle of resultant load for multi-directional load cases.
(where P is load and the subscripts LM, HM, LA, HA indicate low mean, high mean, low amplitude, and high amplitude, respectively, re indicates resultant, and re, peak indicate resultant load at failure)

3.2. Model Caisson

The model caisson dimensions were selected based on potential L/D ratio applicable for geotechnical conditions (especially shallow depth to bedrock) at the University of Maine Deepwater Offshore Wind Test Site offshore of Monhegan Island in the Gulf of Maine (§1.4). Depth to pad eye was selected based literature related to suction caissons with L/D = 2 and the DNV (2006) recommended practice for determining optimum pad eye position based on an estimated normally consolidated undrained shear strength profile. The model suction caisson was machined from a single piece of aluminum alloy 6601 (E = 70 GPa) and has the physical and geometrical properties summarized in Table 3.4.

Table 3.4. Summary of model caisson details.

Property	Model	Prototype
Length (mm)	50	7500
Diameter (mm)	25	3750
Thickness (mm)	1	150
Mass (kg)	0.021	472.7
L/D	2	2
t/D	0.04	0.04
Pad eye location (mm from base)	20	3000
Cap condition	closed	closed
Mooring line dia. (mm)	0.8	120

The top cap of the suction caisson had a 5 mm diameter vent plug/port for the pore pressure transducer, vent port, a tell-tale inclinometer/ installation guide port, and counterweight (for mass symmetry) (Figure 3.6). The installation guide port enabled the connection of the caisson to the vertical actuator for the in-flight jacking installation of the caisson. The caisson vent plug remained open during the jack-in installation (allowing water flow) and was sealed prior to line loading. The tell-tale inclinometer was used in conjunction with the in-flight cameras to determine the angular rotation of the caisson to the nearest 0.1° in x and y directions. A wired pore pressure transducer (PPT) was inserted through the port for in-flight measurement of internal pore pressure below the top cap. The PPT wire was tied to the vertical actuator support so as not

to create an unbalanced load during flight. External pore pressure accumulated during loading was of interest to the program, however, due to equipment limitations, internal pore pressure was measured and provided a basis for inference of internal pore volume change potentially caused by vertical uplift.

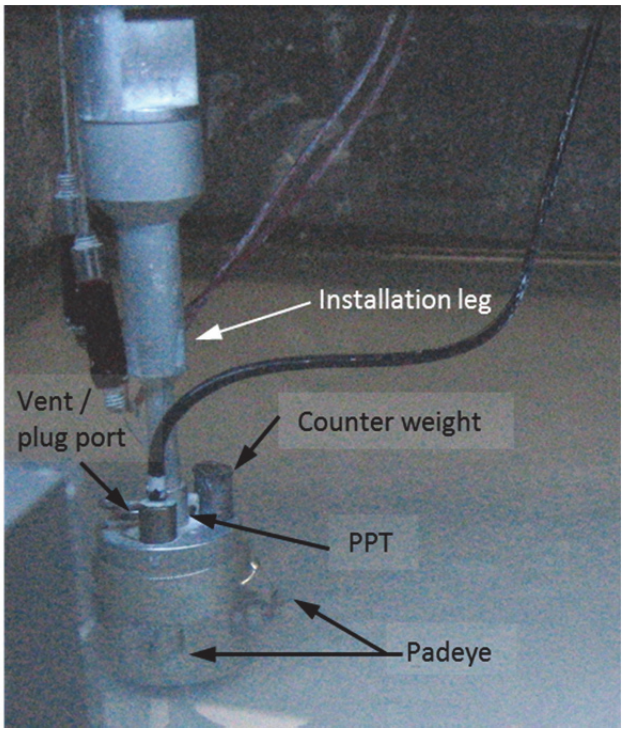

Figure 3.6. Photograph of suction caisson model components

Four pad eyes, manufactured from aluminum alloy 6061-T6, were adhered symmetrically around the caisson body by an epoxy adhesive. The tensile strength of the 2-part epoxy is 43 MPa; the tensile bond strength of the epoxy is 11-15 MPa at 0 °C. With the dimensions of the pad eye attachment surface, the expected capacity of the bond is 1.1 – 1.5 kN. The bond strength was tested to exceed 1.3 kN, sufficient for the anticipated caisson loading and factor of safety.

The mooring line used in the model testing is a low-stretch braided nylon fishing line with a maximum capacity of 24 kg (235 N).

3.3. Instrumentation and Test Setup

Equipment mounted on the soil model strongbox (internal dimensions: 390 mm width by 650 mm length and 325 mm height) included:

- Crossbeams to supporting actuators and loading equipment;
- 2 actuator-driven loading devices (6 kN capacity, 3 mm/s maximum speed) to perform ball penetrometer tests, vertically install the caisson, and load anchor by mooring lines via the pulley setup;
- Pulleys (attached to base plates of the actuators);
- in-flight test monitoring cameras and lighting;
- a subterranean oil-impregnated multi-pressure instrument (STOMPI)- to measure pore pressures within the soil sample (for consolidation / rebound information);
- water feed lines (to maintain constant pressure head throughout a given test).

The two (2) actuators are driven by 24V DC (electrical) servo-motors with two degrees of freedom – vertical and horizontal displacement (and loading). For these tests, only the vertical drive was used for loading. Use of the horizontal drive was limited to positioning between successive tests and test segments. The physical vertical loading capability of each actuator was 6.5 kN and the physical maximum drive speed was 3 mm/s. Each actuator is controlled through data-logging software with theoretical resolution of 0.001 mm/s, although the speed of the data communications for control and monitoring which varies with system performance tends to be the limiting factor

The video monitoring system consisted of an in-flight camera used to monitor the operations of the entire centrifuge, and two test cameras used to monitor the progress of individual caisson installations and caisson loading tests within the soil model. The test cameras were used to obtain test videos, which were post processed with grid analysis program to

determine caisson rotation during caisson loading tests. Caisson rotations about two axes were analysed (Figure 3.7).

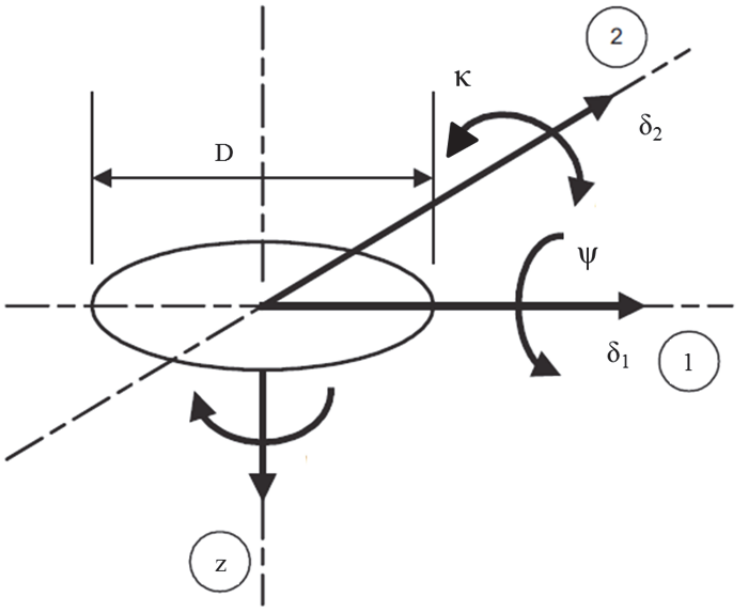

Figure 3.7. Rotation and displacement definitions for suction caisson movement (after Bienen et al. 2006).

Additional instruments used for determination of soil model s_u profile included 'S-type' load cell and ball penetrometer. The S-type load cell was connected inline between the vertical actuator drive shaft and the penetrometer ball attachment (Figure 3.8). The range of the S-type load cell was 180 N with a resolution of 0.01 N. Calibration of the S-type load cell was performed immediately prior to testing. The ball penetrometer attachment consists of a sphere attached to the end of an instrumented shaft, which allows determination of continuous bearing resistance profile during penetration. The ball penetrometer replaced use of the T-bar penetrometer after the first three shear profile tests, as the T-Bar was found to be malfunctioning. The ball penetrometer had a diameter of 15mm.

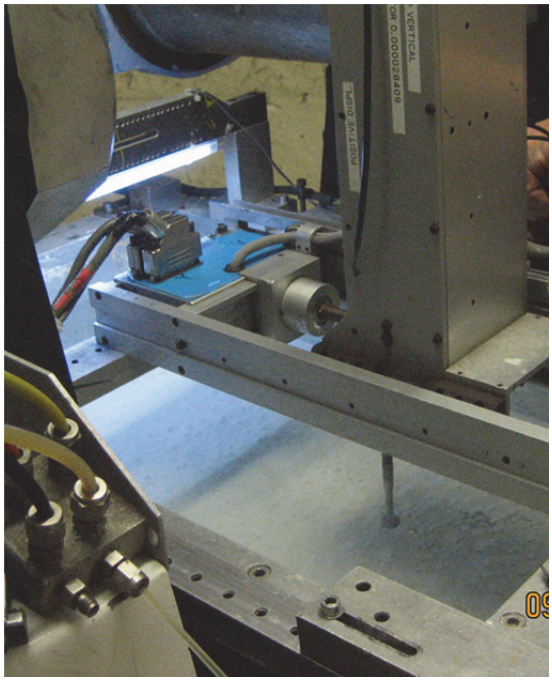

Figure 3.8. Ball penetrometer setup for soil model shear profile testing.

In addition to the actuators and camera systems, instrumentation for the line-load assembly included two column load cells and a pore pressure transducer. The column load cells were connected 'mid-line' along the low stretch braided nylon fishing 'mooring' line (Figure 3.9). Column load cells were positioned along the mooring line such that the load cell would not be penetrated into the clay sample on installation of the caisson, the load cell would be offset from the zone of influence of the caisson during centrifuge spin up, and the load cell would remain underwater throughout caisson loading (Figure 3.9). The capacity of each column load cell was 500 N, the resolution was 0.05 N. Calibration of the column load cells was performed immediately prior to testing. A miniature pore pressure transducer was attached at the underside of the caisson top cap (Figure 3.9). A vertical post extension was also attached to the caisson top cap to facilitate post-processing of caisson rotation using grid analysis on test videos.

For the line loading test setup, vertical actuators were located so the distance between center of caisson and pulley contact is 200 mm (horizontal offset) for both orthogonal loading directions. The setup is as illustrated in Figure 3.10 and Figure 3.11. The intended loading angle

of each mooring line was 45° ± 2° from horizontal, where the angle of loading varied in between tests due to specific caisson penetration depth and during tests due to horizontal and vertical caisson displacement and caisson rotation.

All tests were performed at the beam centrifuge facility at the Centre for Offshore Foundation Systems (COFS) at University of Western Australia, Perth, WA. The beam centrifuge used for the tests is an Accutronic 661 (France), with a 1.8 m radius and 40 giga-tonne payload capacity. More details about the facility are available from Randolph et al. (1991). The centrifuge is housed in a 20.5 deg C temperature controlled room. Visual monitoring of the centrifuge operations was enabled by cameras mounted in the centrifuge and monitoring of the sample/testing activities was enabled by cameras mounted on the soil model strongbox. Electrical actuators and data acquisition systems to control and monitor testing functions were operated from the separate control room.

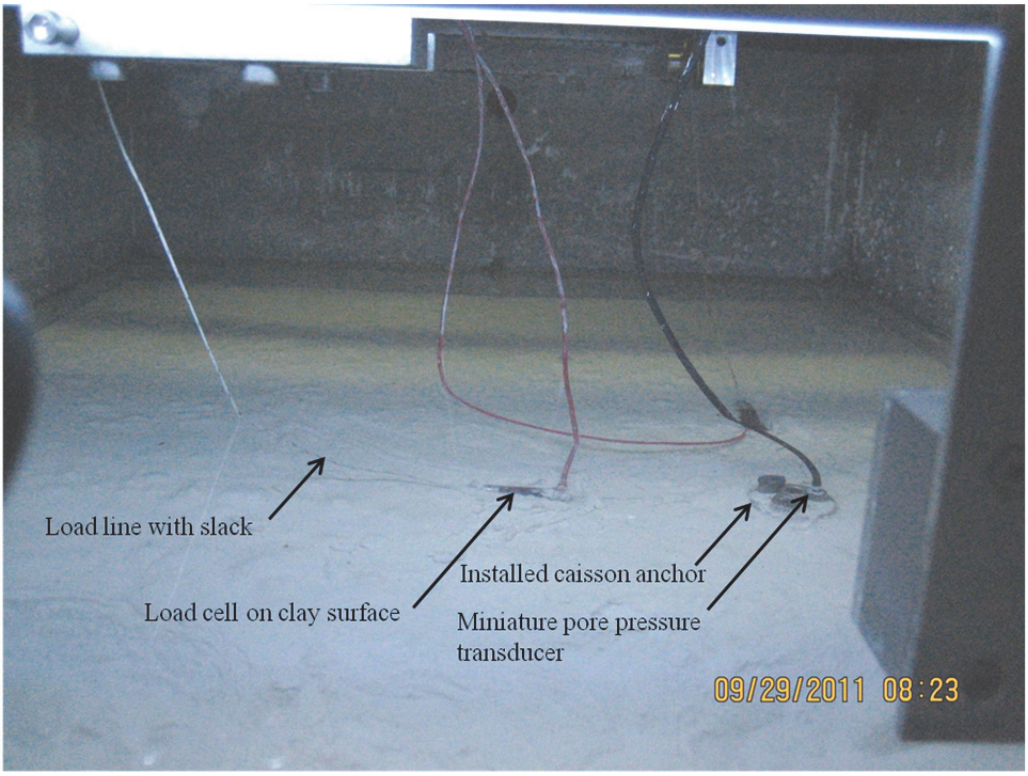

Figure 3.9. Setup for suction caisson line loading.

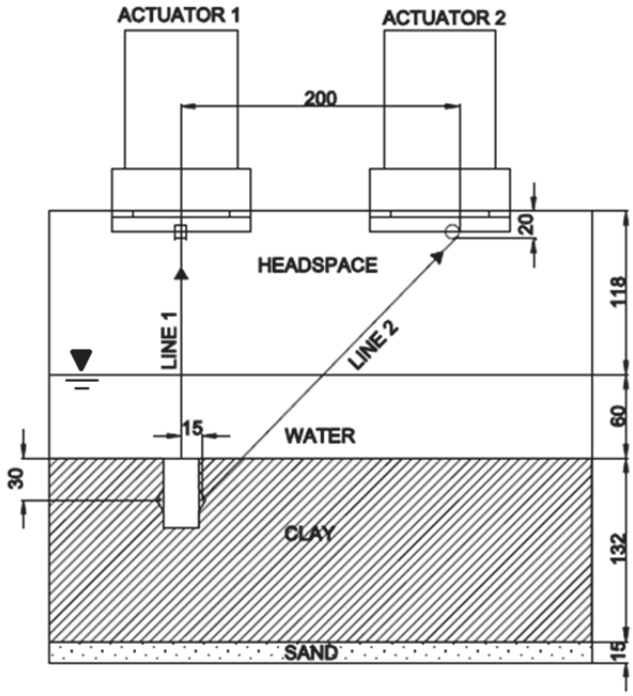

Figure 3.10. Schematic of test setup for caisson multi-directional load resistance tests. (dimensions shown in millimeters)

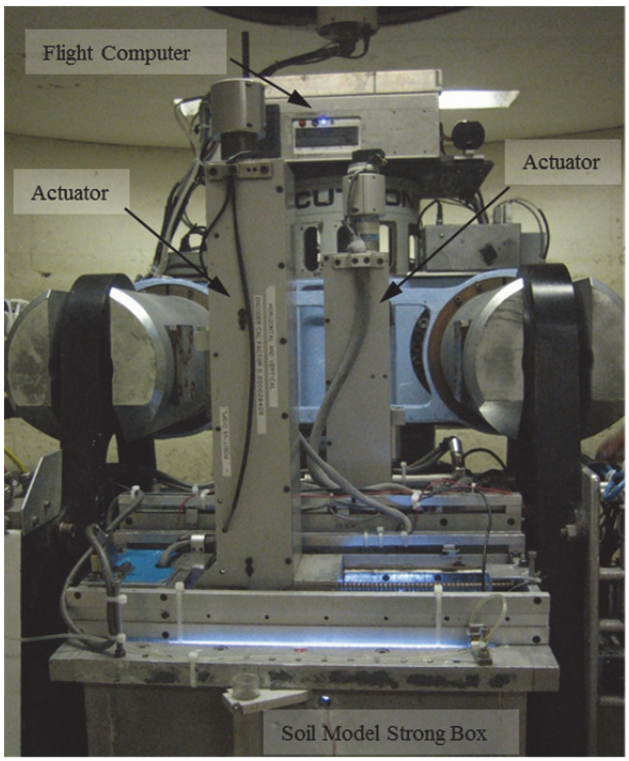

Figure 3.11. Photograph of test setup for caisson multi-directional load resistance tests.

3.4. Soil Model

Manufactured kaolin clay was selected as it has well documented, consistent properties, which allows for better results interpretation and comparison with published literature. Some commonly accepted properties of manufactured kaolin are summarized in Table 3.5. One aspect of kaolin beneficial to this study is the high hydraulic conductivity, which limited the time required for sample consolidation and testing. One of the challenges associated with using kaolin clay with marine installation models is that kaolin does not behave like most typical marine clays. kaolin tends to have a higher coefficient of consolidation and permeability and is non-thixotropic (Andersen 2009), where the latter property considerably affects short term strength gain.

The kaolin sample was prepared by rehydrating dry powdered speswhite kaolin (Prestige™ NY) commercially available from Unimin Australia to a slurry with 120% water content by mass (about twice the liquid limit) with regular tap water. The kaolin sample was prepared in an aluminum strong box with internal dimensions of 390 mm width by 650 mm length and 325 mm height. A single lift measuring 0.260 m thickness was placed over saturated filter paper and 15 mm sand base that provided drainage to the top and bottom of the sample.

Table 3.5. Summary of commonly accepted Kaolin clay properties (after Stewart 1992).

Kaolin Property	**Value**
Liquid Limit, LL (%)	61
Plastic Limit, PL (%)	27
Plasticity Index, PI (%)	34
Specific Gravity, G_s	2.6
Angle of Internal Friction, ϕ (degrees)	23
Consolidation Coefficient, c_v (m^2/yr.)	2
Submerged Unit Weight, γ' (kN/m^3)	5.82
Sensitivity (w = 58%) (Cao 2003)	1.3

To create the normally consolidated soil approximating typical conditions for offshore soils at transitional and deep water depths, the kaolin slurry was consolidated by spinning in the centrifuge at 150 g for 3 days. The pore pressure in the soil sample was monitored using the

STOMPI to aid in determining completion of the sample consolidation. The resulting geometry of the soil sample is summarized in Table 3.6 and a schematic diagram of the samples is shown in Figure 3.10. Schematic of test setup for caisson multi-directional load resistance tests..

Table 3.6. Summary of geometry for Sample 1 and Sample 2.

Sample Component	Thickness (mm)
Headspace	118
Free water on clay surface	46 to 73
Clay	132
Sand	15
Total height of strongbox	325

3.5. Test Procedures

Two (2) sample boxes with the soil model created in the same manner were used over the testing period of two (2) weeks. The number of tests performed was limited by the time allotted on the equipment and the capacity for the configuration of the equipment for the unusual, simultaneous, independently controlled, double line loading. Eleven (11) soil model shear strength tests, and thirteen (13) caisson loading tests were performed. Completion times for each caisson test were typically 3-4 hours for monotonic tests and 4-5 hours for cyclic tests. These times include setup, reconfiguration between installation and line loading, reconsolidation and line load testing.

Test procedures were developed to facilitate four types of suction caisson tests:

i) Monotonic baseline tests;

ii) Single line cyclic followed by monotonic inclined load to failure;

iii) Double line cyclic-sustained followed by monotonic inclined load to failure;

iv) Double line cyclic-cyclic followed by monotonic inclined load to failure.

The general testing progression consisted of the configuration of the centrifuge equipment for caisson installation, installation phase (at 150g), modification of the centrifuge equipment setup for the loading phase (at 1g), reconsolidation of the sample (at 150g), and

loading phase (at 150g). Installation setup and execution were essentially the same for all tests with the exception of the number of load lines attached to the caisson. Configuration of the centrifuge equipment setup was dependent on the number of load lines to be used in the test (one or two). Reconsolidation of the sample was limited due to time constraints of the research program, consistency was the target objective.

3.5.1. Test Layout

A total of 11 soil model shear strength profile tests were performed including: eight (8) ball penetrometer tests, and three (3) T-Bar penetrometer tests. Typically a series of three (3) penetrometer tests were performed prior to, and after completion of caisson tests in each soil model. The ball penetrometer tests were located at the center of width of the soil samples and spaced out along the length of the two (2) soil samples (Figure 3.12 and Figure 3.13).

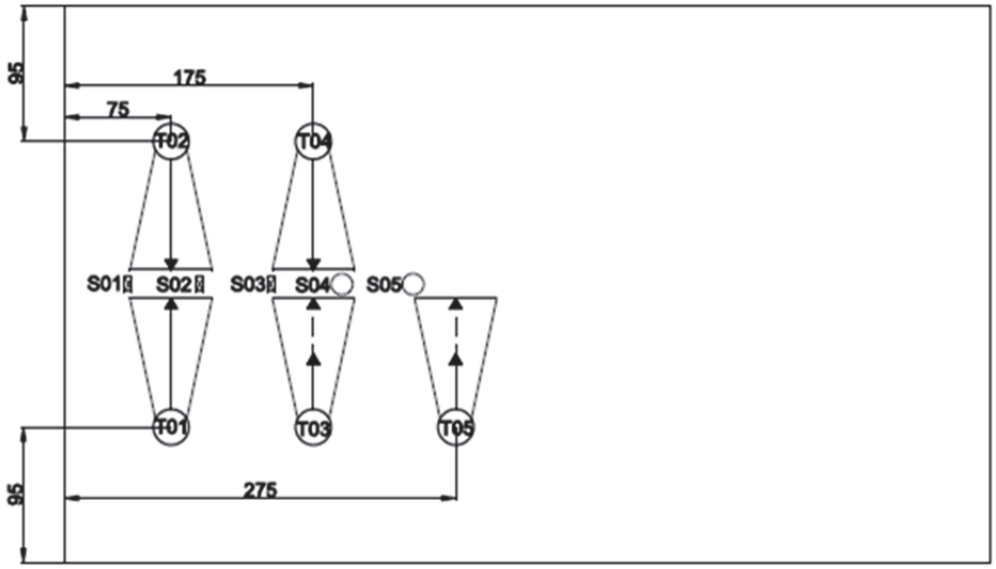

Figure 3.12. Layout of tests performed in test soil model 1 (S1).

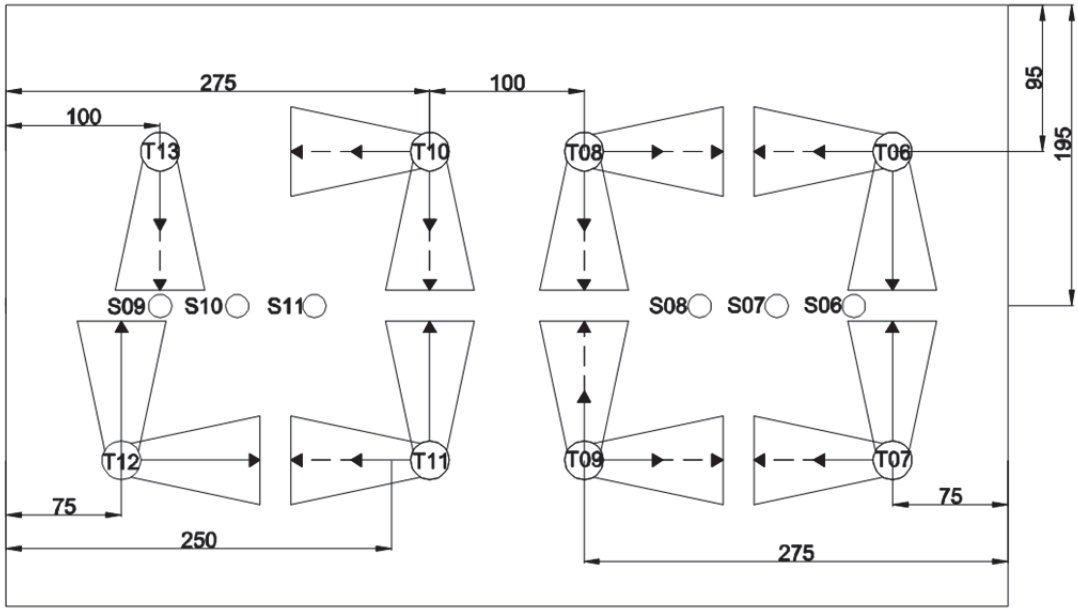

Figure 3.13. Layout of tests performed in soil model two (S2).

Layouts of the caisson loading tests in the two sample boxes were selected to maximize the number of tests that could be performed within schedule limitations and to maintain sufficient offset between tests to limit disturbance effects from adjacent tests. Five (5) tests (S1-T01 to S1-T05) were performed in the first sample box (Figure 3.12). Eight (8) (S2-T06 to S2-T13) tests were performed in the second box (Figure 3.13). A minimum spacing of 4D was maintained to limit interaction between tests (C. Gaudin, personal communications, June 2011) while maximizing the number of test sites available per soil model. Spacing between adjacent test sites were considered for both directions of the perpendicular loading.

3.5.2. Shear Strength of Soil

Shear strength profile through the soil model was measured using ball penetrometer tests performed in-flight at of 150g centrifuge acceleration. Tests were performed prior to and following caisson loading tests in each of the soil model strong boxes (Figure 3.12 and Figure 3.13). The first series of three penetrometer tests in soil model 1 was performed using the T-bar prior to initiation of caisson tests. Post processing of test data indicated problems with T-bar

equipment, thus T-bar results were considered invalid . A second series of two penetrometer tests was performed in soil model 1 using the ball penetrometer following the five soil caisson tests. Prior to commencement of caisson tests in soil model 2, three ball penetrometer tests were performed. Following the eight suction caisson tests conducted in soil model 2, three final ball penetrometer tests were performed. Penetrometer tests were performed at a vertical penetration rate of 1 mm/s. Undrained test conditions were maintained as determined using Equation 3-1 (from Randolph & Hope 2004) resulting in V = 236.

$$V = \frac{vd}{c_h} \qquad [3\text{-}1]$$

where: $V > 30$: for undrained condition
v = penetration rate;
d = penetrometer diameter;
c_h = coefficient of horizontal consolidation.

3.5.3. Model Caisson Installation

Prototype suction caissons are typically installed in the field, by a combination of self-weight and underpressure. Initially, the suction caisson is allowed to penetrate into the seabed under its own weight, then 'suction' is applied to the internal cavity of a suction caisson, to create an underpressure for completion of the installation to design depth. For this investigation, jacking installation of the caisson was selected for simplicity, small size of caisson and focus of testing on relative capacity/behavior of multi-line loading.

For the jacking installation at each test site, the model caisson was manually located over each test site and submerged with the tip slightly above clay surface (approximated visually) prior to centrifuge acceleration. After the centrifuge had reached the design acceleration of 150g and was balanced, the suction caisson was installed by jacking at a constant rate of penetration of 0.1 mm/s, which was controlled by a vertical motor-actuator. Vertical load and vertical displacement were measured, monitored and recorded during caisson installation. The installation penetration continued until the underside of caisson cap came in contact with surface of sample, as identified

by sudden increase in resistance/pore pressure and visual observation (real-time visual camera feed) of clay material exiting top of caisson through vent port.

Performance differences between suction caissons that are installed using various different methods are described by Luke (2003), who reports based on 1g tests, that the side shear component of load resistance is greater when using deadweight installation than for suction caissons using suction installation. Andersen & Jostad (2002) note that excess pore pressures developed during installation are greater for the self weight installation component or driving installation of caissons , due to the greater lateral effective stress and friction created along the outside of the caisson. Therefore, if installation pore pressures are allowed to dissipate prior to loading, the results of this testing program are anticipated to indicate higher load resistance than for suction installed caissons.

3.5.4. Line Load Setup and Reconsolidation

The centrifuge was spun down to 1g between the installation phase and the line loading phase due to the need to rearrange test equipment mounted on the sample box for this stage. This included removal of the rigid connection between vertical actuator and suction caisson, and setup of the two vertical actuators and pulleys for line loading. Based on results from unload-reload triaxial tests on kaolin clay (radial strain prevented) showing that lateral earth pressure returned to the same value after each unload-reload cycle, it was concluded that centrifuge spin down and spin up between installation and loading of the model caisson did not significantly affect lateral stresses in the soil model (Jeanjean et al. 2006).

For the line load setup, the mooring lines (already attached to the pad eye at the caisson) were connected to the vertical actuators through the pulleys (oriented parallel to direction of the line load) on the base plate of the actuators. Sufficient slack in the lines was allowed so that the load cell on each of the load lines was supported on the surface of the clay as shown in Figure

3.9. This amount of slack was maintained so that the load cells did not put load on the caisson during the spin up and sample reconsolidation.

Following this equipment setup, the centrifuge was spun up to 150g and a delay time equal to the 1g setup time plus 15 minutes was allowed before line loading commenced. This allowed for soil reconsolidation to negate the rebound that occurred during the time spent at 1g following spin down (Levy et al. 2007) and to allow for dissipation of the excess pore pressures accumulated during installation (Chen & Randolph 2007). Kaolin, unlike most marine clay, is a non-thixotropic clay (Andersen & Jostad, 2002) and requires pore pressure dissipation for increase in strength. Alternatively, thixotropic clays increase in strength without complete pore pressure dissipation. An example of this is Gulf of Mexico clays, which are considered to achieve full scale setup in 100 prototype days (Jeanjean, 2006).

The time required for complete dissipation of installation pore pressures is dependent on the method of installation and the soil properties. The excess pore pressures generated during suction installation tends to be significantly less than those generated during self-weight or driven installations. The jacking installation of the model caisson is akin to the driving type of installation, where the pore pressure dissipation with time can be estimated based on the coefficient of horizontal consolidation, the "equivalent diameter" of the caisson and the dimensionless time factor.

Using Figure 3.14 and Equation 3-2 (Randolph and Gourvenec 2011) the time to 99% pore pressure dissipation for the model caisson (jacked installation) was calculated as 11.25 prototype years or 263 model scale minutes. It was determined to be non-optimal for the schedule of the investigation program to allow time for 99% pore pressure dissipation for each installation. The effect of percentage installation pore pressure dissipation on caisson capacity was investigated by performing monotonic single line tests with varied elapsed times post-installation, as previously noted in § 3.1.1. The intended percentage pore pressure dissipation for each test was approximately 45% (15 minutes model scale time) for test schedule purposes.

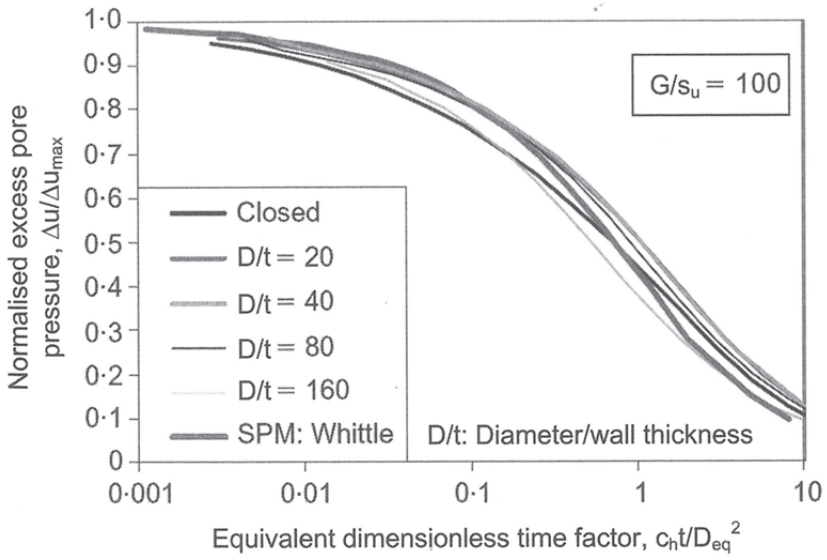

Figure 3.14. Dissipation of pile installation induced pore pressures with time (from Randolph & Gourvenec 2011).

$$T_{90} = c_h t_{90} / D_{eq}^2 \approx 10 \qquad [3\text{-}2]$$

where: T_{90} = Equivalent dimensionless time factor
c_h = coefficient of horizontal consolidation
D_{eq} = equivalent diameter ($D_{eq} = 2\sqrt{(D\ t)}$)

3.5.5. Loading

The line load program was initiated after the reconsolidation period was completed. Line loads were applied using vertical actuators that were digitally monitored and controlled using UWA developed LabView software. The monitoring systems performed control-feedback loops for line loads, pore pressure, and line displacement at 10Hz (resulting in 10 readings/second recorded data). Real time results were displayed graphically and numerically on the test monitoring screens inside the centrifuge control room during testing. Video surveillance of the testing was also displayed and recorded during the testing for monitoring and post-processing of caisson rotation.

Monotonic line load application was displacement controlled at 0.1 mm/s. The rate of testing was selected to maintain undrained conditions (see §3.4.1 , Eq. 3-1), to remain within the capabilities of the equipment (max 3 mm/s), and to be consistent with the loading rates used in

other research programs for comparison. Cyclic line loads parameters such as frequency, P_{mean} and P_{amp} were user selected. Ideal frequency of loading would be the centrifuge scale equivalent of actual offshore loading frequencies. Typical operating conditions in the Gulf of Maine have load period of 10 sec/cycle in prototype scale which would be 0.0677 sec/cycle or 15 Hz at 150g acceleration. The resolution and maximum rate of motion of the actuators was insufficient to achieve these loading rates, thus a loading frequency was selected based on the equipment limitation of 3 mm/s. In the first cyclic load test, 0.5 Hz was selected for load frequency, however the sinusoidal load progression was not adequately maintained to an appropriate resolution by the equipment. The frequency of 0.15 Hz,10% of the equivalent field scale loading, was used to improve load control for the remaining tests, while maintaining the undrained condition.

Three cyclic test categories combining high/low amplitude with high/low mean load used are summarized in §3.2.2 and Table 3.3. The digital control system was pre-programmed with the intended cyclic load parameters (mean load and load amplitude) prior to test initiation. For single line tests, the line-load progression for the full test was pre-programmed into the load control software prior to the start of the test, limiting the required user interaction during the tests. For the more complex double line tests, the loading progressions were programmed as series of loading programs that required the user to upload, start and finish two different loading progression programs for a single test. A summary of the test progressions is provided in Table 3.7 and illustrated in Figure 3.15. Digital override controls were also used during testing if the pre-programmed goal loads were not sufficiently attained.

Table 3.7. Summary of caisson load progressions for various test types.

		Test Step Sequence				
		Initial Loading		**Long Term Loading**		**Failure**
		disp. control		load control		disp. control
		0.1 mm/s rate		cyclic: 0.15 Hz rate		0.1 mm/s rate
Test Type	**Line**	**1**	**2**	**3**	**4**	**5**
Monotonic	L	P_{fail}				
		stop				
Sequential Sustained Monotonic	L1	P_{mean}				
		sustained				
	L2		P_{fail}			
			stop			
1-Line cyclic	L	P_{mean}		P_{mean},P_{amp}		P_{fail}
		sustained		cyclic		stop
2-Line cyclic - sustained	L1	P_{mean}		P_{mean},P_{amp}		
		sustained		cyclic		
	L2		P_{mean}			P_{fail}
			sustained			stop
2-Line cyclic - cyclic	L1	P_{mean}		P_{mean},P_{amp}		
		sustained		cyclic		
	L2		P_{mean}	P_{mean},P_{amp}		P_{fail}
			sustained	cyclic		stop

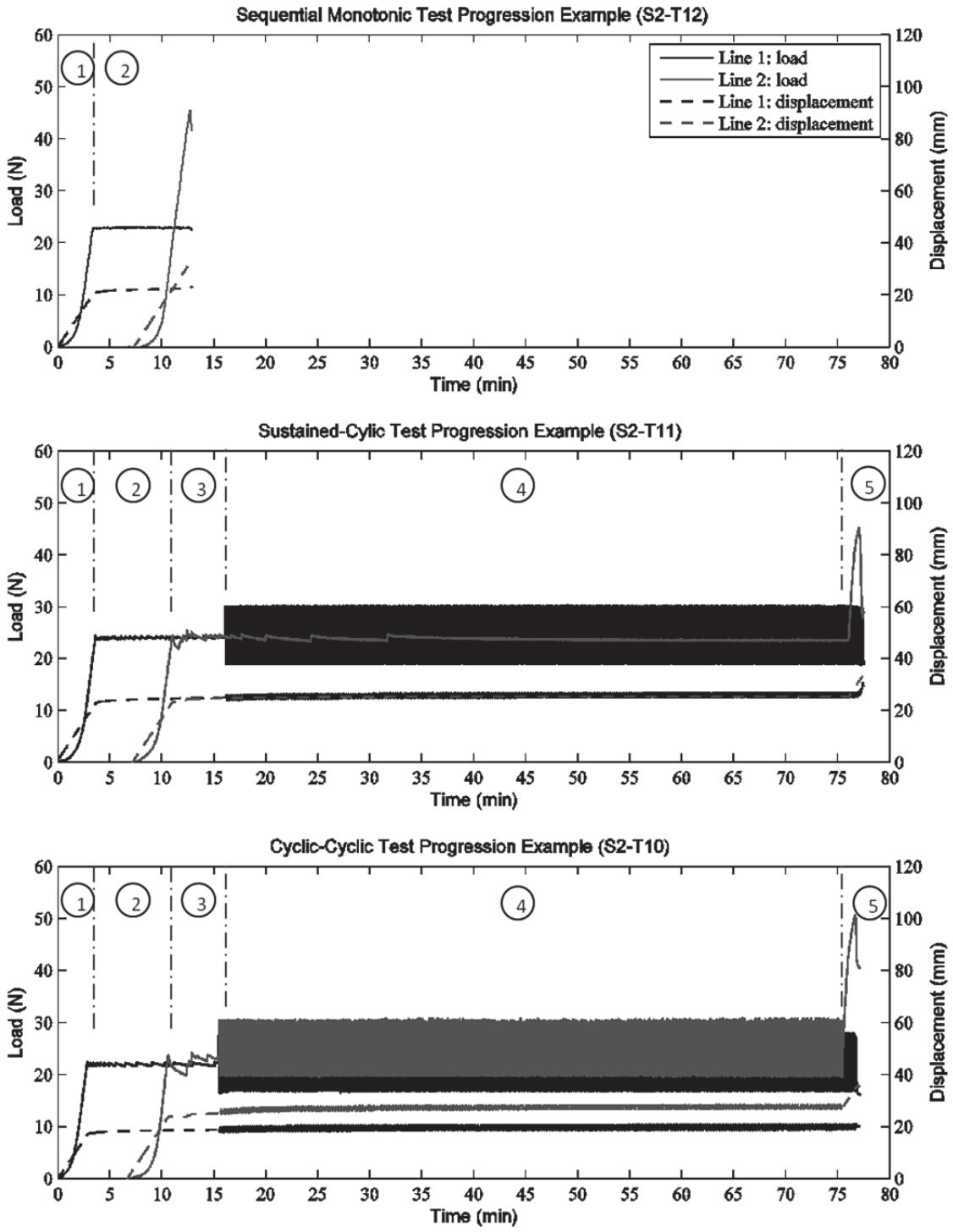

Figure 3.15. Load and displacement progressions for orthogonal load tests.
(circled numbers indicate the loading sequence from Table 3.7)

3.5.6. Baseline Single Monotonic Tests

Two single line monotonic tests were initially intended to be performed. The first test (S1-T01) was not performed satisfactorily due to equipment issues, therefore two more single line monotonic tests were performed (S1-T02 and S1-T04). S1-T02 and S1-T04 were located towards the side of Soil Model 1 (Figure 3.12). The single line load was applied in a direction tangential to the direction of rotation of the centrifuge.

In the single line monotonic tests, the suction caisson was loaded with simple monotonic line load in a single direction until after the peak line load resistance was obtained. The peak line load resistance was interpreted as the failure of the caisson and defined the end of the test. The only variable modified between S1-T02 and S1-T04 was time allowed for reconsolidation and installation pore pressure dissipation between the setup of the line load at 1g and load application.

3.5.7. Baseline Single Cyclic Tests

Three single line cyclic tests were conducted (S1-T03, S1-T05 and S2-T13). The layout of the test sites are shown in Figure 3.12 and Figure 3.13. The estimated percent pore pressure dissipation allowed prior to applying the line loads varied from 0% to 47%. The single line cyclic load was applied from the caisson towards the centerline of the width of the sample, which is tangential to the direction of rotation of the centrifuge. The three loading phases for single line cyclic tests are summarized below and in Table 3.7:

i) monotonic load to P_{mean} at constant displacement rate (see §3.6.4);

ii) cyclic loading at $P_{mean} \pm P_{amp}$ for # cycles

iii) monotonic load to failure following cycling.

3.5.8. Double Line Sustained-Cyclic Tests

Three double line sustained-cyclic tests were performed (S2-T06, S2-T07, S2-T11; Figure 3.13). The range of percent pore pressure dissipation prior to loading was approximately 32% to 42%. For each test, one of the line loads was applied towards the centerline of the width

of the sample (tangential to the direction of rotation of the centrifuge) and the other line load was applied perpendicular to the first (perpendicular to the direction of centrifugal acceleration parallel to the axis of the centrifuge).

The four components of the loading progression are summarized below and in Table 3.7:

i) monotonic load to mean Line 1 to P_{mean} at constant displacement rate (see §3.6.4);

ii) monotonic load to sustained Line 2 to P_{mean} at a constant displacement rate;
(Upon application of the constant loads for both Lines 1 and 2, both loads were sustained and monitored briefly to ensure the loads continued to be maintained.)

iii) cyclic loading Line 1 at P_{amp} for 540 cycles while Line 2 remained at P_{mean};

iv) monotonic load of Line 2 to failure with continued cycling of Line 1.

3.5.9. Double Line Cyclic-Cyclic Tests.

Three double line cyclic-cyclic tests were performed (S2-T08, S2-T09, S2-T10; Figure 3.13). Between the installation of the caisson and the initiation of the line loading the estimated pore pressure dissipation achieved ranged from 54% to 59%. For each test, one of the line loads was applied towards the centerline of the width of the sample (tangential to the direction of rotation of the centrifuge) and the other line load was applied perpendicular to the first (perpendicular to the direction of centrifugal acceleration, parallel to the axis of the centrifuge).

There were five components of the loading progression as summarized below and in Table 3.7:

i) monotonic load to mean Line1 to P_{mean} at constant displacement rate (see §3.6.4);

ii) monotonic load to sustained Line 2 to P_{mean} at a constant displacement rate;
(Upon application of the constant loads for both Lines 1 and 2, both loads were sustained and monitored briefly to ensure the loads continued to be maintained.)

iii) cyclic loading Line 1 at P_{amp} for 540 cycles and 180° phase offset cyclic loading Line 2 at P_{amp} for 540 cycles;

iv) monotonic load of Line 2 to failure with continued cycling of Line 1.

The first phase involved constant rate displacement of line 1 until the mean load for the following (iii) phase was attained, this load was sustained while the line 2 was displaced at a constant rate until mean load for the following (iv) phase was attained. At this point both loads were sustained and monitored briefly to ensure the loads continued to be maintained. The third phase was then initiated with the cyclic load being applied at line 1, with load amplitude and mean load individual to each test. Halfway through the first load cycle on line 1, the cyclic load phase for line 2 was initiated (180 degree phase offset) with load amplitude and mean load individual to each test. After 540 cycles were applied to line 2, line 2 was displaced at a constant rate until failure, while line 1 continued to cycle. The load progressions are summarized in Table 3.7 and illustrated in Figure 3.15.

4. RESULTS AND ANALYSIS

This chapter describes the results of: shear strength profile tests on the two soil models used for centrifuge modeling; monotonic single line tests; three series of single and double orthogonal line cyclic tests as previously described (§3.1)

4.1. Shear Strength Profile

Undrained shear strength profiles were calculated from the measured ball penetrometer resistance force profiles for tests S1-B04, S1-B05, and S2-B06 to S2-B11 (Figure 4.1; Figure 4.2). To resolve the penetration resistance profiles to s_u profiles, a bearing factor N_{ball} = 13.5 (Stewart & Randolph 1994), and 176.7 mm^2 projected area were used. Shear strength profiles were consistent among the three series of penetrometer tests. Average undrained shear strength depth relationships (s_u/z), tabulated in Table 4.1, ranged from 0.88 to 1.04 for the different test series.

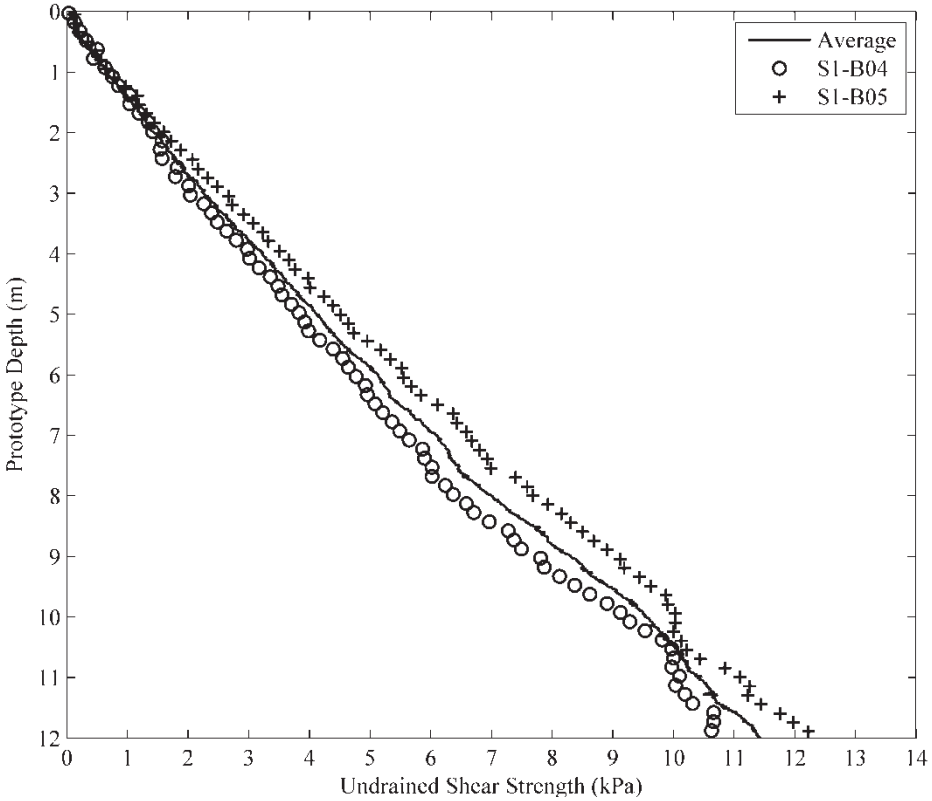

Figure 4.1. Undrained shear strength profile in soils model 1.

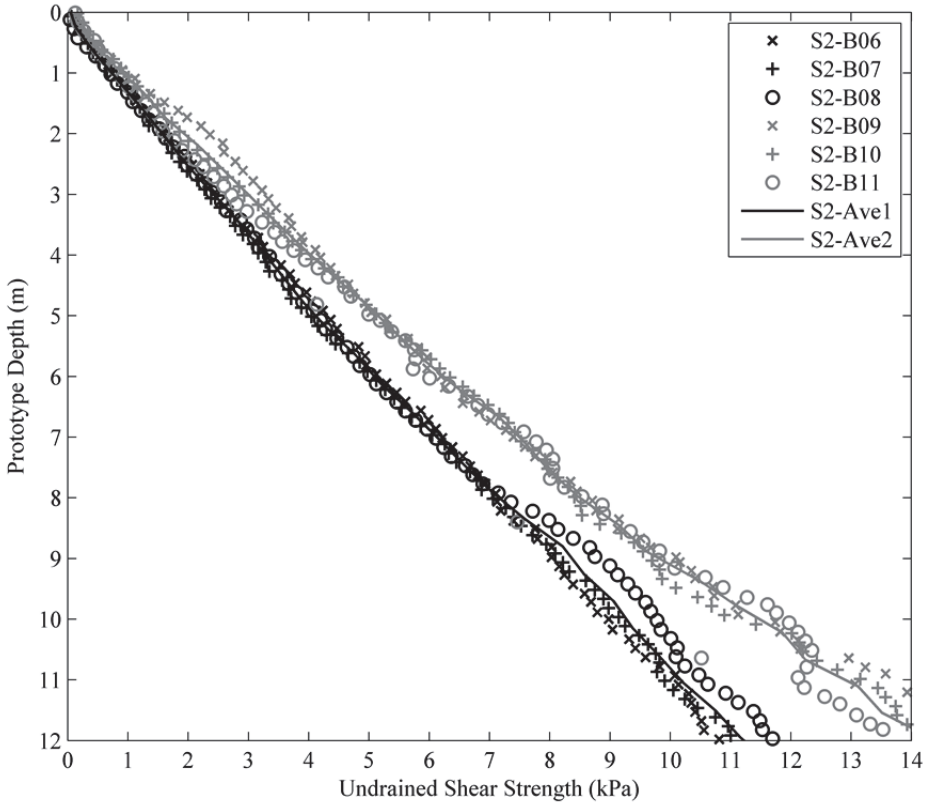

Figure 4.2. Undrained shear strength profile in soil model 2.

Table 4.1. Summary of shear strength tests and results for Soil Models 1 and 2.

Test Numbers	Sequence of Shear Strength Tests	s_u/z	$s_{u,\ z\ =\ 5m}$
S1-B04 to B05	After completion of caisson tests in sample 1	0.92	4.6
S2-B06 to B08	Prior to caisson tests in sample 2	0.88	4.4
S2-B09 to B11	After completion of caisson tests in sample 2	1.04	5.2

4.2. Predicted Single Line Monotonic Behavior

Line load resistance provided by caisson-soil interaction was estimated using Limiting Equilibrium Method (LEM) recommended by DNV RP-303 (DNV 2005; §2.2.4). Applying LEM and using caisson geometry, the measured shear strength profile, typical kaolin properties (Table 3.5), 45° load angle, and estimated internal and external α values (DNV 2005; API 2002), the estimated monotonic single line peak load resistance (normalized by product of undrained shear strength and projected caisson area $s_{u,ave}$ D L) was 9.5N/N (Appendix A). Using the measured shear strength profiles and force-moment equilibrium concepts, optimum pad eye depth below

seabed was calculated as 0.315 L or 16 mm (model scale). The actual position of the pad eye was lower than the estimated optimum position by 8mm (or 16% of the caisson height). As lateral resistance is assumed to be the limiting factor, backwards rotation of the caisson (top rotates opposite to direction of loading) is expected based on the pad eye location below optimum. Additionally, as the line load angle (θ) is 45°, horizontal-vertical resistance interactions were also anticipated.

4.3. Data Collection and Interpretation

Line displacements, line loads, and internal pore pressure (at the caisson cap) were measured and recorded digitally at 10 ms intervals during testing. Rotation of the caisson in the 2 planes of loading (arbitrary designated as the x-z plane for Line 1 and y-z plane for Line 2) was interpreted by post-processing in-flight video recordings of the caisson extension post and using digital grid analysis.

Line load and line displacement data were processed for presentation and comparison using the following interpretations and as illustrated in Figure 4.3. The initial concave upward component of the load – displacement (P-δ) curve resulted from removal of 'slack' from the line and initial 'lifting' of the load cell from the soil surface, prior to the loading of the caisson. This initial curve was considered a test setup artefact and was omitted from the reported results. The second concave upwards component of the P-δ curve was interpreted as a combination of line pulling through the soil model and the initiation of load transfer to the caisson. When the P-δ curve became linear, the applied load was considered to be fully transferred to the caisson. The failure of the caisson is interpreted as the first peak in measured load resistance in each test. Following this, a decrease in load resistance occurred and after substantial caisson displacement, a second peak in P-δ curve occurred. This second peak was a result of backwards caisson rotation and a secondary resistance mechanism which was largely gravitational. The second resistance mechanism is not the focus of the study and is furthermore omitted from the results and analysis.

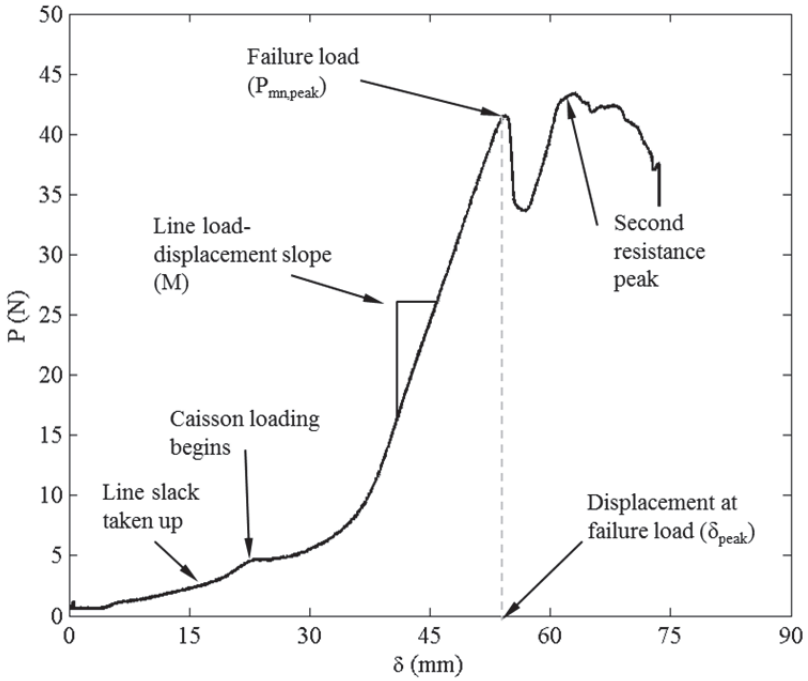

Figure 4.3. Typical line load – displacement progression for monotonic tests.

Reported line loads and displacements for all tests are normalized values for ease of comparison between tests and with literature. The applied line loads are normalized by the product of the undrained shear strength at the depth of the moment centroid of the caisson ($s_{u,2/3L}$) caisson length, L, from caisson top), and the projected side area of the caisson (D L). The displacement is normalized by the caisson diameter (D).

Caisson displacement in the x, y and z directions and load angle (θ) (Figure 4.4) were not measured due to geometric limitations and are not resolvable, as only line displacement (δ) was measured (1 known and 4 unknown variables). Alternatively, a simplifying assumption of constant load angle (45°) was assumed to approximate the x, y and z caisson displacements. Based on measured pre-failure line displacements, maximum error in resolved load magnitude and displacement resulting from the simplifying assumption in the x, y, and z directions is limited to 5%, 2% and 4%, respectively. With respect to the accuracy and resolution of the tests, the error is accepted and $\theta = 45°$ is maintained for further analyses.

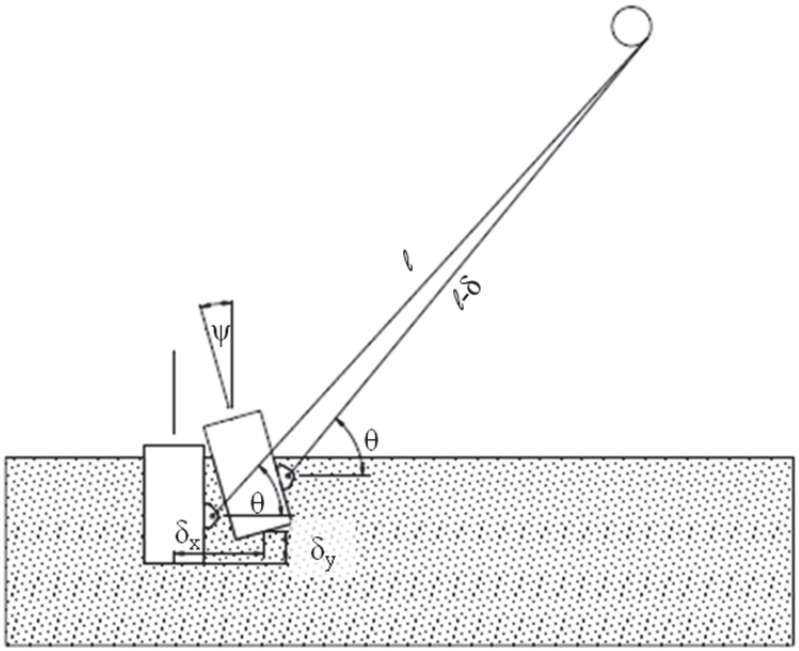

Figure 4.4. Schematic of measured and unknown variables during caisson load tests.

Internal pore pressure (u) data was processed to exclude initial effects of removal of load line slack and lifting of the load cell off the sample surface. Excess pore pressures from installation are not reflected in pore pressure measurements due to the location of the pore pressure transducer at the top of the caisson, vented jacking installation of the model caisson, and a progression of centrifuge spin-down/spin up between installation and loading. Pore pressure corresponding to the interpreted point of initial caisson loading was taken as hydrostatic condition. Due to variations in the depth of water above the saturated soil model between the two soil models and between each test, initial hydrostatic conditions were not the same for all tests. Within a given sample, the water depth varied up to 6 mm between tests, resulting in variation of hydrostatic water pressure up to 9 kPa at 150g. Pore pressure data for each test was normalized by the hydrostatic conditions of each test for comparison purposes.

4.4. Baseline Monotonic Loading

Results from single line, double line, monotonic and cyclic tests are compared to investigate relative performance of the various loading geometries and progressions. Single line

monotonic test results were taken as baselines for all other tests and for baseline comparison to results in literature. The first series of cyclic tests progressed in complexity from single line cyclic, to double line cyclic-sustained to double line cyclic-cyclic. The results from this first series provide insight on the caisson performance and behavior in response to increasingly complex cyclic loads. The second series of cyclic tests were performed with increased cyclic load amplitude to investigate the effects on caisson performance and behavior. The third series of cyclic tests were performed with increase mean cyclic load to investigate effect of mean load on caisson performance and behavior. Caisson anchor performance was compared on the basis of load-displacement behavior, peak monotonic load resistance and pore pressure response.

4.4.1. Single Line Monotonic Tests

Single line monotonic load resistance is the standard (DNV 2006, API 2005) for design of anchor caissons, thus, single line monotonic test results are the baseline for comparison to other test results and to literature. Three single line monotonic inclined load tests were performed. Two tests were performed with varied delay times after installation to compare the effects of percent dissipation of installation pore pressure on performance and behavior. The method of determining percentage installation pore pressure dissipation described by Randolph & Gourvenec (2011) was used for all tests (§3.5.4). The monotonic inclined load to failure was after approximately 28% installation pore pressure dissipation in test S1-T02 and after approximately 99% installation pore pressures dissipation in test S1-T04.

The slope of the load-displacement (P-δ) curve, although not a true modulus, is indicative of the stiffness of the caisson-soil system. The slope of the linear component of the P-δ curve (M_{in}) was greater in S1-T04 than S1-T02 (Figure 4.5), indicating a stiffer response where greater installation pore pressure had dissipated. M_{in} of S1-T04 = 114% M_{in} of S1-T02. A summary of M_{in} values are provided in Table 4.2.

Table 4.2. Summary of load – displacement slopes for caisson load tests.

Load Type	Test No.	Line	Line Load-Displacement (P-δ) Slope		
			M_{in}	M_{pc1}	M_{pc2}
Mono-tonic	S1-T02	-L-M	8.6	-	-
	S1-T04	-L-M	9.8	-	-
	S2-T12	-L1-S	9.2	-	-
		-L2-M	9.9	-	-
Cyclic 1 LMLA	S1-T03	**-L-CM**	**10.5**	**18.5**	**8.5**
	S2-T06	-L1-C	13.6	-	-
		-L2-SM	**13.1**	**18.5**	**8**
	S2-T08	-L1-C	12	-	-
		-L2-CM	**12**	**22.6**	**8.1**
Cyclic 2 LMHA	S1-T05	**-L-CM**	**10.9**	**22.8**	**9.2**
	S2-T07	-L1-C	9.2	-	-
		-L2-SM	**10.5**	**21.8**	**6.6**
	S2-T09	-L1-C	10.1	-	-
		-L2-CM	**10.2**	**26.7**	**8.3**
Cyclic 3 HMLA	S2-T13	**-L-CM**	**10.2**	**25.5**	**7.8**
	S2-T11	-L1-C	9.9	-	-
		-L2-SM	**9.9**	**24.5**	**8.2**
	S2-T10	-L1-C	9.9	-	-
		-L2-CM	**10.2**	**26.7**	**8.6**

Symbols: M_{in} = initial linear slope (to cyclic mean load); M_{pc1} = first post-cyclic linear slope; M_{pc2} = second post-cyclic linear slope (see Figure 4.9).

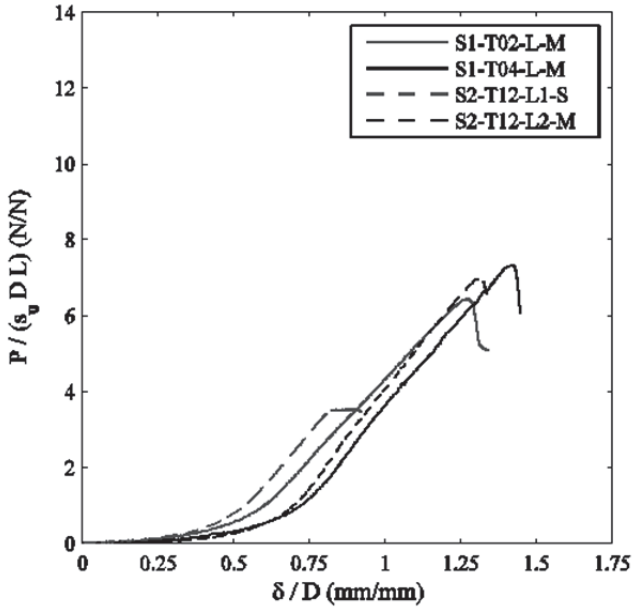

Figure 4.5. Normalized load resistance and line displacements in monotonic tests

Line load resistance provided by the anchor caisson is increased with increased installation pore pressure dissipation prior to caisson loading. Line load resistance is 13.8% greater in S1-T04 having 99% excess pore pressure dissipation, than in S1-T02 having 28% pore pressure dissipation. Line load-displacement plots are illustrated in Figure 4.5 for the single line case**,** and line load and displacements at failure are provided in Table 4.3 and Table 4.4, respectively. Reference monotonic load resistances were established for all other tests performed at various percentage pore pressure dissipation (Figure 4.6) from interpolation/ extrapolation of the results of these two single line monotonic tests (S1-T02 and S1-T04). Linear interpolation/ extrapolation was applied since monotonic load resistance varies directly with s_u, which varies directly with effective stress, which varies directly with percentage pore pressure dissipation.

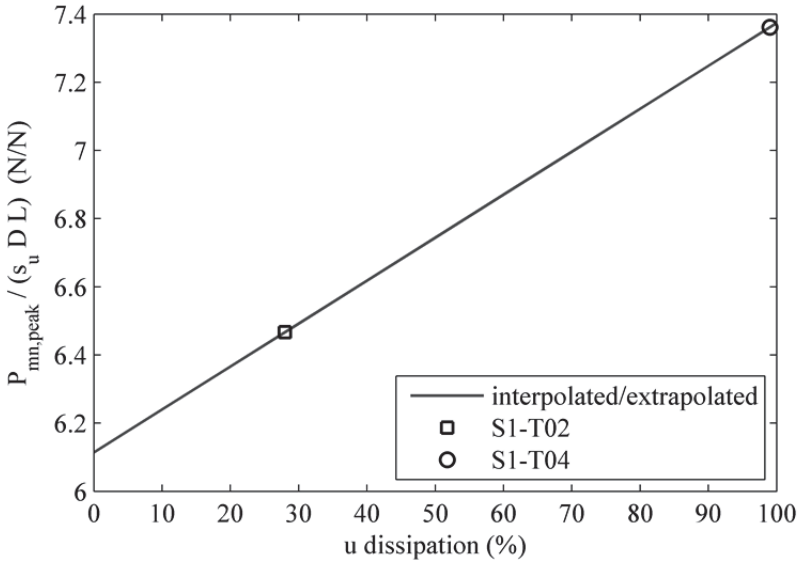

Figure 4.6. Interpreted reference monotonic load resistance varying with percentage pore pressure dissipation.

Table 4.3. Summary of caisson load details.

Load Type	Test No.	Line	Est. Δu[1] Disp. (%)	$\mathcal{N}$ (N)	Normalized Loads (N/N)				Loading (Fraction of $P_{mn,\,peak}$)		
					Monotonic	Cyclic Loading		Monotonic	Monotonic	Cyclic Loading	
					P_{in}	P_{mean}	P_{amp}	P_{peak}	P_{in}	P_{mean}	P_{amp}
MONO-TONIC	T02	-L-M	28	5.75	-	-	-	6.47	-	-	-
	T04	-L-M	99	5.75	-	-	-	7.36	-	-	-
	T12	-L-S	99	6.50	3.51	-	-	3.97[2]	0.54	-	-
		-L2-M			-	-	-	7.06	-	-	-
CYCLIC 1 LMLA	T03	**-L-CM**	0	5.75	**2.25**	**1.97**	**1.05**	**7.68**	**0.306**	**0.268**	**0.143**
	T06	-L1-C	32	5.50	2.58	2.70	0.94	2.99[2]	0.336	0.352	0.122
		-L2-SM			**2.53**	**2.12**	**0.00**	**7.71**	**0.329**	**0.277**	**0.000**
	T08	-L1-C	54	5.50	2.61	2.65	0.94	2.48[2]	0.340	0.345	0.122
		-L2-CM			**2.55**	**3.01**	**1.00**	**8.28**	**0.332**	**0.392**	**0.130**
CYCLIC 2 LMHA	T05	**-L-CM**	42	5.75	**2.49**	**2.33**	**1.84**	**10.29**	**0.339**	**0.318**	**0.251**
	T07	-L1-C	42	5.50	2.10	2.43	1.55	2.76[2]	0.274	0.317	0.201
		-L2-SM			**3.26**	**2.51**	**0.00**	**8.89**	**0.306**	**0.327**	**0.000**
	T09	-L1-C	59	5.50	2.55	2.81	1.61	2.68[2]	0.332	0.367	0.210
		-L2-CM			**2.66**	**3.07**	**1.92**	**9.01**	**0.347**	**0.400**	**0.250**
CYCLIC 3 HMLA	T13	**-L-CM**	47	6.50	**3.73**	**4.03**	**0.79**	**8.59**	**0.574**	**0.620**	**0.122**
	T11	-L1-C	40	6.50	3.76	3.78	0.86	3.31[2]	0.579	0.581	0.133
		-L2-SM			**3.73**	**3.71**	**0.00**	**6.96**	**0.575**	**0.571**	**0.000**
	T10	-L1-C	54	6.50	3.45	3.43	0.84	3.33[2]	0.531	0.528	0.129
		-L2-CM			**3.66**	**3.87**	**0.85**	**7.79**	**0.563**	**0.596**	**0.131**

NOTE: [1]using method of Randolph and Gourvenec (2011); [2]cyclic line load concurrent with peak monotonic resistance achieved in orthogonal direction.
SYMBOLS: $P_{mn,peak}$ = reference monotonic peak pullout resistance; $d_{mn,peak}$ = displacement at reference monotonic peak pullout resistance; P_{amp} = load amplitude; $P_{calc,peak}$ = calculated peak load resistance; $\mathcal{N} = s_{u,2/3L} D L$ or normalization parameter.

Table 4.4. Summary of line displacements and caisson rotations.

Load Type	Test No.	Line	Normalized Line Displacement			Caisson Rotation (°)	
			Mono.		Mono.	Mono.	Cyclic
			δ_{in}	δ_{cyc}	δ_{peak}	ψ_{in}	ψ_{cyc} or $\varkappa_{cyc}$
Mono-tonic	T02	-L-M	-	-	1.28	-	-
	T04	-L-M	-	-	1.39	-	-
	T12	-L-SM	0.817	-	0.91	-	-
		-L2-M	-	-	1.28	-	-
Cyclic 1 LMLA	T03	**-L-CM**	**0.885**	**	**1.14**	**	**
	T06	-L1-C	0.639	0.024	0.70	0.0	0.2
		-L2-SM	**0.776**	**0.029**	**1.34**	**0.0**	**0.0**
	T08	-L1-C	0.596	0.058	0.66	0.2	0.5
		-L2-CM	**0.693**	**0.058**	**1.19**	**0.0**	**0.7**
Cyclic 2 LMHA	T05	**-L-CM**	**0.579**	**0.032**	**1.24**	**0.0**	**0.4**
	T07	-L1-C	0.650	0.059	0.77	0.1	0.4
		-L2-SM	**0.805**	**0.011**	**1.70**	**0.0**	**0.0**
	T09	-L1-C	0.807	0.072	0.89	0.0	0.4
		-L2-CM	**0.799**	**0.058**	**1.31**	**0.0**	**0.8**
Cyclic 3 HMLA	T13	**-L-CM**	**0.916**	**0.053**	**1.41**	**0.4**	**0.8**
	T11	-L1-C	0.994	0.043	1.03	0.8	0.9
		-L2-SM	**0.984**	**0.024**	**1.25**	**0.7**	**1.0**
	T10	-L1-C	0.754	0.010	0.80	0.3	0.7
		-L2-CM	**1.005**	**0.080**	**1.38**	**0.4**	**1.0**

SYMBOLS: d_{in} = initial line displacement to mean load; d_{cyc} = accumulated line displacement during cyclic loading; d_{peak} = line displacement at peak monotonic load resistance; r_{in} = initial angular rotation at zero load; r_{cyc} = accumulated permanent rotation during cyclic loading.

As described in §4.2, the theoretical normalized load resistance provided by the suction caisson is 9.5 N/N (model scale). Measured normalized load resistance of S1-T04 was 78% of the resistance estimated by the LEM. The difference between the estimated and measured resistance may be explained, in part, by the location of the pad eye at a non-optimum position. The position of the pad eye approximately 9.5 mm lower than optimum position resulted in backward caisson rotation, which does not provide maximum resistance. Additionally, Aubeny et al. (2003) report a reduction in caisson line load resistance as the line load angle deviates from either purely vertical

or purely horizontal loading, resulting in an 'interaction' between different load resistance mechanisms. The load angle at which horizontal-vertical (H-V) load interaction significantly affects peak load resistance is dependent on load attachment depth and aspect ratio (L/D). Aubeny et al. (2003) report that for a caisson with L/D = 2, H-V load interaction is typically significant for load angles between approximately 30-45 degrees from horizontal (dependent on soil conditions). Thus, the 45° line load angle in S1-T02 and S1-T04 may have resulted in H-V resistance interaction and subsequent reduction in peak load resistance. H-V resistance interaction is accounted for in the LEM through roughness factors which define the fraction of s_u mobilized at the active and passive soil wedges and caisson tip for design purposes (DNV 2005). Roughness factors are typically determined through optimization of plasticity theory equilibrium equations which are dependent on relative displacement between the structure and soil (DNV 2005). No roughness factors were included in the estimate of caisson resistance as 3D finite element analysis of this model had not yet been performed.

S1-T04 test conditions and corresponding results compare well with results reported by Jeanjean et al. (2006) with respect to the aspect ratio, load angle and pad eye depth. The peak load resistance (P_{peak}) measured in S1-T04 was 97% P_{peak} of a similar test reported by Jeanjean et al. (2006). Centrifuge studies of monotonic inclined loading on suction caissons in overconsolidated and layered clay conducted by Jeanjean et al. (2006) and normally consolidated clay by Clukey et al. (2004) are summarized in Table 2.3 for comparison.

Line displacements and corresponding estimates of caisson displacement at peak monotonic load resistance were considerably large, compared to literature. Line displacement at peak resistance was 130% diameter (D) and 140% D, for S1-T02 and S1-T04, respectively. Approximating constant 47° load angle results in lateral caisson displacement of 97% D and 95% D for S1-T02 and S1-T04, respectively. Comparable tests on caisson anchors have typically reported lateral displacements of 10% D to 50% D at peak load resistance. Based on the results obtained, the cause of the high displacements is not clear. Potential sources of the high

displacement at peak resistance may be stretching of the line load or pull through of the line at the connection points. Further testing of the line material and knotting / connection methods used would be required to confirm if these are the true sources of high apparent line displacement.

Internal pore pressure response to monotonic loading progresses as the inverse to line load progression, as shown in Figure 4.7. Pore pressure decrease is initially non-linear, corresponding to the non-linearity of the loading progression as the mooring line pulls through the soil and applied loads are not fully transferred to the caisson (Figure 4.8(d)). Following the non-linear progression of pore pressure decrease, a local minimum is attained as the sustained load is reached in the first line. The minimum pore pressure for the test is reached as the peak monotonic load is reached in line 2 (Figure 4.8 e), f), g), h), and i)). Internal pore pressures measured do not include pressures generated during installation as the caisson was vented during jacking installation, and the PPT was set to zero at 1G, prior to centrifuge start up for caisson loading.

In S1-T02 (Figure 4.8 a)) the internal pore pressure at failure is 13.5 kPa below hydrostatic. Pore pressure for test S1-T04 is unavailable due to measurement errors. Table 4.5 provides a summary of internal pore pressure measured during the test progressions and normalized by the initial hydrostatic pressure.

Internal pore pressure decrease during loading increase may be caused by vertical caisson displacement. As the caisson was displaced upwards void volume inside the caisson was increased and internal pore pressure was reduced. Based on results, soil permeability is insufficient to allow equalization of u at the rate of loading. Creation and maintenance of pore pressure differential is the premise of suction caisson installation and a component of vertical load resistance.

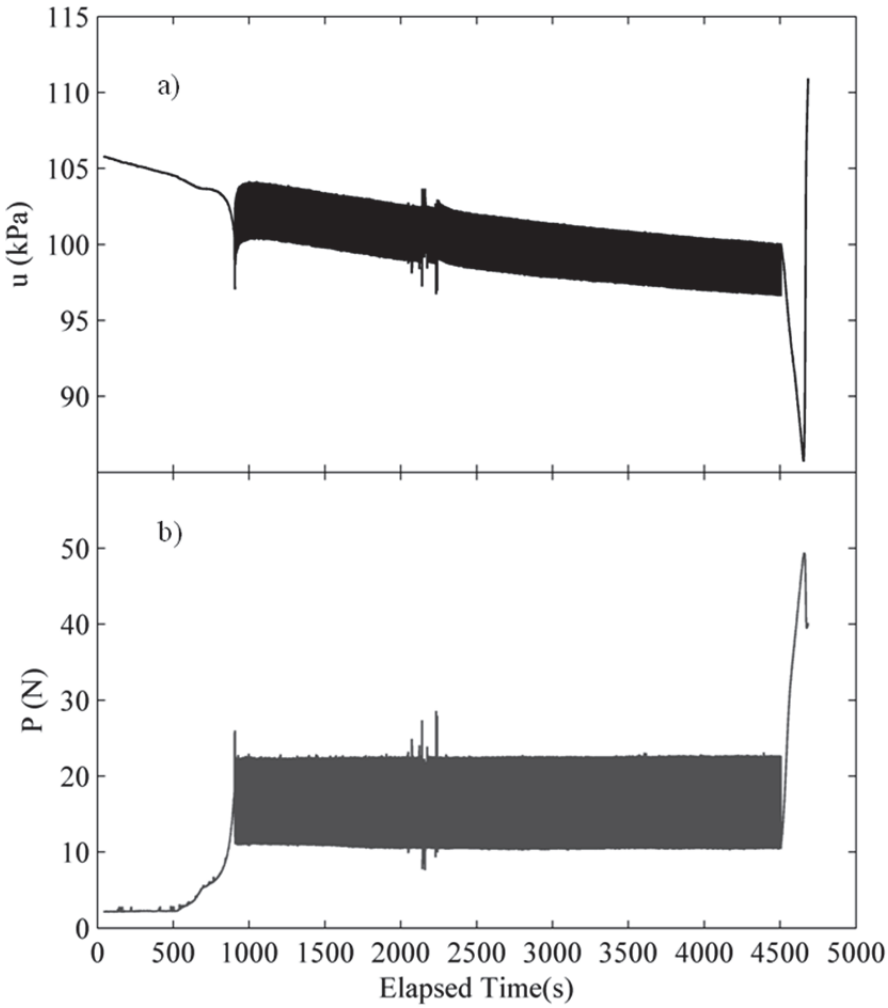

Figure 4.7. Example of pore pressure (u) progression vs. load progression with time.

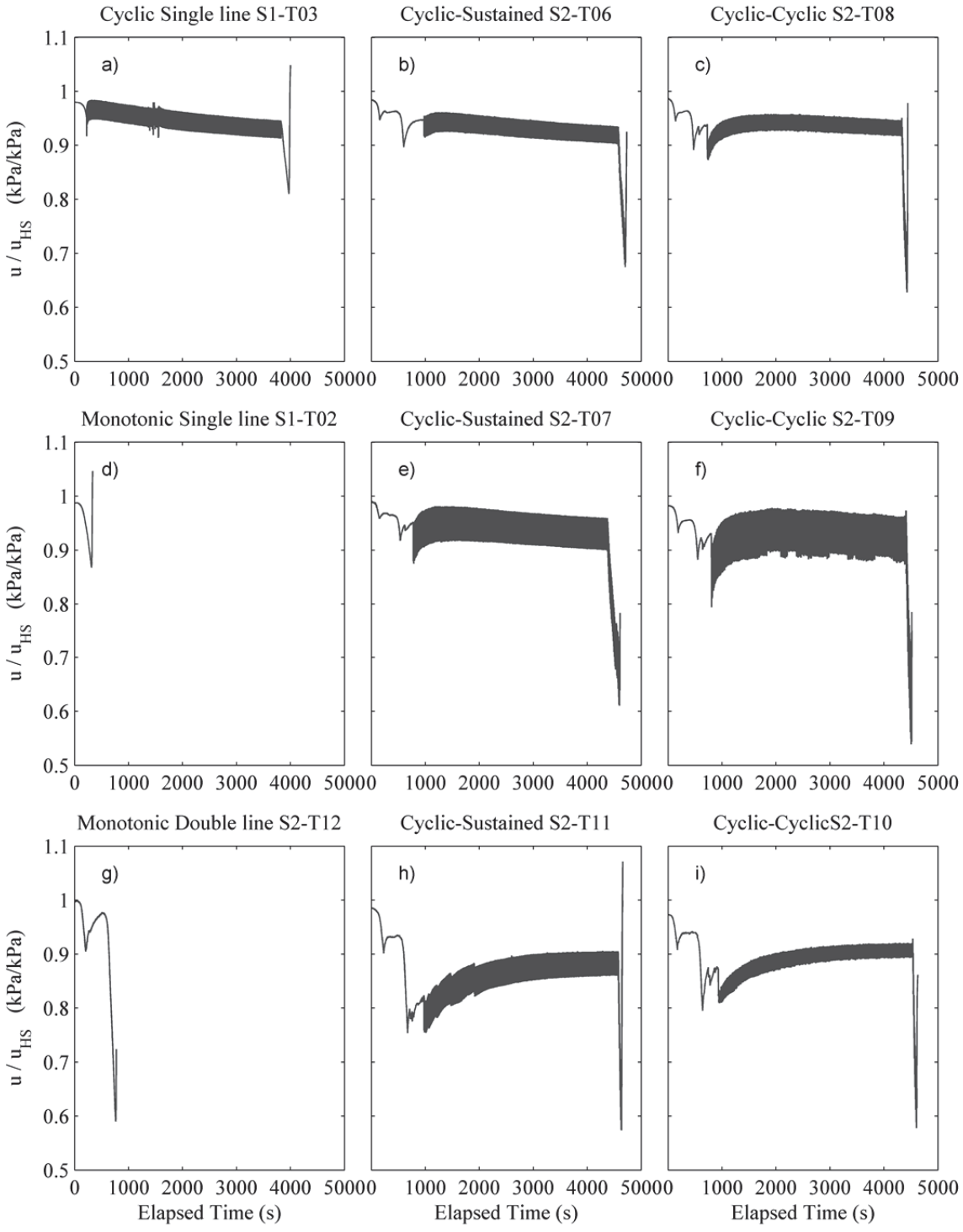

Figure 4.8. Normalized pore pressure progression during caisson load tests.

Table 4.5. Summary of internal pore pressure response.

LOAD TYPE	TEST NAME		u_{hs}	u_{peak}	NORMALIZED INTERNAL PORE PRESSURE (kPa/kPa)							
					u_0	u_{in}		peak range u		low range u		u_{peak}
						L1	L2	high	low	high	low	
MONO-TONIC	S1-T02	-L-M	109.1	95.1	0.988	-	-	-	-	-	-	0.872
	S1-T04	-L-M	-		-	-	-	-	-	-	-	-
	S2-T12	-L1-S / L2-M	67.8	40.1	0.997	-	-	-	-	-	-	0.591
CYCLIC 1 LMLA	S1-T03	-L-C	105.8	85.8	0.980	0.918	-	0.985	0.949	0.946	0.913	0.811
	S2-T06	-L1-C / L2-SM	80.1	56.1	0.984	0.948	0.896	0.961	0.925	0.934	0.903	0.700
	S2-T08	-L1-C / L2-CM	74.9	51.5	0.989	0.949	0.892	0.956	0.924	0.947	0.917	0.688
CYCLIC 2 LMHA	S1-T05	-L-C	-	-	-	-	-	-	-	-	-	-
	S2-T07	-L1-C / L2-SM	80.9	52.9	0.998	0.962	0.937	0.981	0.916	0.959	0.901	0.654
	S2-T09	-L1-C / L2-CM	73.6	43.1	0.981	0.932	0.883	0.976	0.891	0.962	0.876	0.586
CYCLIC 3 HMLA	S2-T13	-L-C	-	-	-	-	-	-	-	-	-	-
	S2-T11	-L1-C / L2-SM	78.0	48.1	0.986	0.913	0.781	0.905	0.860	0.905	0.860	0.617
	S2-T10	-L1-C / L2-CM	78.3	49.2	0.973	0.912	0.866	0.921	0.894	0.920	0.894	0.628

4.4.2. Double Line Monotonic Test

One double line monotonic test S2-T12 was performed to obtain baseline multi-line loading caisson performance. The loading progression consists of maintained load on one line while the orthogonal line is loaded monotonically to failure. Comparison of the load-displacement, peak load resistance, and pore pressure responses to the single line monotonic results indicates relative performance and behavior of a multi-line loaded anchor caisson.

Initial P-δ slope (M_{in}) of first line load of the double line monotonic tests was less than M_{in} of the baseline monotonic test (Table 4.2). M_{in} of S2-T12-L1 was 94% M_{in} of S1-T04, which is likely due to sample variability or minor installation differences. A stiffer P-δ response occurred for S2-T12-L2, which had a sustained load on the perpendicular line 1, where M_{in} of S2-T12-L2 was 108% of M_{in} for S2-T12-L1 and 101% of M_{in} for T04. Peak monotonic load resistance (P_{peak}) measured along the line loaded to failure is less for the caisson subject to a sustained perpendicular load (Table 4.3, Figure 4.5), where P_{peak} for the double line monotonic test (T12) is 4% less than that of the reference single line monotonic test (T04).If the total resultant peak resistance is considered, reference monotonic inclined load resistance is exceeded in this case where the caisson is subject to double line loading with the sustained load perpendicular to the line subjected to monotonic load to failure. Resolved loads at peak failure show the double line test has 31% more capacity than the single line monotonic test. A summary of resolved loads at peak monotonic load resistance is provided in Table 4.6.

Line displacement and approximated caisson displacement at peak monotonic load resistance in the direction of applied monotonic load to failure (Table 4.4) were the same for double line monotonic and single line monotonic tests. Double line loading, however, did result in larger percent reduction in internal pore pressure. A decrease of 40.8% of the initial hydrostatic pressure occurred as the double line reached peak resistance compared to a 12.8% decrease at the point of peak resistance for the single line. This indicates more uplift occurred in the double line test which is consistent with the greater uplift load resulting from the two lines loaded at 45°.

Table 4.6. Summary of resultant displacements, loads and load angles for multi-directional load tests.

Load Type	Test Name		Resultant Displacements (mm/mm)			Resultant Loads (N/N)			Resultant Load Angle	
			Mono.	Cyclic	Mono.	Cyclic Loading		Mono.	ω_{sweep} (deg)	ω_{peak} (deg)
			d_{in}	d_{cyc}	d_{peak}	P_{mean}	P_{amp}	P_{peak}		
Cyclic 1 LMLA	S2-T06	-L1-C / L2-SM	1.227	0.050	1.792	4.18	0.89	9.92	20.0	38.6
	S2-T08	-L1-C / L2-CM	1.138	0.095	1.630	4.97	0.62	10.46	37.6	44.1
Cyclic 2 LMHA	S2-T07	-L1-C / L2-SM	1.260	0.100	2.188	4.26	1.39	11.38	38.3	40.5
	S2-T09	-L1-C / L2-CM	1.446	0.101	1.919	5.18	1.28	11.76	61.8	58.8
Cyclic 3 HMLA	S2-T11	-L1-C / L2-SM	1.711	0.055	1.982	6.43	0.83	10.00	13.2	25.9
	S2-T10	-L1-C / L2-CM	1.524	0.086	1.905	6.36	0.59	10.51	26.0	31.6
Monotonic	S2-T12	L1-S/L2-M	-	-	1.910	-	-	9.68	-	-

NOTE: [1]See Figure 3.5

SYMBOLS: d_{in} = line displacement at initial load (cyclic mean load), d_{cyc} = accumulated permanent line displacement during cyclic loading; d_{peak} = line displacement at peak pullout resistance; P_{mean} = cyclic mean load; P_{peak} = peak pullout resistance; P_{amp} = load amplitude;;ω_{sweep} = resultant load sweep angle; ω_{peak} = load offset angle at peak resistance.

4.5. First Cyclic Loading Series: Low Mean Low Amplitude (LMLA) Loading

The first series of single line cyclic, double line cyclic-sustained, and double line cyclic-cyclic tests was performed to observe effects of increased load configuration complexity on load-displacement (P-δ) behavior, accumulated permanent cyclic displacement (δ), caisson rotation (ϰ and ψ) post-cyclic peak monotonic load resistance (P_{peak}) and pore pressure response (u). Single line cyclic test S1-T03 was performed in Soil model 1 (Figure 3.12), and both double line cyclic tests were performed in Soil model 2 (Figure 3.13).

Low cyclic mean load and low cyclic load amplitude (LMLA) were selected for the first series of tests. These loads were chosen with respect to the peak load for the single line monotonic tests, and §3.1 provides a justification for the selected loading ratios. A summary of loads applied in each of the single line cyclic (S1-T03), double line cyclic-sustained (S2-T06), and double line cyclic-cyclic (S2-T08) tests is provided in Table 4.3.

4.5.1. Line Load-displacement Behavior

For cyclic tests followed by monotonic load to failure, there were two distinct periods of monotonic loading which are of interest (Figure 4.9). The first monotonic load period was initial caisson loading to the mean cyclic load, prior to initiation of cyclic loading. During this initial monotonic loading, the trend of the load displacement (P-δ) slope is linear. The second monotonic load period occurred following the cyclic loading, and continued until caisson failure. In this second monotonic loading, the P-δ response resembles a piecewise jointing of two unique linear components, the first of which is steeper than the latter.

Steepness of the initial P-δ slope (M_{in}) for the first line loaded in each test: single line monotonic test (S1-T02/ S1-T04), single line cyclic test (S2-T03), double line cyclic-sustained test (S2-T08), and double line cyclic-cyclic test (S2-T08) varied between the tests (Figure 4.10a; b; c; Table 4.2). The softest initial response occurred in the single line monotonic test (S1-T03) and the stiffest response occurred in line 1 of the double line cyclic-sustained test (S2-T06) which

was loaded following line 1 loading to the desired sustained load. Notably, M_{in} of line 1 in the double-line cyclic-sustained test (S2-T06) was 130% M_{in} of the single line cyclic test (S1-T03). The standard deviation of M_{in} for the single line test and L1 of the double line test was 14.6% of the mean M_{in} value. M_{in} values were more variable than expected. Theoretically M_{in} should be similar in the single line tests and the first line of each of the double line tests, if percentage installation pore pressure dissipation and installation depth were similar, since no variables were intentionally modified to this point. M_{in} for load line 2 (L2) of the two double line tests (S2-T06 and S2-T08) were consistent between tests. For S2-T06 and S2-T08, the standard deviation of M_{in} was 0.07, less than 1% of mean M_{in}.

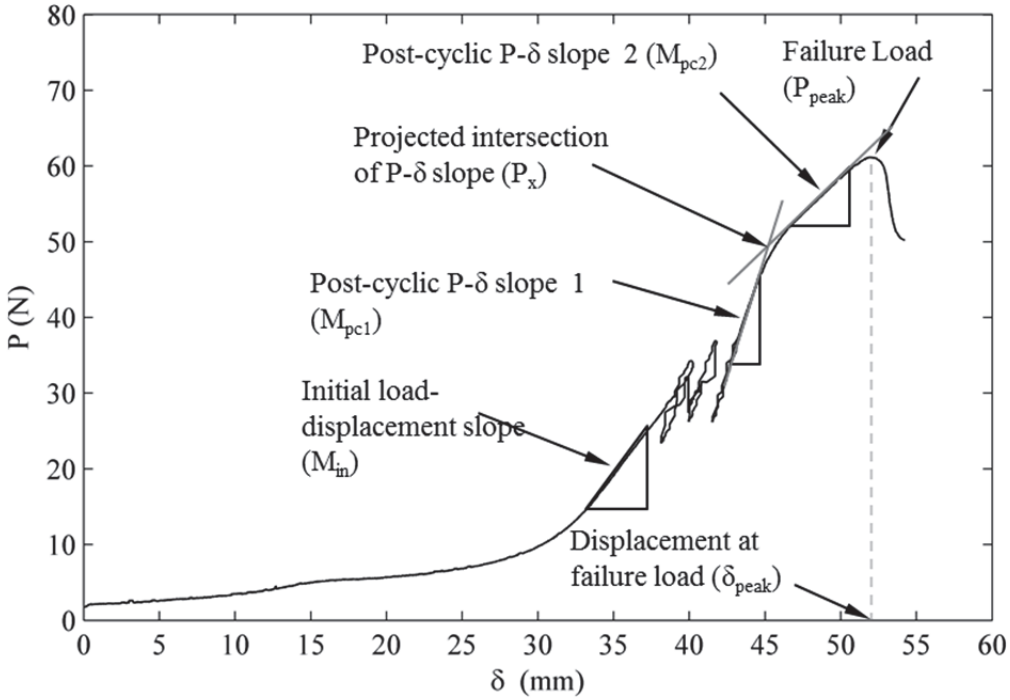

Figure 4.9. Typical line load – displacement progression for cyclic tests.

The increase in steepness of the first linear component P-δ slope (M_{pc1}) during post-cyclic monotonic loading (relative to M_{in}) is larger where the monotonic load was applied to a load line previously subjected to cyclic loads (Figure 4.10a; b; c; Table 4.2). In the single line cyclic test (S1-T03), and L2 of double line cyclic-cyclic test (S2-T08), M_{pc1} values are 176% and 188% of the respective M_{in} values. Less increase in steepness of the first linear component of P-δ slope

during post-cyclic monotonic loading was observed where monotonic loading was not preceded by cyclic loading on a given load line. For L2 of S2-T06, where monotonic load to failure was applied orthogonally to the direction of cyclic preloading, M_{pc1} is 141% of M_{in}. The results appear to indicate greater increases in stiffness (relative to monotonic loading without cyclic preload) occur where cyclic preload is applied in the same direction as the monotonic load to failure. Increased stiffness of P-δ response was also observed by Watson & Randolph (2006) in an investigation of sustained and cyclic preload effect on load-displacement response of suction caissons.

Change in P-δ slope from the steeper first post-cyclic slope to the milder second post-cyclic slope occurs at a similar load magnitudes relative to maximum cyclic load ($P_{cy,max} = P_{mean} + P_{amp}$) for the tests where cyclic pre-loading is applied in the same direction as the monotonic load to failure (Figure 4.10a; b; c; Table 4.2). In both single line cyclic test (S1-T03) and double line cyclic-cyclic test (S2-T08), the projected intersection (P_x) of M_{pc1} and M_{pc2} slopes occurred at 150% $P_{cy,max}$ of each test. In double line cyclic-sustained test S2-T06, where cyclic pre-loading was applied in a perpendicular direction to the monotonic load to failure, P_x = 120% $P_{cy,max}$.

A decrease in P-δ slope was observed during the second linear component of post–cyclic monotonic loading (M_{pc2}), relative to M_{in} (Figure 4.10a; b; c; Table 4.2). Larger decrease in P-δ slope occurred in cyclic-sustained (S2-T06) and cyclic-cyclic (S2-T08) double line tests where $M_{pc\,2}$ is 61% and 68% of the respective M_{in} values. A smaller decrease in P-δ slope occurred in cyclic single line test (S1-T03), where M_{pc2} is 81% of M_{in}. The results indicate a softening response in the second linear component of P-δ slope during all post-cyclic monotonic tests, with the most softening occurring where post-cyclic monotonic load is applied orthogonal to cyclic preloading.

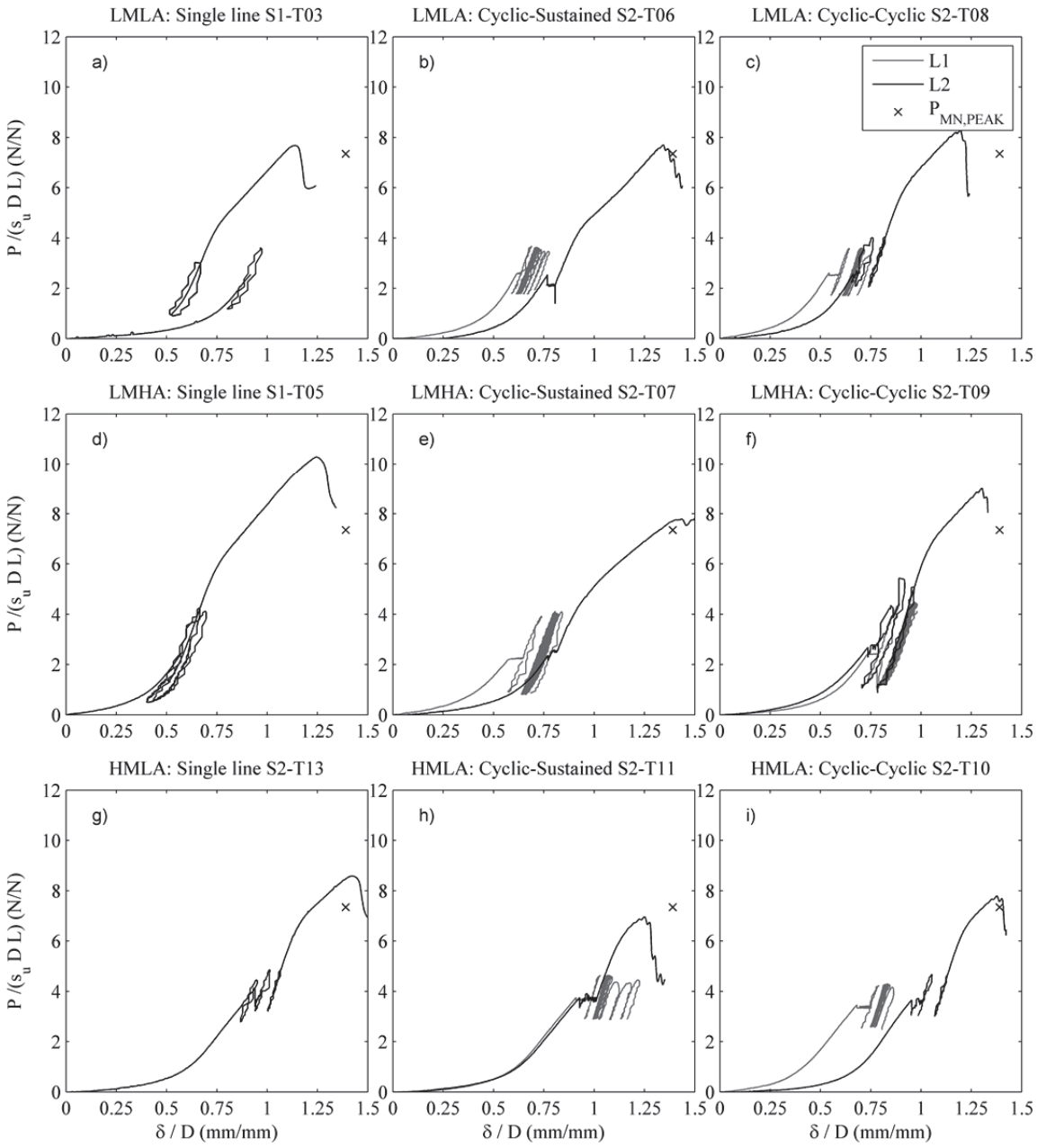

Figure 4.10. Normalized line load – displacement progression during cyclic load tests.

Similar stiffness changes were reported by Levy et al (2007) from a study of piles subjected to multi-stage loading in orthogonal directions. In the study, a pile was loaded in one direction to the intended load, immediately offloaded, and then reloaded in the orthogonal direction to failure. Elapsed time between the initial offloading and reloading in the orthogonal direction was limited to 2-4 minutes. The initial slope of the second stress strain curve was steeper than the first, confirming a stiffening of the soil pile system in the reload stage following initial loading. At some discrete point, the stress strain slope changes to a less steep linear slope maintained until failure.

4.5.2. Accumulated Displacements

Permanent cyclic displacement is non-recoverable displacement accumulated over a load cycle that is maintained following load release. Accumulated permanent cyclic displacement (δ_{cyc}) plotted against the log number of load cycles (n) indicates the fatigue response of the soil-structure system.The slope of the displacement versus number of cycles (δ_{cyc}-n) plot indicates the rate of change in accumulated displacement. The trend appears linear on the semi-log plot, indicating a decreasing rate of displacement accumulation representing low fatigue response as number of cycles continues to increase.

Cycling in both of the orthogonal directions results in increased initial rate of displacement accumulation, compared to the effect of a perpendicular sustained load combined with cyclic loading (Figure 4.11 a and b). The initial δ_{cyc}-n slope (for n = 0 - 20) of S2-T08-L2 was 650% of the δ-n slope of S2-T06-L2. As the number of cycles increases, the difference between cyclic-cyclic and sustained-cyclic loading on the displacement accumulation rate diminishes. The slope over the last 100 cycles (n = 440 - 540) in S2-T08-L2 is 62% of the δ_{cyc}-n slope of S2-T06-L2.

S1-T03 load-displacement results reveal an anomaly of decreasing displacement with increasing number of cycles (inconsistent with all other tests) is considered an outlier. S1-T03 displacement results will not be used for comparisons.

As a consequence of the greater initial rate of displacement with cyclic loads applied in perpendicular directions, a greater percentage of total displacement was accumulated in a fewer number of cycles. In cyclic-cyclic test S2-T08-L1, 50% of total displacement was accumulated over 50 cycles ($n_{50} = 50$), whereas in cyclic-sustained test S2-T06-L1, 50% of total displacement was accumulated in 80 cycles ($n_{50} = 80$).

Greater total displacement accumulation occurred where cyclic loading in both orthogonal directions was applied. Accumulated displacements, δ_{cyc}, normalized by the caisson diameter, D, for (cyclic-cyclic) S2-T08-L1 and S2-T08-L2 were 0.058 mm/mm each. These are 240% and 200% of δ_{cyc} of (cyclic-sustained) S2-T06-L1 and S2-T06-L2. Displacement accumulated during cyclic loading was a small percentage of the displacement at failure for both cyclic sustained and cyclic-cyclic tests. Accumulated cyclic displacements for S2-T06-L1 and S2-T06-L2 accounted for 3.4% and 2.2% of peak failure displacement (δ_{peak}) respectively. For S2-T08-L1 and S2-T08-L2, accumulated cyclic displacement was 8.8% and 4.9% of δ_{peak}, respectively.

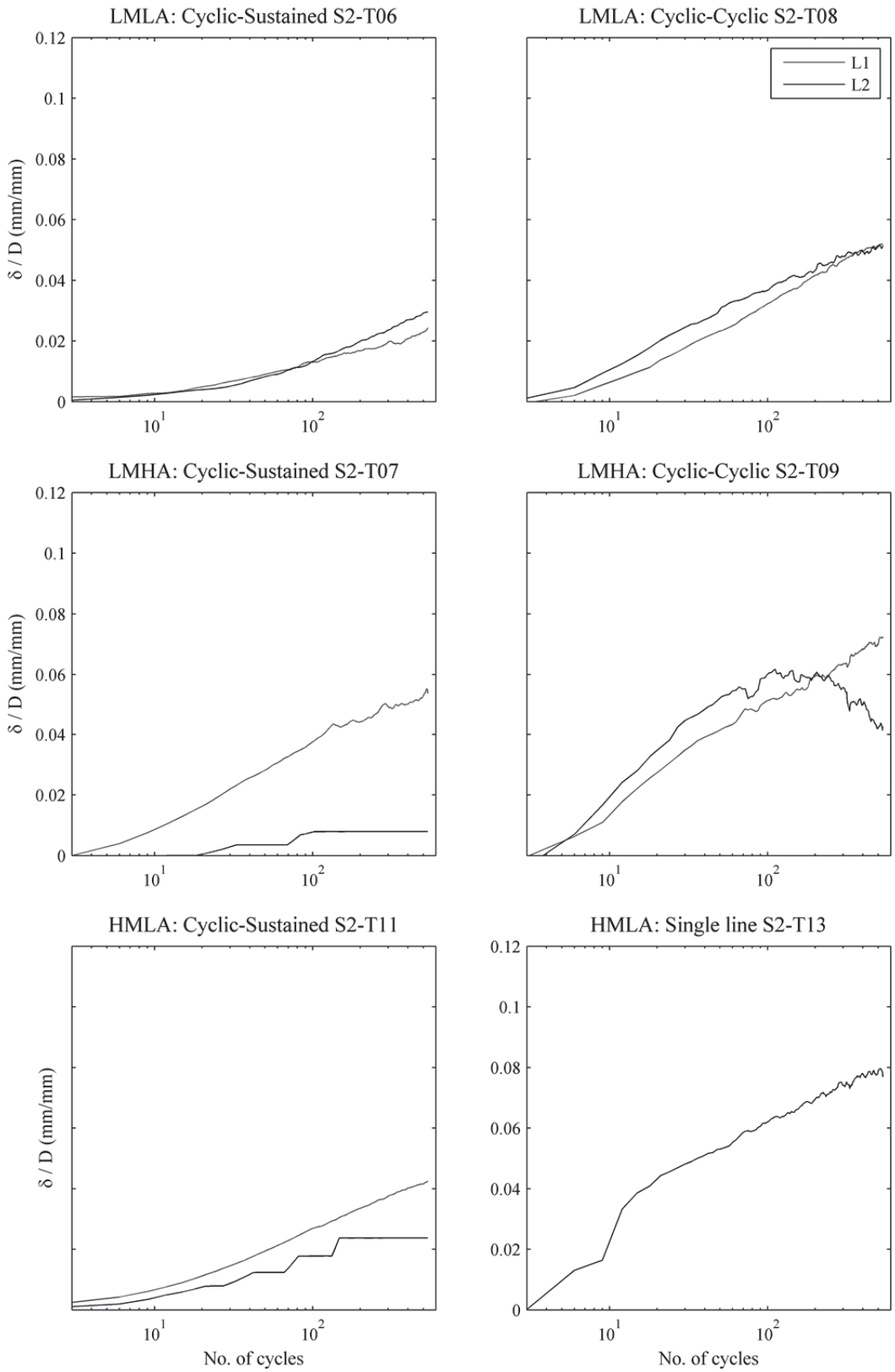

Figure 4.11. Permanent displacement accumulated during cyclic tests.

4.5.3. Caisson Rotation

In all tests performed, caisson rotation was observed during loading, indicating non-optimum position of pad eye and less than maximum resistance mobilized by the suction caisson. Caisson rotation is described here by two terms of rotation, one in each of the two planes of loading (Figure 3.7). Rotation in the plane of the monotonic load to failure is designated by ψ, and rotation in the plane perpendicular to the monotonic failure load is $\varkappa$.

Greater caisson rotation in both planes of loading ($\varkappa$ and ψ) occurred when cyclic loads were applied in both orthogonal directions than when cyclic loading was applied only in the direction orthogonal to monotonic load to failure (Table 4.4; Figure 4.12). Accumulated caisson rotation in double line cyclic-cyclic test (S2-T08), was 280% and 200% of the respective $\varkappa$ and ψ values of cyclic-sustained test (S2-T06) (Table 4.4; Figure 4.12 a; b; c; d). These results may indicate that cyclic inclined loads on a suction caisson in normally consolidated (kaolin) clay result in greater caisson rotations than for sustained inclined loads. This is consistent with expectations as cyclic loading tends to cause strain-softening to a greater extent than sustained loading (Koutsoftas 1978; Matsui et al. 1980; Chaney and Fang 1986; Zhou and Gong 2001).The greater rotation in test S2-T08 might also be partially attributed to the unintentionally higher P_{mean} applied to L2, and correspondingly higher resultant mean load $P_{re,mean}$. Caisson rotation results for single line test (S1-T03) are not available due to incompatibility between obtained video quality and post-processing grid analysis of rotation.

Maximum load resistance is achieved when the pad eye is located at optimum position resulting in only translational displacement (Andersen and Jostad 1999; DNV 2005). Thus, the observed caisson rotation during the tests performed indicates that the pad eye was not located in its optimal position and the maximum capacity possible for the caisson size, was not fully mobilized. A higher resistance may be achieved by relocating the pad eye to the true optimal position, potentially based on *resultant* load angle and soil strength properties.

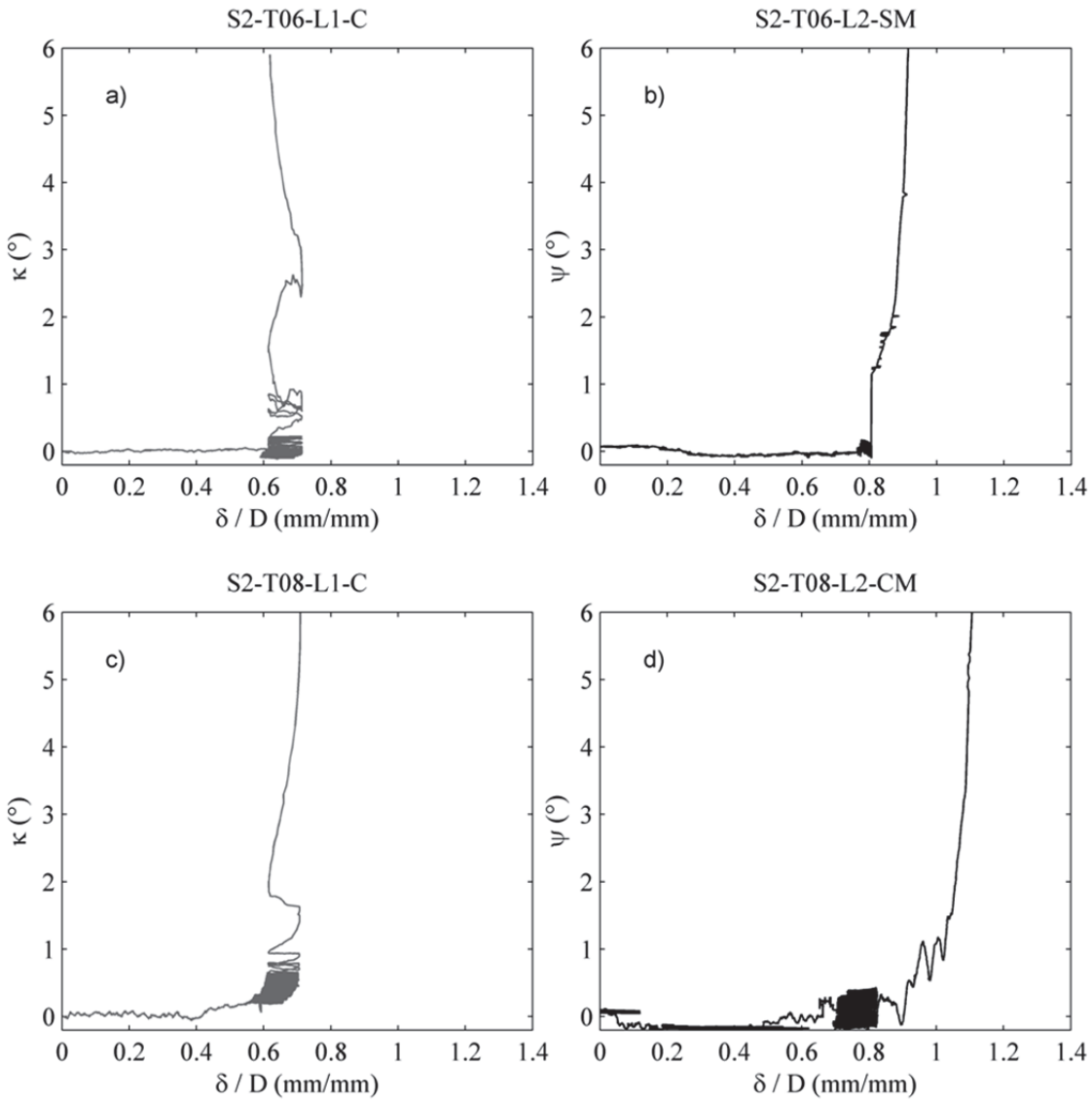

Figure 4.12. Progression of suction caisson rotation relative to normalized line displacement for Low Mean Low Amplitude cyclic tests.

4.5.4. Peak Load Resistance

Peak monotonic load resistance (P_{peak}) is typically the primary focus for caisson anchor design. In these series of tests P_{peak} was identified at the point of maximum load resistance attained during the post-cyclic monotonic loading (equal to the point of failure), as shown in Figure 4.9. The reference load resistance for each test ($P_{mn,peak}$) was determined based on results from monotonic single line tests (S1-T02 and S1-T04), for the appropriate percentage installation

pore pressure dissipation (§4.5.1; Figure 4.6). All P_{peak} values reported were normalized by the product of s_u, D, and L, for comparison purposes between tests and with literature. A summary of the interpreted peak resistances (Figure 4.9) is provided in Table 4.3 and Figure 4.10.

Cyclic pre-loading increased P_{peak} attained during post-cyclic monotonic loading, compared to $P_{mn,peak}$ attained during monotonic loading alone. The greatest increase in P_{peak} measured during post-cyclic monotonic load to failure occurred in single line test (S1-T03), where cyclic preload was applied only in the direction of monotonic load to failure. For single line cyclic test S1-T03, post-cyclic P_{peak} is 126% of the reference $P_{mn,peak}$. The second largest increase in P_{peak} occurred where cyclic preloading was applied in both the same direction as, and the direction orthogonal to the post-cyclic monotonic load to failure (S2-T08), where P_{peak} is 122% of $P_{mn,peak}$. The smallest increase in P_{peak} occurred where cyclic preload was applied orthogonally to the monotonic load to failure (S2-T06), where P_{peak} is 118% of $P_{mn,peak}$. Based on these results it appears that for suction cyclic preloading of a suction caisson that does not cause failure during load cycling, results in increased post-cyclic monotonic resistance for a given line, when compared to monotonic load resistance without cyclic preloading. Furthermore, the increase in monotonic load resistance is greatest when the applied cyclic preload shares the same zone of influence in the soil as the following post-cyclic monotonic load.

Observation of increased resistance due to cyclic preload is consistent with results obtained by Clukey et al. (1995) for approximately vertically loaded suction caissons with aspect ratio L/D = 2. Increases in monotonic load resistance following cyclic pre-loading were related to the load amplitude applied during cyclic pre-loading (Clukey et al. 1995). Respectively, gains of 5%, 19% and 35% in post cyclic monotonic load resistance, relative to peak resistance attained in monotonic-only loading, occurred with cyclic pre-load amplitudes of 0.27 to 0.30, 0.30, and 0.43 of the calculated peak monotonic load resistance, respectively.

Double line tests apply greater total load magnitude to the caisson, as determined from vector addition of the two orthogonal loads to obtain a single resultant load vector. Resultant peak

load resistance ($P_{re,peak}$) for both cyclic-sustained and cyclic-cyclic tests are substantially higher than the baseline single monotonic peak resistance (Figure 4.13). For cyclic-sustained test (S2-T06) $P_{re,peak}$ is 152% of $P_{mn,peak}$. For cyclic-cyclic test (S2-T08), $P_{re,peak}$ is 153% of $P_{mn,peak}$. Therefore, the increase in monotonic load resistance resulting from cyclic preloading is even greater in terms of resultant load resistance than for a single line within the double line configuration.

The increase in total resultant monotonic load resistance ($P_{re,peak}$) following post-cyclic preloading, appears to reflect the increase in angle of sweep (ω_{sweep}) (Table 4.6). Where ω_{sweep} is defined by the relative magnitudes of P_{amp} and P_{mean} of the orthogonal loads, along with the phase offset (§3.6), ω_{sweep} is least (ω_{sweep} is 0) for single line cyclic (S1-T03) and largest for double line cyclic-cyclic (S2-T08). This is similar to the increase in resultant monotonic load resistance where the least increase in resistance is in single line cyclic ($P_{re,peak}$ is the same as $P_{mn,peak}$), the greatest increase is in double line cyclic-cyclic $P_{re,peak}$ is 158% $P_{mn,peak}$. The resultant peak resistance correlates well to the angle of sweep (ω_{sweep}) of the resultant (resolved) cyclic load vectors.

4.5.5. Pore Pressure Response

Internal pore pressure change is typically indicative of pore volume change. Pore pressure increase indicates pore volume decrease and pore pressure decrease indicates pore volume increase. Pore volume increase in soils inside a caisson may result from uplift of the caisson. Internal pore pressure relative to external/hydrostatic pressure affects hydraulic flow into the caisson, ‘seal condition’ of the caisson, and environmental pressure on the caisson.

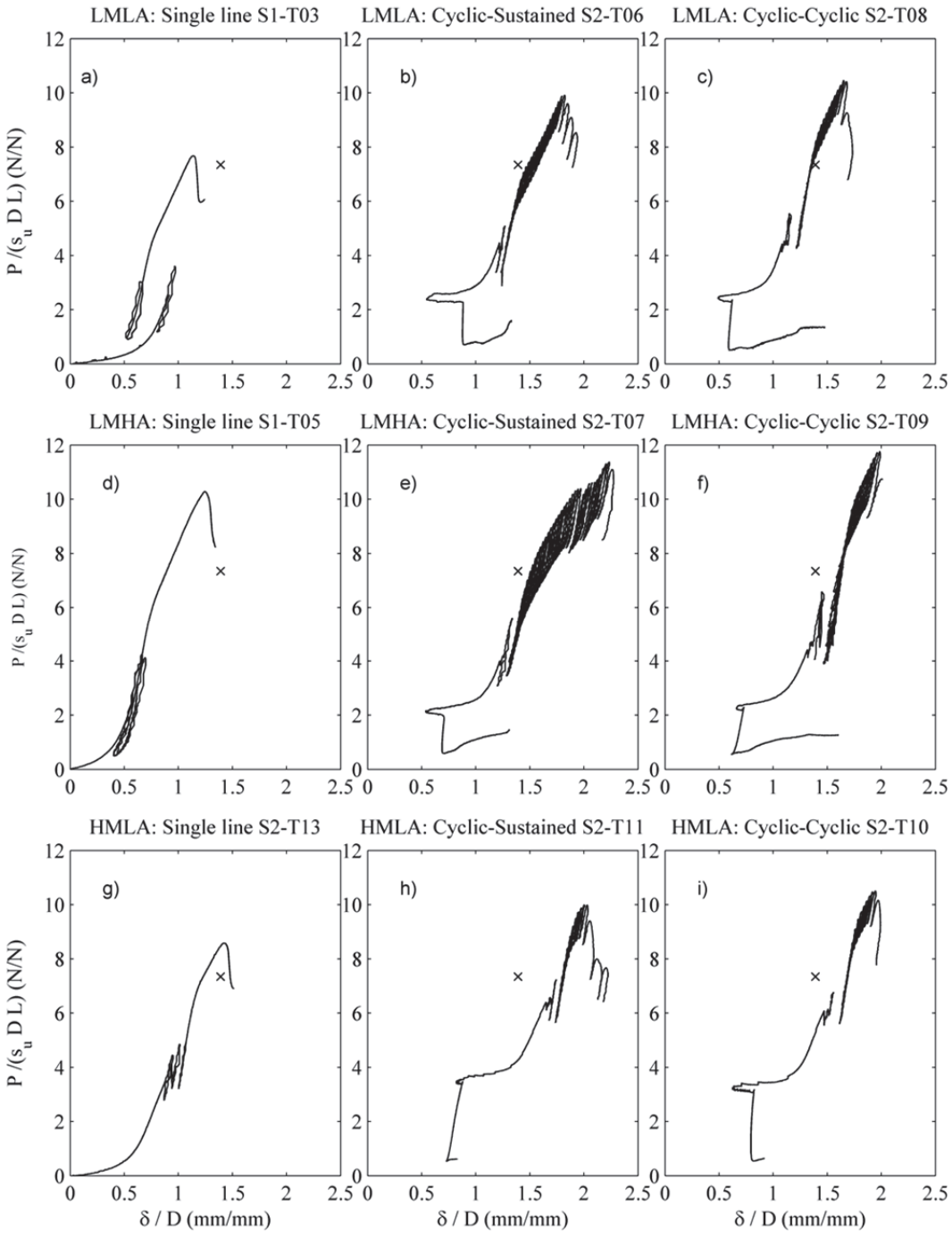

Figure 4.13. Normalized resultant load – displacement progression for cyclic tests.

Internal pore pressures changed throughout the test progression for all tests, varying with the displacement and associated volume change in the fluid-occupied spaces inside the suction caisson (Figure 4.7). Pore pressure progression during the initial monotonic loading to P_{mean} in all LMLA tests progressed similarly to the monotonic single line tests (§4.4.1). All pore pressure values presented were normalized by the hydrostatic pressure for comparison purposes. Following the monotonic loading to P_{mean}, the pore pressure response was cyclic reflecting the cyclic load applied (Figure 4.8 a), b), and c)). The trend of the mean pore pressure was an initial decrease at the start of cyclic loading, increasing to a similar mean pore pressure as had occurred at the completion of the monotonic loading to P_{mean}, followed by a consistent decrease mirroring the consistent (but low) rate of increase in line displacement. This general trend was observed in all three LMLA tests (S1-T03, S2-T06 and S2-T08).

There are slight differences in the pore pressure trends measured during cyclic loading for each of the LMLA tests. Decrease in mean pore pressure during cyclic loading, for single line cyclic (S1-T03), double line cyclic-sustained (S2-T06) and double line cyclic-cyclic (S2-T08) were 3.7%, 2.5% and 0.8% of the respective initial hydrostatic pore pressures. The largest decrease in mean pore pressure was in the single line cyclic tests, indicating that the largest suction force was invoked by the single line configuration.

4.5.6. Gap Formation and Sample Surface at Failure

Gap formation potentially reduces frictional resistance of the caisson (Huang et al. 2003). There has not been conclusive research defining conditions that will or will not result in formation of a gap between the soil and backside of a caisson (with respect to load attachment). Classic earth pressure theory provides a simple method for estimation of whether or not a gap will form, that has been both supported and countered by modeling results. Theoretically, if the reduction in total stress on the backside of the caisson is greater than the initial horizontal stress, a gap may form. However, in normally consolidated clay, undrained shear strength is typically

insufficient to support the near –vertical face that would result in gap formation (El-Sherbiny 2005; Rauch et al. 2005). Some studies have shown that gapping may occur in normally consolidated soils where high amplitude cyclic loads are applied to the caisson (Houlsby et al. 2005) or where large lateral displacements of the caisson occur (Huang et al. 2003).

Based on visual observations following completion of the tests, there was visible gapping on the backside for S1-T03, S2-T06 and S2-T08 (Figure 4.14). The point at which gapping was initiated during the load progression is unknown as video camera positioning and clarity of water over top of the soil model were not ideal for this type of observation. Gapping may have occurred for various reasons, including large lateral displacements or uplift failure of the caisson due to shearing at the soil structure interface Potentially, gapping observed for each test may not have been caused by the same mechanism, as evidenced by difference in the appearance of the sample surface at failure for tests S1-T03, S2-T06 and S2-T08. In tests S1-T03 and S2-T06, there were obvious ‘slumps’ in the sample behind the caisson (opposite to direction of resultant load at failure; Figure 4.14 a), and b)). In test S2-T08, the sample appeared to have tension cracks behind the caisson rather than a ‘slump’ (Figure 4.14 c)).

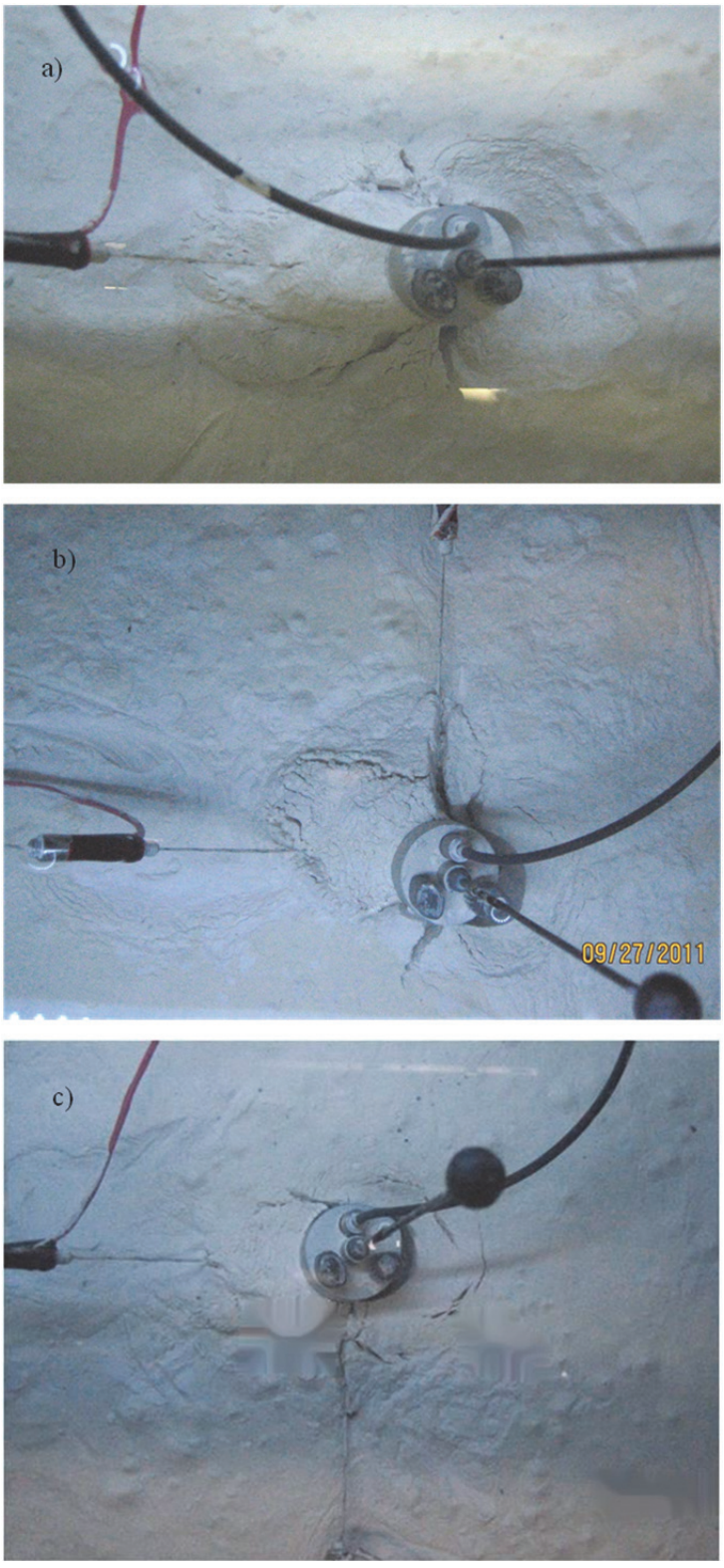

Figure 4.14. Photos of post-post monotonic failure sample surfaces for LMLA tests. (a) S1-T03; (b) S2-T06; (c) S2-T08.

4.5.7. Summary of Behavior

Behavior of suction caissons for three configurations of cyclic loading are compared in terms of accumulated displacement, caisson rotation and pore pressure response. Initially, a higher rate of displacement accumulation occurs in double line cyclic-cyclic tests when compared to double line cyclic sustained test. The result of the higher rate of displacement accumulation is a higher total displacement occurring in the cyclic-cyclic test than in the cyclic-sustained test. Rotation of a suction caisson during loading indicates that the pad eye location is not optimized, therefore the maximum load resistance of the caisson is not mobilized. Pore pressure response during cyclic loading is also cyclic, with mean pore pressure trend that decreases on initiation of cyclic loading, increases towards hydrostatic pressure, then decreases steadily.

Post-cyclic monotonic behavior and strength of a suction caisson previously subjected to three configurations of cyclic loading are described through load-displacement behavior, peak monotonic load resistance, and physical disturbance observations. During post-cyclic monotonic loading, P-δ relationship resembles two adjoined linear components. The first linear component M_{pc1} is steeper than M_{in}, whereas the second linear component M_{pc2} is less steep than M_{in}. Greater increase in M_{pc1} relative to M_{in} occurs where cyclic preload was applied in the same direction as the post-cyclic monotonic load. Greater decrease in M_{pc2} relative to M_{in} occurs where cyclic preload is applied only in the direction orthogonal to the monotonic load to failure. For all tests Peak monotonic load resistance is increased by cyclic preloading. The largest increase of P_{peak} occurred where cyclic preloads were applied in the same and orthogonal to the direction of monotonic load to failure. Gap formation on the soils adjacent to the backside of the caisson occurred in all LMLA tests. Cause of the gap formation is unknown although it appears, from the variations in the soil surface at failure, causes may have differed between single cyclic, cyclic-sustained and cyclic-cyclic tests.

4.6. Effects of Increased Cyclic Load Amplitude on Double Line Loading

A second series of single line cyclic, double line cyclic-sustained, and double line cyclic-cyclic tests were performed with increased cyclic load amplitude to observe effects on load-displacement (P-δ) behavior, accumulated permanent cyclic displacement (δ), caisson rotation ($\varkappa$ and ψ) post-cyclic peak monotonic load resistance (P_{peak}) and pore pressure response (u). Mean load was maintained similar to the initial set of cyclic tests while cyclic load amplitude was increased, thus the test set is designated 'Low Mean High Amplitude' (LMHA). A summary of loads applied in each of the single line cyclic (S2-T05), double line cyclic-sustained (S2-T07), and double line cyclic-cyclic (S2-T09) tests is provided in Table 4.3. All LMHA tests were performed in soil sample 2 (Figure 3.13).

Actual loading for each line is shown in Table 4.3. Actual loads applied to the load lines vary from the intended loads due to testing conditions, the magnitude of 'zero load' identified as the point at which caisson loading begins (Figure 4.9) and the capability of the actuators to maintain a load-controlled sinusoidal load function. Similar conditions were maintained as closely as possible between tests, however differences in length of line slack, caisson installation depth and depth of water, resulted in variations in the 'zero load' for each test. Since 'zero load' was determined only in post processing only an estimate of the zero load was able to be made during testing, resulting in initial and mean load values different than intended. Amplitude of load cycles should have been maintained by the actuator – digital data acquisition and control system, however, due to equipment operating error amplitudes were also different than intended. The differences between actual and intended loads affect the suction caisson response, however, due to the limited tests performed in this program, the effect is not defined. For the purpose of analysis, the effects of these differences are ignored, but in order to confirm results, additional tests are required.

Load-displacement (P-δ) slope (M_{in}) during the initial monotonic loading of the first load line to the mean or sustained loads tended to be lower, but more consistent in higher amplitude

tests than in lower amplitude tests (Table 4.2; Figure 4.10). The maximum difference in M_{in} values for loading of the first line in high amplitude tests was 18%, which occurred between S1-T05 and S2-T07-L1. Standard deviation of M_{in} was 0.85, 7.9% of the mean M_{in} for tests S1-T05, S2-T07 and S2-T09. Consistent values of M_{in} were expected for all low mean tests, including both high and low amplitude cyclic tests (no load variables were manipulated to this point), however the mean value of M_{in} for loading of the first line in high amplitude tests was 84% of M_{in} of low amplitude tests. M_{in} values for the second load line in high amplitude cyclic tests (S2-T07-L2 and S2-T09-L2) were also lower, and similarly consistent in comparison to low amplitude cyclic tests. For loading of the second load lines, standard deviation of M_{in} was 0.21, 2.0% of the mean M_{in} for S2-T07-L2 and S2-T09-L2. Values of M_{in} for second load lines were also expected to be consistent for all low mean tests, however, the mean M_{in} of the second load line in the high amplitude tests was also 84% of M_{in} of low amplitude tests.

Increased cyclic load amplitude tended to result in steeper P-δ slope during post-cyclic monotonic loading (M_{pc1}) relative to initial P-δ slope (M_{in}) (Table 4.2; Figure 4.10). For single line cyclic tests, M_{pc1} is 209% of M_{in} in high amplitude test (S2-T05), whereas M_{pc1} is 176% of M_{in} for low amplitude test (S1-T03). For cyclic-sustained tests, M_{pc1} is 208% and 141% of their respective M_{in} values for high amplitude (S2-T07) and low amplitude tests (S2-T06), respectively. For cyclic-cyclic tests M_{pc1} is 262% and 188% of the respective M_{in} values for high amplitude and low amplitude tests, respectively. The greater increase in initial P-δ slope during post-cyclic monotonic loading in high amplitude tests indicates a greater increase in stiffness response for caisson anchors previously subjected to high amplitude cyclic when compared to caisson anchors subjected to low amplitude cycling.

Higher amplitude cyclic preloading typically resulted in lower changeover points (P_x) between first and second linear components of the P-δ slope during post-cyclic monotonic loading, than in corresponding lower amplitude cyclic tests (Table 4.2; Figure 4.10). For single line cyclic tests, P_x occurred at 141% of $P_{cy,max}$ in high amplitude cyclic tests, whereas P_x occurred

at 156% of $P_{cy,max}$ in low amplitude cyclic tests. For cyclic-sustained tests, P_x occurred at 81% and 85% of the respective $P_{cy,max}$ values for high amplitude and low amplitude cyclic tests, respectively. For cyclic-cyclic tests, P_x occurred at 102% and 109% of the respective $P_{cy,max}$ values for high amplitude and low amplitude cyclic tests, respectively. The decreases in P_x relative to $P_{cy,\,max}$ for tests with higher amplitude cyclic preloading are relatively small, indicating only slight reduction of the point during post-cyclic monotonic loading load where the P-δ response softens.

There were similar reductions in the steepness of the second linear component of P-δ slope of post-cyclic monotonic loading (M_{pc2}), relative to $M_{in,}$ for higher amplitude and lower amplitude tests (Table 4.2; Figure 4.10). For single line cyclic tests, M_{pc2} is 84% of M_{in} in high amplitude test (S2-T05), whereas M_{pc2} is 81% of M_{in} for low amplitude test (S1-T03). For cyclic-sustained tests, M_{pc2} is 63% and 61% of M_{in} for high amplitude (S2-T07-L2) and low amplitude (S2-T06-L2) tests, respectively. For cyclic-cyclic tests M_{pc2} is 81% and 68% of the respective M_{in} values for high amplitude and low amplitude tests, respectively. Increase in cyclic pre-loading amplitude does not appear to have a definitive effect on the softening P-δ response occurring after P_x has been exceeded during the post-cyclic monotonic loading.

Cycling at higher amplitude resulted in higher initial displacement accumulation rate (δ-n slope) (Figure 4.11). Based on results from cyclic-sustained tests S2-T06 and S2-T07, initial displacement accumulation rate (secant, n = 0 to 20) for high amplitude cyclic-sustained δ-n slope was 600% of the rate resulting from cycling at lower amplitude. In both high and low amplitude tests rate of displacement accumulation decreased with increasing number of cycles until an approximately constant rate was reached at 300cycles. There was greater reduction in δ-n slope for the higher amplitude test, resulting in a lower rate of displacement accumulation in the higher amplitude test at a high number of cycles. Between 440 and 540 cycles, δ-n secant slope of high amplitude test S2-T07 was 91% δ-n secant slope for low amplitude test S2-T06. Progression of accumulated displacement of double line cyclic-cyclic test S2-T09 were not used for comparison,

due to irregular negative δ-n secant slope after 140 cycles that was not observed in any other tests. Although the pattern of rate of accumulation of displacement from test S2-T09 did not appear consistent with other tests, the measured total displacement is provided (Table 4.4) for reference, although values may be errant.

Fewer cyclic load repetitions at higher amplitude were required to attain a given displacement in comparison than lower amplitude load cycles (Figure 4.11). For double line cyclic-sustained tests the number of cycles required to reach 50% of the total accumulated cyclic displacement (δ_{cyc}) was 35 cycles ($n_{50} = 35$) and 80 cycles for high amplitude and low amplitude tests, respectively.

Higher amplitude cyclic loading resulted in more accumulated permanent displacement during cyclic loading (Table 4.4; Figure 4.11). Total permanent cyclic displacement (δ_{cyc}) accumulated after 540 cycles in the direction of the line undergoing cyclic loading at high amplitude (S2-T07-L1) was 246% of δ_{cyc} for the low amplitude cyclic test, S2-T06-L1. For cyclic-cyclic tests, δ_{cyc} accumulated for line 1 and line 2 of high amplitude test S2-T07 was 124% and 100% of the corresponding δ_{cyc} values of low amplitude test S2-T06. Based on these results, it appears that increased amplitude of cyclic loading on a caisson anchor results in increased accumulation of permanent displacement, for a given number of cycles.

Increased cyclic load amplitude does not appear to have a unique effect on the amount of permanent cyclic displacement relative to total displacement at peak post-cyclic monotonic load (failure). Permanent cyclic displacement accumulated during cyclic loading (δ_{cyc}) for L1 and L2 of high amplitude cyclic-sustained test S2-T07 are 7.7% and 0.6% of the respective δ_{peak} values, respectively. Permanent cyclic displacement accumulated during cyclic loading (δ_{cyc}) for L1 and L2 of low amplitude cyclic-sustained test S2-T06 are 3.4% and 2.2% of the respective δ_{peak} values, respectively.

Permanent caisson rotation occurring during cyclic loading was similar in higher load amplitude and lower cyclic load amplitude tests. For high amplitude and low amplitude cyclic-

sustained tests, S2-T07 and S2-T06, no caisson rotation was accumulated during cyclic loading (applied only to the orthogonal line) in the direction orthogonal to the cyclic load (ψ), however, accumulated rotation in the direction of the cyclic loading (ϰ) for high amplitude test S2-T07 was twice rotation accumulated for low amplitude test S2-T06 (Table 4.4; Figure 4.15). For cyclic-cyclic tests, high amplitude cycling resulted in accumulated rotation in the direction of cycling (ψ) and accumulated rotation in the second direction of cycling (ϰ) were 125% and 114% of the respective rotations for low amplitude tests.

Caisson rotation during post-cyclic monotonic load to failure progressed similarly in high amplitude test S2-T09 as in the low amplitude test S2-T06 (Figure 4.15). The rate of increase in ψ was similar between the two tests, likely dominated by the rate of loading (0.1 mm/s) rather than the amplitude of the cyclic pre-load applied, or the concurrent cyclic load applied in the orthogonal direction. The progression of caisson rotation (ψ) during post-cyclic monotonic loading in high amplitude cyclic-sustained test S2-T07 was not consistent with other tests, it is therefore considered an outlier and will not be discussed further. Progression of caisson rotation in the x-z plane (ϰ) and y-z plane (ψ) for test S2-T09 are provided in Figure 4.15 c) and d)

Cyclic pre-loading with high cyclic amplitude resulted in higher post-cyclic peak monotonic load resistance in comparison to tests with low cyclic amplitude pre-loading (Table 4.3). For single line cyclic tests, P_{peak} is 155% and 126% of their respective $P_{mn,peak}$ values, for high amplitude and low amplitude cyclic tests, respectively. For cyclic-sustained tests, P_{peak} is 134% and 118% of their respective $P_{mn,peak}$ values, for high amplitude and low amplitude cyclic tests, respectively. For cyclic-cyclic tests, P_{peak} is 131% and 122% of their respective $P_{mn,peak}$ values, for high amplitude and low amplitude cyclic tests, respectively. Based on these results, increased cyclic load amplitude (about a given mean load) results in increased post-cyclic peak monotonic load resistance.

When total resultant loads are considered, higher amplitude cyclic pre-loading results in even greater increases of post-cyclic monotonic load resistance (Table 4.6; Figure 4.13). For

cyclic-sustained tests, the resultant load at peak resistance ($P_{re,peak}$) were 171% and 152% of the respective $P_{mn,peak}$ for high amplitude (S2-T07) and low amplitude tests (S2-T06), respectively. For cyclic-cyclic tests, the resultant load at peak resistance ($P_{re,peak}$) were 171% and 153% of the respective $P_{mn,peak}$ for high amplitude and low amplitude tests, respectively. Resultant peak resistance for double line high amplitude cyclic tests also correlated well with angle of sweep of resultant load vectors, where larger sweep angles resulted in increased resultant peak resistance.

The general trend of pore pressure response in tests with higher cyclic amplitude was similar to pore pressure response for tests with lower cyclic amplitude (Figure 4.8). During the monotonic load components of the cyclic tests (initial loading of line 1/line 2 and loading to failure), pore pressure response is similar to response observed in baseline monotonic tests. During cyclic loading, as the cyclic load magnitude follows a symmetric sinusoidal waveform about a constant mean, pore pressure response correlates to both temporary cyclic displacement and progressive displacement accumulation. The range of pore pressure induced during cyclic loading is greater in tests with higher amplitude cyclic loading. For double line cyclic-sustained tests, the pore pressure range generated in high amplitude test S2-T07 is twice the pore pressure range generated in low amplitude test S2-T06. For double line cyclic-cyclic tests, the pore pressure range generated in high amplitude test S2-T09 is three times the pore pressure range generated in low amplitude test S2-T08.

No gapping was observed on the backside of the caisson for tests S1-T05, S2-T07, or S2-T09 (Figure 4.17). In S1-T05, a tension crack set back from the backside of the caisson was visible, however in tests S2-T07 and S2-T09, ‘slumps’ and associated depressions were observed on the backside of the caisson. Differences in sample surface in front of the caisson, in comparison to the low amplitude tests, were most obvious for tests S2-T07 and S2-T09. In both S2-T07 and S2-T09, the areas of affected sample surface were larger than in corresponding tests S2-T06 and S2-T08.

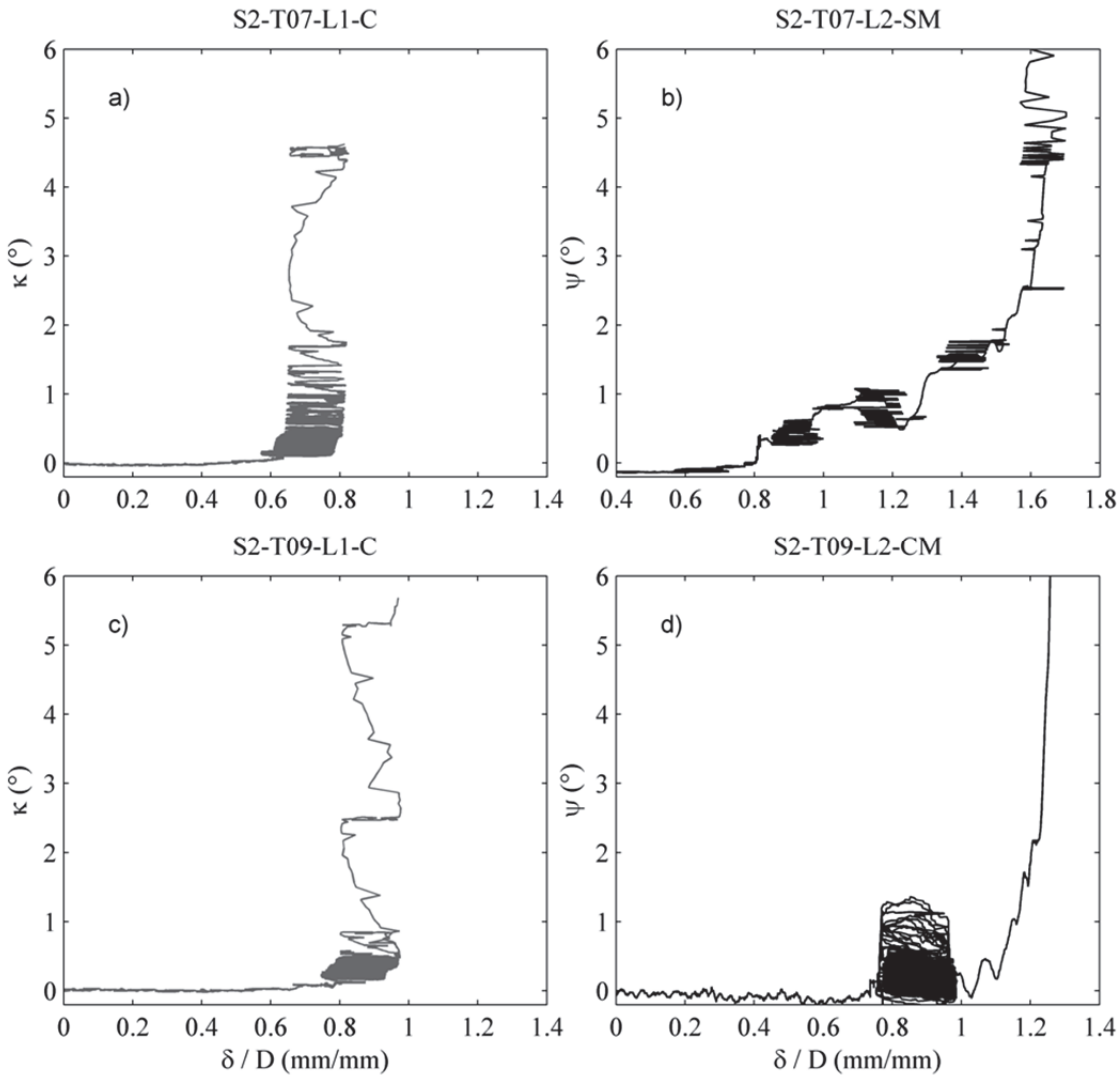

Figure 4.15. Progression of suction caisson rotation relative to normalized line displacement for Low Mean High Amplitude cyclic tests.

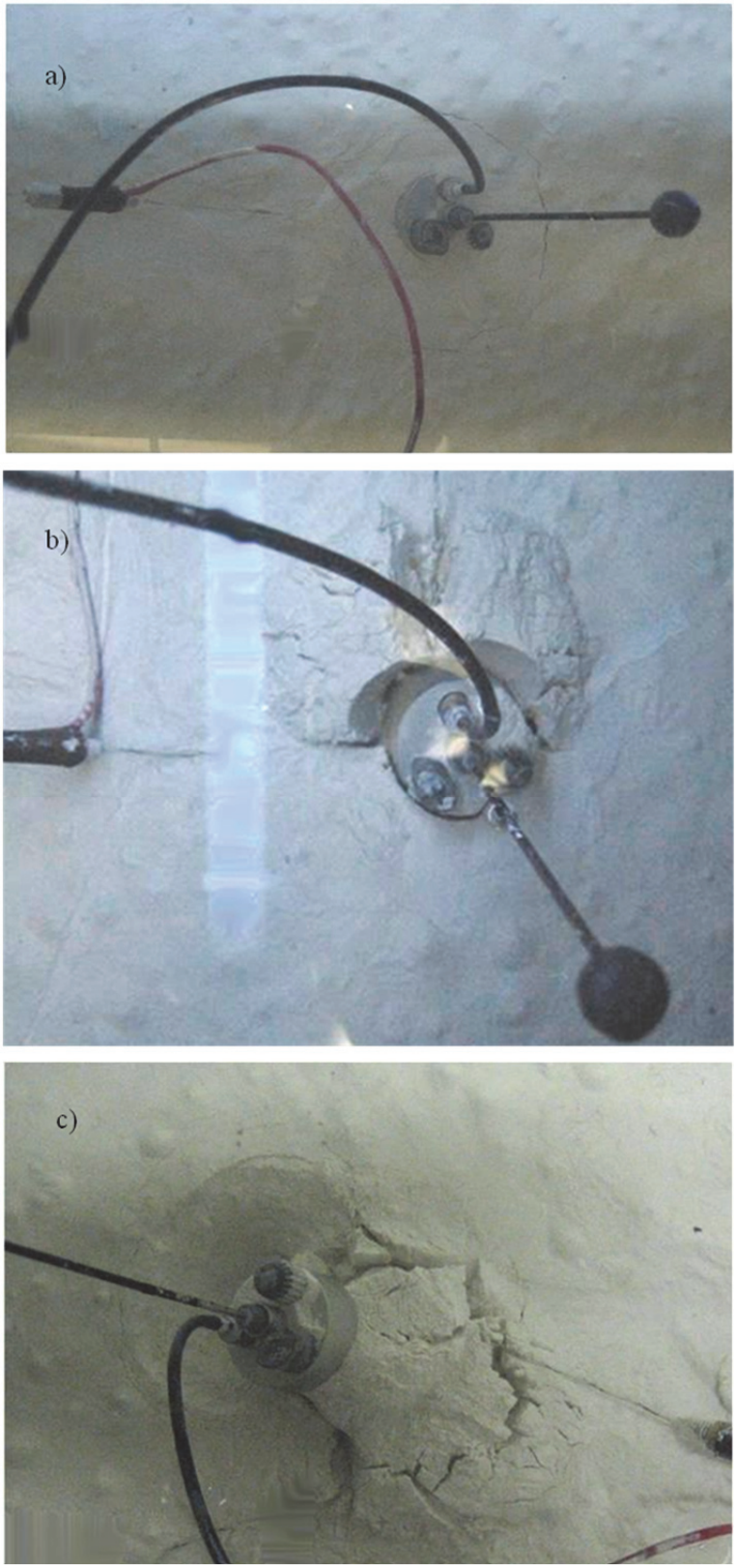

Figure 4.16. Photos of post-post failure sample surfaces for LMHA tests.
(a) S1-T05; (b) S2-T07; (c) S2-T09.

4.7. Effects of Increased Cyclic Mean Load on Double Line Loading

A second series of single line cyclic, double line cyclic-sustained, and double line cyclic-cyclic tests were performed with increased cyclic mean load to observe effects on load-displacement (P-δ) behavior, accumulated permanent cyclic displacement (δ), caisson rotation ($\varkappa$ and ψ) post-cyclic peak monotonic inclined load resistance (P_{peak}) and pore pressure response (u). Load amplitude was maintained similar to the initial set of cyclic tests (LMLA) while cyclic mean load was increased, thus the test set is designated 'High Mean Low Amplitude' (HMLA). A summary of loads applied in each of the single line cyclic (S2-T13), double line cyclic-sustained (S2-T11), and double line cyclic-cyclic (S2-T10) tests is provided in Table 4.3. All LMHA tests were performed in soil sample 2 (Figure 3.13).

Load-displacement (P-δ) slope (M_{in}) during the initial monotonic loading of the first load line to the mean or sustained loads tended to be more consistent in higher mean load tests than in lower mean load tests (Table 4.2; Figure 4.10). The maximum difference in M_{in} values for loading of the first line in high mean low amplitude tests was 3% which occurred between single line (S2-T13) and cyclic-sustained test (S2-T11). Standard deviation of M_{in} was 0.17, 1.7% of the mean M_{in} for test S1-T13, S2-T11 and S2-T1. M_{in} values for Line 2 of the double line tests (S2-T11 and S2-T10) were consistent, and on average, 80% of M_{in} of low amplitude tests.

Increased cyclic mean load tended to result in steeper P-δ slope during the first part of post-cyclic monotonic loading (M_{pc1}) relative to initial P-δ slope (M_{in}) (Table 4.2; Figure 4.10). For single line cyclic tests M_{pc1} is 250% of M_{in} in high cyclic mean load test (S2-T13), whereas, M_{pc1} is 176% of M_{in} low cyclic mean load test (S1T03). For cyclic-sustained tests, M_{pc1} is 211% and 141% of their respective M_{in} values for high mean (S2-T11) and low mean tests (S2-T06), respectively. For cyclic-cyclic tests M_{pc1} is 262% and 188% of the respective M_{in} values for high amplitude and low amplitude tests, respectively. The greater increase in initial P-δ slope during post-cyclic monotonic loading in high amplitude tests indicates a greater increase in stiffness

response for caisson anchors previously subjected to cycling about a high mean load when compared to caisson anchors subjected to cycling about a low mean load.

Higher mean load cyclic preloading typically resulted in lower changeover points (P_x) between first and second linear components of the P-δ slope during post-cyclic monotonic loading, than in corresponding lower mean cyclic load tests (Table 4.2; Figure 4.10). For single line cyclic tests P_x occurred at 141% of $P_{cy,max}$ in high mean test (S2-T13), whereas P_x occurred at 156% of $P_{cy,max}$ in low mean tests (S1-T03). For cyclic-sustained tests, P_x occurred at 83% and 85% of the respective $P_{cy,max}$ values for high mean and low mean tests, respectively. For cyclic-cyclic tests, P_x occurred at 92% and 109% of the respective $P_{cy,max}$ values for high mean (S2-T10) and low mean cyclic (S1-T08) tests, respectively. The decreases in P_x relative to $P_{cy,\,max}$ for tests with higher mean cyclic preloading are relatively small, indicating only slight reduction of the point during post-cyclic monotonic loading load where the P-δ response softens.

There were similar reductions in the steepness of the second linear component of P-δ slope of post-cyclic monotonic loading (M_{pc2}), relative to $M_{in,}$ for higher mean and lower mean tests (Table 4.2; Figure 4.10). For single line cyclic tests, M_{pc2} is 76% of M_{in} in high mean test (S2-T05), whereas M_{pc2} is 81% of M_{in} for low amplitude test (S1-T03). For cyclic-sustained tests, M_{pc2} is 82% and 61% of M_{in} for high mean (S2-T11) and low mean (S2-T06) tests, respectively. Although M_{pc2} of S2-T11 may not be as precise since the P-δ line has a larger radius of curvature at P_x and the duration of loading over this P-δ is short (see Figure 4.10 h). For cyclic-cyclic tests M_{pc2} is 84% and 68% of the respective M_{in} values for high mean and low mean tests, respectively. Increase in cyclic pre-loading amplitude does not appear to have a definitive effect on the softening P-δ response which occurs after P_x is exceeded during the post-cyclic monotonic loading.

Cycling about a higher mean load resulted in higher initial displacement accumulation rate (δ-n slope) (Figure 4.11). Based on results from cyclic-sustained tests S2-T06 and S2-T11, initial displacement accumulation rate (secant, n = 0 to 20) for high mean cyclic-sustained δ-n

slope was 280% of the rate resulting from cycling about a lower mean. In both high mean and low mean tests, rate of displacement accumulation decreased with increasing number of cycles until an approximately constant rate was reached at 350 cycles. There was greater reduction in δ-n slope for the higher mean test, resulting in a lower rate of displacement accumulation in the higher mean test at a high number of cycles. Between 440 and 540 cycles, δ-n secant slope of high mean test S2-T11was 73% δ-n secant slope for low mean test S2-T06. Progression of accumulated displacement of double line cyclic-cyclic test S2-T10 was not used for comparison, due to inconsistencies in cyclic load frequency caused by equipment errors. Although the pattern of rate of accumulation of displacement from test S2-T10 did not appear consistent with other tests, the measured total displacement is provided (Table 4.4) for reference.

Fewer cyclic load repetitions at higher mean load were required to attain a given displacement in comparison to cycles about lower mean load (Figure 4.11). For double line cyclic-sustained tests the number of cycles required to reach 50% of the total accumulated cyclic displacement (δ_{cyc}) was 60cycles ($n_{50} = 60$) and 80 cycles for high amplitude and low amplitude tests, respectively.

Cycling loading about a higher mean resulted in more accumulated permanent displacement during cyclic loading (Table 4.4; Figure 4.11). Total permanent cyclic displacement (δ_{cyc}) accumulated after 540 cycles in the direction of the line undergoing cyclic loading about a high mean (S2-T11) was 185% of δ_{cyc} for the low amplitude cyclic test (S2-T06). For the case tested, cyclic loading about a higher mean results in increased accumulation of permanent displacement, for a given number of cycles.

Increased cyclic load amplitude does not appear to have a unique effect on the amount of permanent cyclic displacement relative to total displacement at peak post-cyclic monotonic load (failure). Permanent cyclic displacement accumulated during cyclic loading (δ_{cyc}) for L1 and L2 of high mean cyclic-sustained test S2-T11 are 4.2% and 1.9% of the respective δ_{peak} values, respectively. Permanent cyclic displacement accumulated during cyclic loading (δ_{cyc}) for L1 and

L2 of low mean cyclic-sustained test S2-T06 are 3.4% and 2.2% of the respective δ_{peak} values, respectively.

Permanent caisson rotation occurring during cyclic loading was greater in higher mean load tests than in lower cyclic mean load tests (Table 4.4; Figure 4.17). For cyclic-sustained tests, accumulated rotations ψ and $\varkappa$ were 1° and 0.7° greater in high mean test (S2-T11) than in low mean test (S2-T06). For cyclic-cyclic tests, accumulated rotations ψ and $\varkappa$ were 0.3° and 0.2° greater in high mean test (S2-T11) than in low mean test (S2-T06). Therefore, increased suction caisson rotation occurs with increased cyclic mean load which is expected because of the higher load applied to the caisson and the tendency for the caisson to rotate in response to loading.

Cyclic pre-loading about a high mean resulted in some increases and some decreases in post-cyclic peak monotonic load resistance in comparison to tests with low cyclic amplitude pre-loading, depending on the load configuration (Table 4.3). For single line cyclic tests, P_{peak} is 128% and 126% of their respective $P_{mn,peak}$ values, for high mean and low mean tests, respectively. For cyclic-sustained tests, P_{peak} is 105% and 118% of their respective $P_{mn,peak}$ values, for high mean and low mean tests, respectively. For cyclic-cyclic tests, P_{peak} is 115% and 122% of their respective $P_{mn,peak}$ values, for high mean and low mean tests, respectively. Based on these results, increased cyclic mean may result in increased or decreased post-cyclic peak monotonic load resistance depending on the load configuration.

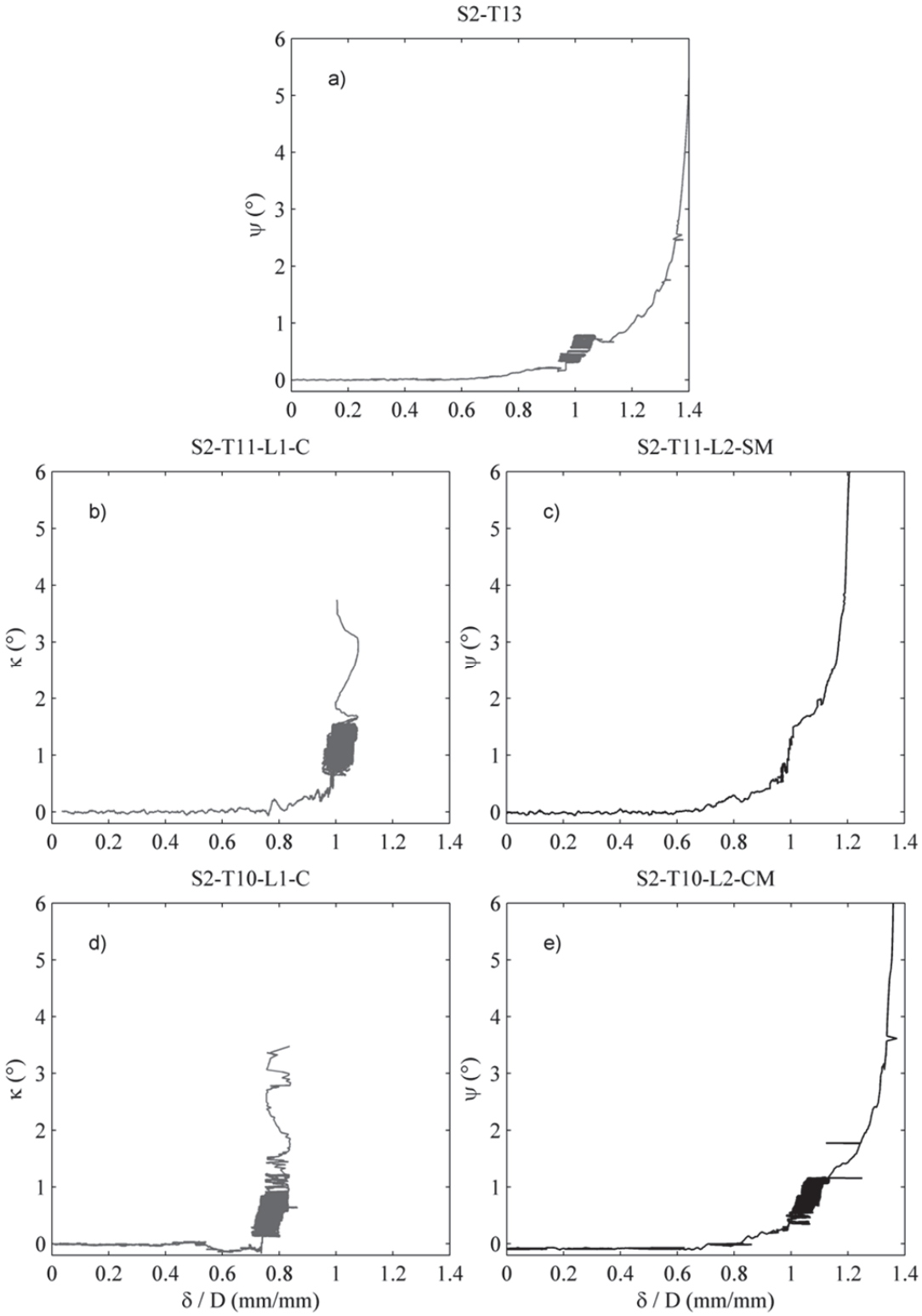

Figure 4.17. Progression of suction caisson rotation relative to normalized line displacement for High Mean Low Amplitude cyclic tests.

When total resultant loads are considered, cyclic pre-loading about a higher mean appears to have minimal effect on post-cyclic monotonic load resistance (Table 4.6; Figure 4.13). For cyclic-sustained tests, the resultant load at peak resistance ($P_{re,peak}$) were 151% and 152% of the respective $P_{mn,peak}$ for high mean (S2-T11) and low mean tests (S2-T06), respectively. For cyclic-cyclic tests, the resultant load at peak resistance ($P_{re,peak}$) were 155% and 153% of the respective $P_{mn,peak}$ for high mean (S2-T10), and low mean (S1-T08) tests respectively. Resultant peak resistance for double line high mean cyclic tests also correlated well with angle of sweep of resultant load vectors, where larger sweep angles resulted in increased resultant peak resistance.

The general trend of pore pressure response in tests with higher cyclic mean was slightly different than in tests with lower cyclic mean (Figure 4.8). During the monotonic load components of the cyclic tests (initial loading of line 1/line 2 and loading to failure), pore pressure response is similar to response observed in baseline monotonic tests. During cyclic loading, as the cyclic load magnitude follows a symmetric sinusoidal waveform about a constant mean, pore pressure response correlates to both temporary cyclic displacement and progressive displacement accumulation. Whereas there was a decreasing trend for mean pore pressure in low mean tests, the mean pore pressure tended to stability in high mean tests. Pore pressure response during post-cyclic monotonic load to failure was similar between high mean and low mean tests.

Gapping was observed on the backside of the caisson in both double line tests S2-T11 and S2-T10, but not in single line test S2-T13 (Figure 4.18). Contrastingly to previous tests sets, in all three HMLA tests a tension crack appeared, set back from the soil-structure interface at the backside of the suction caisson. In front of the suction caisson (towards loading directions), no failure wedge was obvious in single line test S2-T13, although a crack formed parallel to the loading direction. For tests S2-T11 and S2-T10, areas of soil sample mobilized during monotonic inclined load to failure (in front of caisson) were larger than in corresponding low mean load tests (S2-T06 and S2-T08). The soil within the area affected by failure in test S2-T10, appeared to be in a more brittle condition as indicated by numerous cracks throughout.

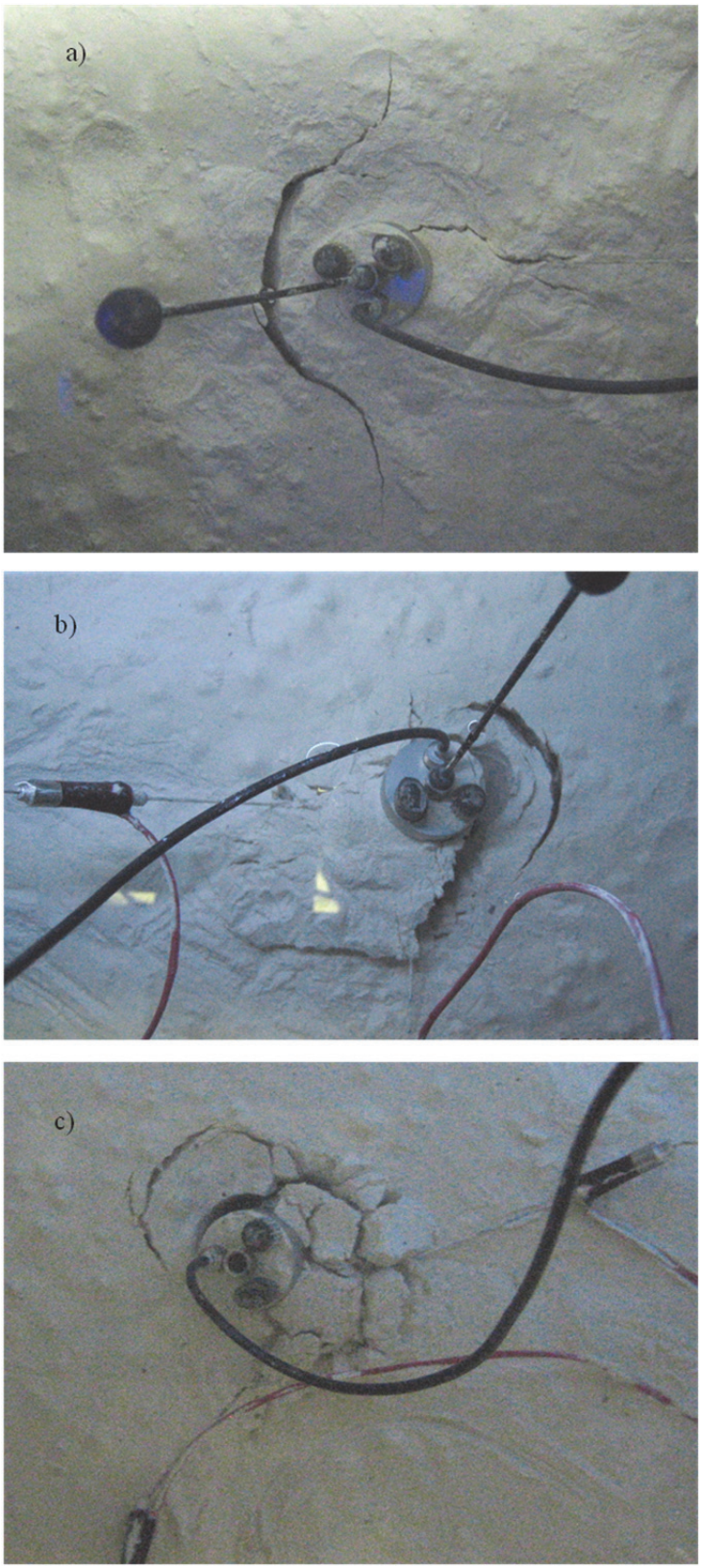

Figure 4.18. Photos of post-post failure sample surfaces for HMLA tests.
(a) S2-T13; (b) S2-T11; (c) S2-T1.

5. DISCUSSION

An assessment of suction caisson capability to resist multi-directional line loads with application to floating offshore wind turbine platforms was conducted through a comparison of single and double line loaded model-scale anchor performance with regard to conditions/requirements of floating wind turbine platforms. This chapter addresses performance of the model suction caisson anchor, limitations of the design, and an assessment of existing methods of design for application to multi-directionally loaded suction caissons.

5.1. Comparison of Orthogonally Loaded and Single Line Loaded Suction Caisson Performance

Monotonic load resistance (without cyclic preloading) was reduced by 4% when an applied load of 54% of peak load resistance was sustained on an orthogonal line. If total resultant load is considered for monotonic load resistance (without cyclic preloading) the resultant monotonic resistance is 31% greater than the reference monotonic single line load resistance. Monotonic resistance for a given line was increased an average of 20% where cyclic pre-loading was applied by orthogonal loads. The increase in monotonic resistance was 36% where cyclic pre-loading was applied only in the same direction of the failure load. If total resultant load is considered for post-cyclic monotonic load resistance with cyclic preloading by orthogonal loads, the average increase of load resistance is 59%.

Acceptable lateral platform displacement (horizontal offset) resulting from mooring system performance depends on platform equipment limitations (DNV 2008). Operational and storm survival criteria for pitch and roll rotational offsets of a wind turbine (Figure 5.1) are typically defined by the turbine manufacturer to maintain efficient operation and appropriate levels of safety (Butterfield et al. 2007; Mercier 2010). The contribution of anchor displacement to platform rotation is dependent on the mooring system configuration. In taut line mooring systems, platform stability is provided through vertical and horizontal tension forces in opposing directions, thus anchor displacements may be particularly significant for these configurations.

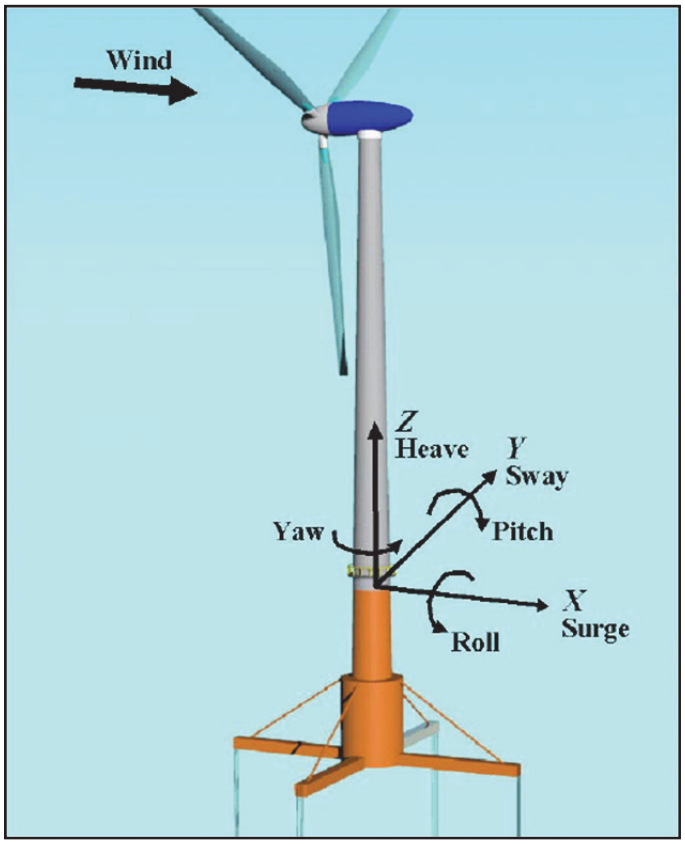

Figure 5.1. Degrees of freedom of a floating wind platform (from Jonkman 2007).

This study performed focused on the taut line mooring configuration. In the majority of double line tests performed in this program, peak resistance was typically attained at maximum resultant displacement of 1.8 D (Figure 4.10). For single line tests, however, peak resistance was attained at line displacement of 1.3 D. Therefore, peak resultant resistance for orthogonal double line loading occurs at larger line displacements in the failure line. Depending on other project specifics such as type of application, mooring line stretch, depth of water, caisson diameter, manufacturer-specified pitch/roll tolerances, etc., the increase in total resultant line displacement occurring from multi-directional loading of suction caissons may or may not be significantly detrimental to the operations. In the case where the equipment manufacturer has smaller tolerances for displacement, an excess 0.5 D anchor displacement and the associated creation of

line slack, may not be acceptable. However, in the case where tolerances are large for equipment motions, a soft response and larger strains would not be problematic.

The API requires mooring test loads to be applied to the anchored mooring line prior to attachment to the floating facility (API 2005). The mooring line is to be loaded to 80% of the identified critical condition loads for a minimum of 15 minutes in order to: ensure sufficient holding capacity, reduce slack in the lines, and aid in detecting damages in the mooring line, anchor or connection (API 2005). Test loading of the mooring line and anchor invokes the displacement response of the mooring line and anchor, potentially resulting in non-recoverable displacements prior to attachment of the platforms. Following attachment of the mooring lines to the platform, the corresponding displacement at the critical condition might be reduced by the previous non-recoverable displacement accumulated; further tests are required to confirm this.

Internal pore pressure during loading of a suction caisson reflects the seal condition (i.e., the capability to maintain a pressure differential between the inside and outside of the caisson) and the resistance mechanisms acting against the vertical component of the applied line load. Where an appreciable pore pressure differential is maintained, the seal is considered intact and additional capacity is provided not only by the differential itself, but by the substantial inverse end bearing mechanism (Figure 2.3) mobilized by the sealed condition. In both single line and double line tests performed in this program, internal pore pressures below the hydrostatic (i.e., suctions) due to the applied loads were induced and maintained throughout the duration of cyclic and post-cyclic monotonic loading. Therefore, for these tests, internal/external pore pressure differential was maintained, as was the pressure differential and resistance to uplift.

5.2. Limitations of Orthogonally Loaded Suction Caisson Model and Tests

Multi-directional line loaded suction caissons are applicable only to catenary/taut/semi-taut mooring systems; they are not a viable option for TLP systems due to vertical tendon configuration. Suction caisson resistance mechanisms are affected by load incline angle, soil

properties, and caisson aspect ratio. Where taut and semi-taut mooring systems have greater load incline angles, vertical resistance mechanisms may dominate. Additional mooring lines on a single caisson in taut and semi-taut mooring configurations will impose resultant loads having greater vertical load components, which will increase the likelihood of failure in vertical uplift. Therefore current pad eye position design may require revising, as the design for optimized lateral resistance may become less critical.

Based on cyclic load tests of a monopile in sand (LeBlanc 2004), the critical resultant cyclic load condition lies between one-way cycling (e.g. cyclic load varies from 0 to some predetermined shear stress level (τ)) and two-way cycling (e.g. cyclic load varying from $-\tau$ to τ). Load amplitudes and directions tested in this research program were one-way only, due to equipment limitations with regard to the complexity of the orthogonal loading progressions. One-way loading may not be representative for all multi-platform wind farm matrices, thus may not be representative of the true critical cyclic loading conditions (between one-way and two way). It is anticipated that the results of this one-way cyclic program may indicate better performance than would be expected for the true condition.

Frequency of cyclic loading in the model tests was 0.15 Hz (except for S1-T03 at 0.5 Hz) equal to a period of 6.76 s/cycle in model time, or 1000 s/cycle in prototype time. Low frequency testing was required due to equipment limitations. The true period of the load cycles would be in the range of 8s to 12s (Andrew Goupee, personal correspondence, 2011). Thus, tests performed were slow cyclic tests and not representative of the true load conditions. As soil strength, and therefore caisson resistance, is load rate dependent the measured peak resistance cannot be scaled directly from model scale to prototype scale.

Mean load and load amplitude were not consistent for all tests in a given series (e.g. LMLA). Within each LMLA, LMHA and HMLA series, P_{mean} varied by up to 23%, 14%, and 13% of the respective intended P_{mean} values, and P_{amp} varied by up to 43%, 33%, and 33% of the respective intended P_{amp} values (Table 3.1; Table 4.3). Inconsistencies can be attributed to two

major factors, equipment error and lack of real time data processing. Equipment error was the main cause of discrepancies in the P_{amp} values. Target load amplitude was digitally programed for each load actuator at the beginning of each test, however, equipment error prevented the true target load amplitude from being adequately attained during testing. Lack of data processing during testing resulted in inconsistent P_{mean} values within a given series. Visual approximation from live graphical tracking of load cell readings was used to identifying the start of caisson loading (Figure 4.9), the target P_{mean} was then set based on that approximation. The resulting inconsistency of P_{mean} and P_{amp} within a given test series renders analysis of results and identification of trends difficult due to the change of multiple variables per test.

All tests were performed with 45° line load inclination angle. In orthogonally loaded double line tests, resultant load inclination angles at failure (resulting from vector addition of two line loads at 45°) varied from 51° to 67°. Load inclinations in the reference single line monotonic tests were maintained at 45°. Caisson rotation was inconsistent between tests, likely a function of the varying load inclinations, the permanent position of the padeye, and the resulting moment applied to the caisson. It is likely that H-V resistance interaction and mobilized failure mechanism were different for each individual test, due to variation of load inclination angle.

As previously discussed (§3.4) kaolin clay was selected as the material for the soil model for its high coefficient of consolidation reducing dissipation time for soil model consolidation, in order to meet test schedule requirements and for comparison to literature. However, there are differences in the properties and behavior of kaolin clay in comparison to natural seabed soils at the Monhegan Island Ocean Energy Demonstration sites. In particular clays from the Monhegan Island site tend to have higher liquid limits, higher plastic limits, lower consolidation coefficient and higher sensitivity (Table 5.1). In comparison to model tests performed in kaolin clay, differences in physical and mechanical soil properties are likely to affect the performance and behavior of suction caisson anchors. For example, higher sensitivity of Monhegan site soils

would result in lower initial shear strength, thus lower load resistance provided by the suction caisson anchors until strength was regained either through thixotropic behavior or installation pore pressure dissipation.

Table 5.1. Summary of Monhegan Island Site clay properties (after Landon Maynard and Chung 2011).

Monhegan Clay Property	**Value**
Liquid Limit, LL (%)	97
Plastic Limit, PL (%)	62
Plasticity Index, PI (%)	35
Specific Gravity, G_s	2.74
Consolidation Coefficient, c_v (m^2/yr.)	1.2
Submerged Unit Weight, γ' (kN/m^3)	4.9
Sensitivity (w = 97%)	4.4

5.3. Evaluation of Existing Design Guidance for Application to Orthogonally Loaded Suction Caissons

Suction caissons are considered a "mature" technology in offshore oil and gas platform foundation design and various design standards have been developed by regulatory bodies, based on the oil and gas experience. These existing design standards for suction caissons are intended for evaluation of capacity and behavior resulting from mooring line loading applied in a single direction. Observation of differences in load resistance and behavior during loading for orthogonally loaded caissons in comparison to single line loaded caissons prompts an evaluation of the applicability these existing standards to multi-line loaded suction caissons.

The two most commonly cited standards addressing design of suction caissons are API RP-2SK (API 2005) and DNV RP-E303 (DNV 2005). API RP-2SK (API 2005) provides general guidance on suction caisson design that is not specific to use of caissons as anchors (flexible connection), implicitly directed to offshore oil and gas industry. Recommended in API RP-2SK (API 2005) are various design methods including Limiting Equilibrium Method (LEM), Finite Element Analysis (FEA), Plastic Limit Analysis and beam-column method. DNV RP-E303 (DNV 2005) provides specific guidance for suction caisson design anchors in clay for floating offshore platforms, although not unique to wind turbine platforms. DNV recommended practice is

not limited to a single method of design, instead suggests specific considerations: soil strength profile, realistic failure mechanisms, horizontal-vertical resistance coupling, 3D effects, soil-structure interface setup effects, and potential vertical crack. DNV RP-E303 (DNV 2005) recommends use of the LEM and/or FEA that address the above issues. LEM is identified as the most commonly used method for estimating capacity, and was developed for use with a single line load and limiting assumptions regarding 3D effects, resistance mechanisms, and design parameters.

In assessing the applicability of existing standards for orthogonally loaded suction caisson anchors there are two key areas for consideration: failure mechanism, and assigned soil parameters. The failure mechanism is the conceptual model of the soil-structure interactions, soil volumes and failure paths providing resistance at the point of failure (taken here to coincide with peak resistance). Relevant soil parameters are those strengths, characteristics and properties assigned to the soil contributing to the failure mechanism.

5.3.1. Evaluation of Failure Mechanism

For a suction caisson loaded in a single direction, DNV RP-E303 (DNV 2005) defines the LEM resistance mechanism to be composed of four major components: active and passive wedge associated with the projected area, soil flow around the bottom of the caisson, shear along the base of the caisson, and side shear along the wedges and side of the caisson (Figure 2.4; §2.1.7). The width of the active and passive soil wedges is approximated as the diameter of the caisson, and the length of the wedges are defined by classic earth pressure theory. The active and passive wedges are oriented parallel to the load direction. The soil volume involved in the reaction mechanism is herein referred to as the zone of influence.

For all orthogonally loaded double line tests (monotonic and cyclic), the resultant load direction (as determined by vector addition) is not constant (Figure 3.4). Conceptually, as the direction of the resultant load changes, the zone of influence changes resulting in a larger total

zone of influence contributing to load resistance throughout the load progression (Figure 5.2). This leads to the question of whether it is only the LEM prescribed zone of influence at the instant of failure that provides load resistance or if there are some other contribution from the total zone of influence that affect peak load resistance. Test results from monotonic double line test (S2-T12) do not appear to support the case that only the LEM-prescribed zone of influence at the instant of failure resists the failure load. Where the sustained load of 54% $P_{mn,peak}$ was applied to one line while the orthogonal line was increasingly loaded, failure would be expected to occur when the load on the orthogonal line reached 62% $P_{mn,peak}$ (by vector addition the resultant load would then be 100% $P_{mn,peak}$) , if zone of influence was limited to the LEM-prescribed failure mechanism. However, failure did not occur until 96% $P_{mn,peak}$ was reached on the orthogonal line. The additional resistance mobilized could indicate an altered reaction mechanism for orthogonal loading, although, due to the difference in resultant load angle at failure in the double line monotonic test compared to the reference monotonic test, further investigation would be required to confirm or dispel this theory.

A visual analysis of post-failure photographs (Figure 4.14; Figure 4.16; Figure 4.18) was performed in attempt to identify lateral extent of failure mechanisms. The failure mechanism for each test was not easily identifiable and estimates / interpretations of zones of influence appeared inconsistent with no recognizable trends. Findings regarding failure mechanism and zone of influence in this program are inconclusive. Further studies including additional modeling with injected dye lines or laboratory testing on samples in orthogonal directions may provide better indication of the failure mechanism and zone of influence contributing to resistance of orthogonal loads.

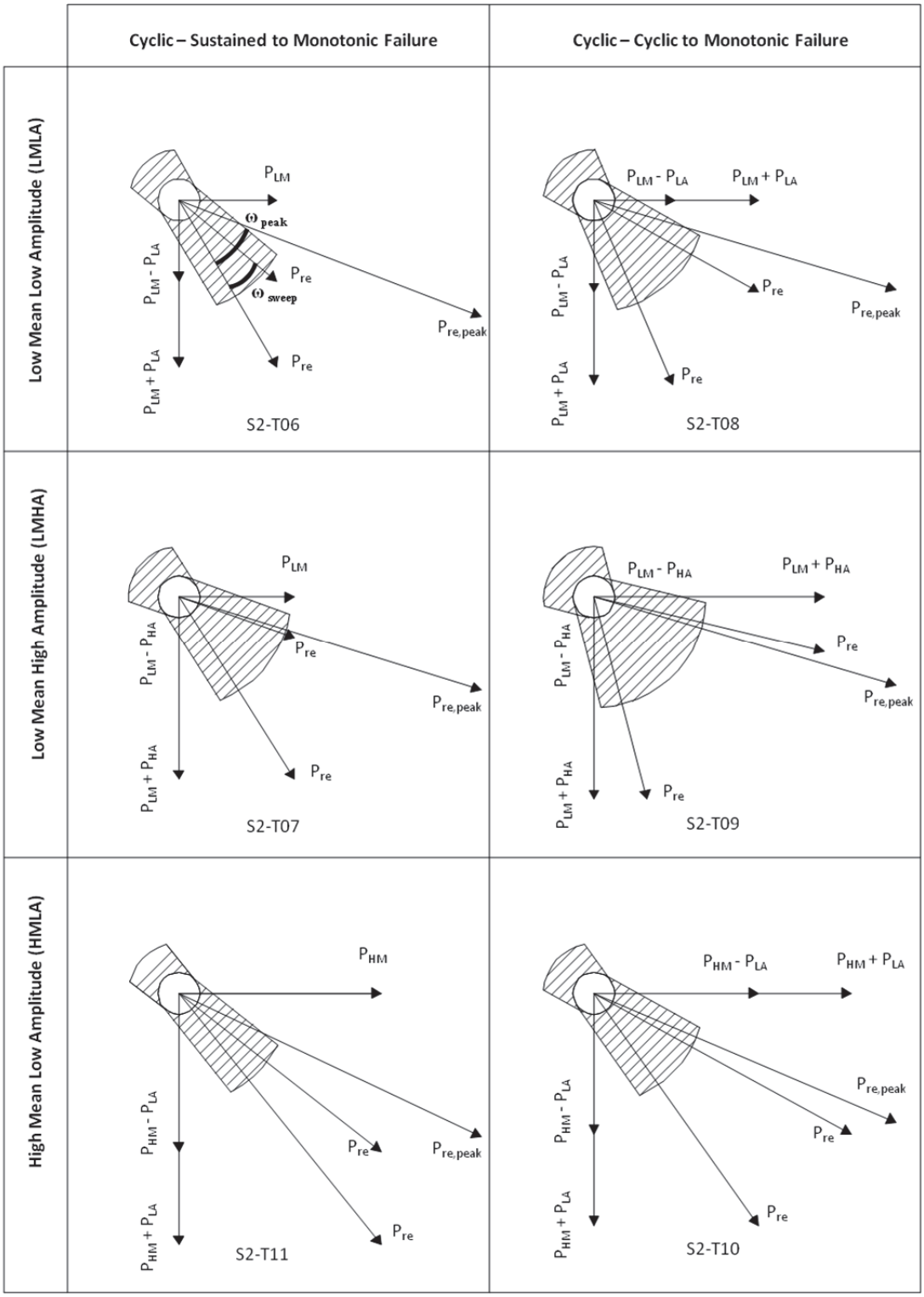

Figure 5.2. Conceptual zone of influence for LEM active and passive wedge components developed during cyclic loading from two orthogonal taut mooring lines (see Figure 3.4).

Another important consideration regarding failure mechanism is the variable load inclination that results from changing x, y, and z-direction load ratios of the orthogonal loads (Figure 5.3). For single line configuration, load inclination remains constant and its effect is incorporated in the LEM through optimized side shear parameters which address Horizontal-Vertical (H-V) resistance interaction for the given soil, and caisson geometry at a specific angle of load inclination (e.g.Figure 5.4). However, during orthogonal loading where the load inclination varies, H-V resistance interaction also varies and would not be adequately addressed through use of constant side shear parameters as suggested by LEM. In this research program, the effect of changing load inclination and H-V resistance interaction could be a contributing factor to the difference between the reference monotonic load resistance (assumed constant 45° load inclination) and the measured load at failure. Depending on the magnitudes of the applied load components, the rate of change in resultant load inclination may be substantial, causing the determination of H-V interaction effect on peak load resistance to be challenging.

Additionally, as indicated in DNV RP-E303 (DNV 2005), there is an optimum pad eye depth for a given load inclination and soil strength profile, that results in translational-only failure and provides maximum load resistance. However, for multi-directional loading, as the resultant load inclination varies, the optimum depth of the pad eye also varies. The physical limitation of a fixed pad eye may result in periods of rotational and translational displacement, which does not follow the assumption for use of the LEM and may not provide maximum load resistance.

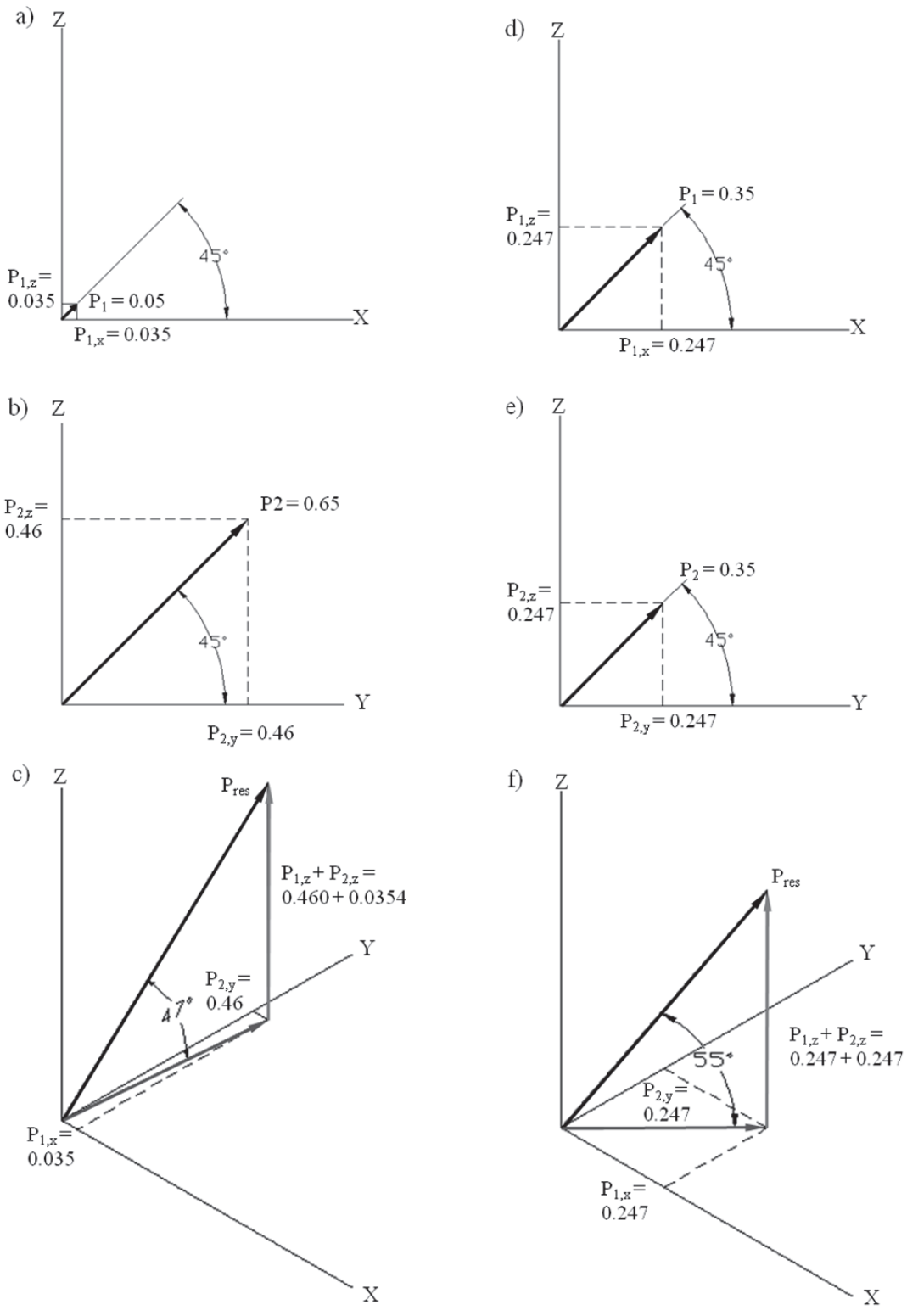

Figure 5.3. Variation of resultant load inclination in LMHA test during cyclic loading

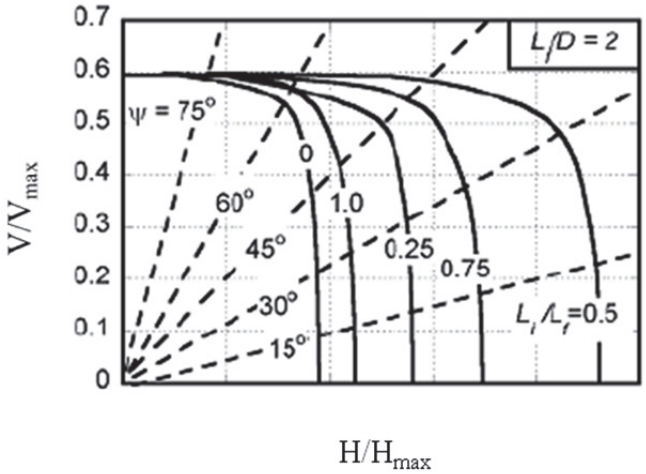

Figure 5.4. Example horizontal-vertical (H-V) resistance interaction diagram. for suction caisson in soil with uniform strength profile, where Vmax and Hmax are the maximum resistances when loaded in purely vertical or purely horizontal directions, respectively(from Aubeny & Murff 2005).

5.3.2. Alternative Failure Mechanism for Evaluation

To overcome some limitations of LEM failure mechanism, another analytical method developed for embedded suction anchors (ESA) may be appropriate for estimation of resistance capacity for suction caissons. ESA resistance analysis is based on force and moment limit equilibrium, which may be more appropriate for multi-directional loading as it takes into account true 3-D behaviors such as development of 3-D normal and shear stresses, a 3-D soil failure wedge, and the rotation response to vertical loading applied at a given pad eye depth (Kwag et al. 2010). The inclined capacity is calculated as the resistance resulting from combination of fractions of the ultimate horizontal and ultimate vertical resistance components (Kim et al. 2009). ESA resistance estimation, similar to LEM, is dependent on the angle of loading, which is variable for out-of-phase cyclic multi-directional loading used in this research program. The importance of this variable resultant load inclination may or may not be significant, depending on the mooring line configuration and properties, water depth, and soil profile.

5.3.3. Evaluation of Recommended Soil Parameter Selection

Selection of soil parameters for engineering analysis and design are typically based on the critical load condition. The critical load condition occurs where the highest loads are applied to the caisson or the lowest factor of safety exists for the caisson design. There is an important difference between the critical load condition for offshore oil and gas and the critical load condition for offshore wind turbine platforms. For oil and gas platforms, the highest applied loads occur during storm conditions. A design storm is designated (typically 3-hour storm with 100 year return period) and the corresponding dead and live loads are identified as critical load conditions (DNV 2005, API 2000). Since offshore wind turbines are non-operational during storm conditions (for protection of the structure and turbine), loads applied to the structure and platform during storm conditions are lower than loads applied during typical operating conditions (Goupee 2010). The critical load condition for offshore floating wind turbine platforms is therefore the long-term operational condition.

Not only does the definition of critical load condition affect the design loads, but also the design soil parameters which are load-dependent and are affected by parameters such as load rate, cyclic load parameters, loading time, etc. For design of offshore oil and gas platform anchors, DNV RP-E303 (DNV 2005) recommends that the undrained cyclic shear strength ($\tau_{f,cy}$) associated with the critical load condition (characteristic design storm) should be used to evaluate the line load resistance of the caissons. This strength is the applied shear stress that causes failure *at the number of cycles defined by the design storm*, and is a function of average shear stress, cyclic shear stress amplitude, and load frequency (Andersen 2009). Based on studies of cyclic loading on Drammen Clay (Andersen 2009), $\tau_{f,cy}$ is less than the monotonic (static) undrained shear strength (τ_f) for typical conditions of a 3 hour storm having 500 to 1000 cycles.

The DNV RP-E303 determined undrained shear strength may not be appropriate for design of anchors for floating offshore wind turbine platforms, where the critical load condition is the operational condition and involves *an essentially unlimited number of load cycles*. Instead, a

more appropriate definition of $\tau_{f,cy}$ for the critical operational condition might be the "stability threshold" (Lefebvre & LeBoeuf 1989), also referred to as 'threshold cyclic stress ratio' (Sangrey et al 1978) or 'critical level of repeated loading (CLRL)' (Chaney & Fang 1986). All three terms reference a similar concept: the load at which continued cycling does not cause further degeneration of soil structure or strength with increasing number of cycles (Figure 5.5). Use of the CLRL as the $\tau_{f,cy}$ would imply non-failure at any applied cyclic stress below $\tau_{f,cy}$, even with ongoing (unlimited) cycling, and progressive failure at any cyclic stress greater than $\tau_{f,cy}$.

All tests performed in this research program involved cyclic loads below CLRL of kaolin clay, as indicated by pore pressure and strain response which attained equilibrium states in all cyclic tests. Where the CLRL is not exceeded, an equilibrium is reached during cyclic loading where no further degradation (strain accumulation) results. In all nine cyclic tests, equilibrium state in both strain and pore pressure with continued cycling was reached (Figure 4.8).

A separate, but related issue is the effect of cycling at a level below the CLRL on the post-cyclic peak monotonic load resistance. Whereas cyclic loading at levels greater than the CLRL have been shown to reduce undrained shear strength due to the accumulation of pore pressure and the approach of the failure envelope(Andersen 1975; Castro & Christian 1976), cyclic loading below the CLRL(as addressed previously), typically results in post-cyclic monotonic failure at similar or greater applied stresses than without cyclic preloading (Lefebvre et al. 1989; Moses & Rao 2007; Dutt et al. 1992), as illustrated in Figure 5.6. The failure envelope is not modified by the undrained cyclic loading, however, the stress path differs from that of a normally consolidated monotonic loading without cyclic pre-loading. The latter stress paths resemble those of overconsolidated materials (Figure 5.7), resulting in undrained shear strengths not reduced by the accumulated pore pressure (Hyde & Ward 1985; Matsui et al. 1980; Yasuhara et al. 1992). This maintenance or increase of undrained shear strength throughout cyclic loading was observed in all tests performed in this program. For all nine cyclic tests performed, the post-cyclic monotonic peak resistance exceeded the reference monotonic peak resistance

without cyclic preload. This concept of maintained undrained shear strength with accumulated, stabilized pore pressures should be considered in designing offshore wind turbine platform anchors. Where the post-cyclic monotonic undrained shear strength is increased by the undrained cyclic loading, use of the CLRL as $\tau_{f,cy}$ is conservative.

Where cyclic preloading below the CLRL results in apparent overconsolidation and increased s_u, it would logically follow that the lateral extent of increased s_u is defined by the region subjected to cyclic preload. Based on interpretation of LEM caisson failure mechanism as the zone of influence of a load at a given instant, the total zone of influence is the cumulative region inclusive of all reaction mechanisms invoked throughout a load progression and this region is the extent of s_u increase (Figure 5.2). It would be expected then, that if a caisson previously subjected to cyclic preloading below CLRL is loaded to failure, a higher resistance would be attained if the failure load was applied in a direction such that the reaction mechanism at failure was contained within the total zone of influence of the cyclic preloading. In terms of this test program, ω_{sweep} indicates the angular range of resultant load direction, a larger ω_{sweep} results in a larger total zone of influence, therefore a larger later extent of increased s_u. If ω_{peak} is less than ω_{sweep}, the failure mechanism would be fully contained within the extent of increased s_u and the peak load resistance should be highest in this case. As ω_{peak} increases with respect to ω_{sweep} the peak load resistance should decrease as the failure mechanism is no longer contained within the region of s_u increase. This trend is modeled in the test results, as the highest load resistance was measured in the only test where ω_{peak} was less than ω_{sweep}, and as ω_{peak} increases relative to ω_{sweep} the measured peak load resistance decreases (Table 4.6; Figure 3.5). It appears that orthogonal cyclic preloading resulting in ω_{sweep} encompassing ω_{peak} results in the highest load resistance, however, load inclination effects should be further investigated.

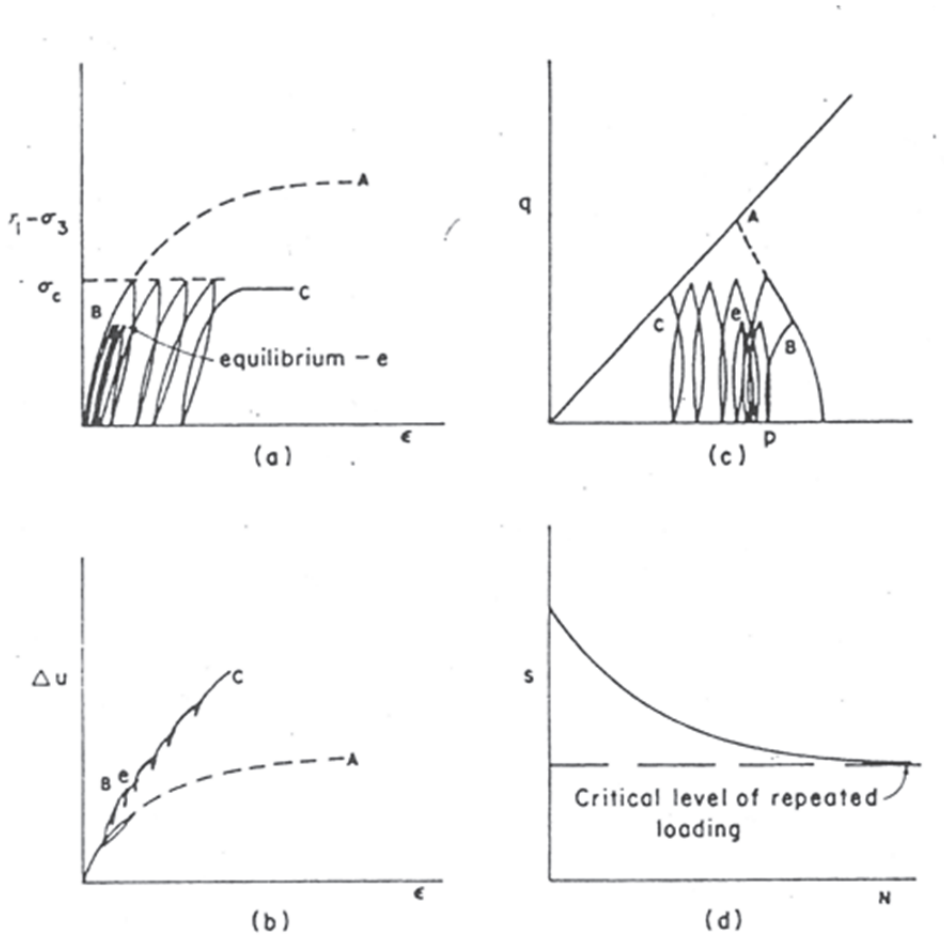

Figure 5.5. General behavior of soils subjected to three different loading conditions. Represented by a) stress-strain behavior; b) change in pore pressure with strain; c) stress path; d) cyclic stress (s) vs number of cycles to failure. For load condition (A) monotonic load; (B) cyclic load (below CLRL) reaching equilibrium state; (C) cyclic load (above CLRL) proceeding towards failure state (from Chaney & Fang 1986)

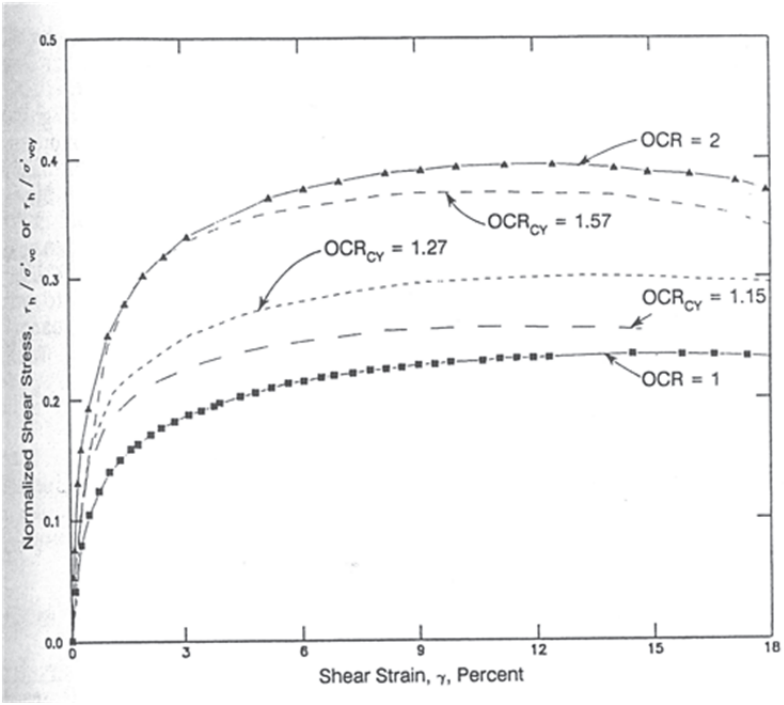

Figure 5.6. Stress-strain data from post-cyclic monotonic tests compared to reference monotonic tests on overconsolidated Gulf of Mexico clay (Garden Banks Area) (from Dutt et al. 1992).

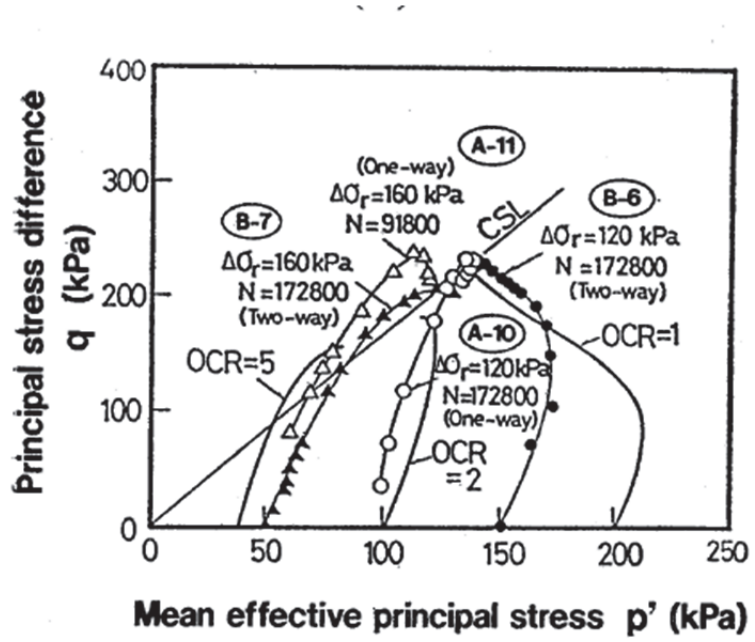

Figure 5.7. Effective stress paths of post-cyclic monotonic triaxial tests on normally consolidated Ariake clay compared to stress paths of overconsolidated Ariake clay with σ'_p = 200 kPa, ($\Delta\sigma_r$ = 2 τ_{amp}) (from Yasuhara et al. 1992).

6. CONCLUSION

This chapter provides a summary of the research program, conclusions about the performance and behavior of suction caisson anchors loaded with orthogonal lines and suggests additional concepts for further research.

6.1. Summary of Research Program

Physical modeling of suction caissons with aspect ratio L/D = 2, in normally consolidated kaolin clay, was conducted in a geotechnical centrifuge to assess resistance and behavior when subjected to non-catastrophic cyclic loads from two orthogonal load lines at 45°. The intent of the program was to investigate the potential for 'combining' anchor points to support more than one floating offshore wind platform, as an economical foundation solution. The testing program was developed for comparison of the standard design case of monotonic single line loading to: double line monotonic loading, single line cyclic with post-cyclic monotonic loading, double line cyclic-sustained with post-cyclic monotonic loading and double line cyclic-cyclic with post-cyclic monotonic loading. The effects of varied cyclic mean load and cyclic load amplitude were also investigated.

Load-displacement behavior during monotonic and cyclic load components, caisson rotation, peak load resistance and internal pore pressure at the caisson top cap were compared for the various mooring line configurations and load progression types. Pore pressure was monitored throughout testing. Caisson rotation was post-processed from video footage. Measured suction caisson resistance and soil-structure behavior was compared between varied load progressions, analytical estimates, and results in literature. Based on test results, an evaluation of the suitability of existing design methods was performed including considerations for alternate or modified methods.

6.2. Summary of Results

6.2.1. Baseline Monotonic Tests

Two single line monotonic load tests were performed to define the effect of dissipation of installation pore pressures prior to monotonic loading and serve as baseline results for comparison. A stiffer response and higher capacity were observed in the test with higher percentage pore pressure dissipation as anticipated. The capacity measured for the higher percent pore pressure dissipation corresponds well to results for similar tests in literature. Measured normalized load resistance of S1-T04 was 78% of estimated capacity using Limiting Equilibrium Method from DNV 2005, for a suction caisson with pad eye assumed to be at optimum location and similar undrained shear strength profile. The lower than expected peak monotonic load resistance is likely due, in part, to location of the pad eye below the single line optimum position, resulting in rotation of the caisson, and vertical-horizontal load interaction occurring from the 45° line load angle (Andersen and Jostad 1999; DNV 2005). Measured displacement at peak resistance was substantially greater than in comparable tests in literature. For instance, peak load resistance (P_{peak}) measured in S1-T04 was 97% P_{peak} of Test 2 reported by Jeanjean et al. (2006). Line displacement at peak resistance was 181% to 950% of displacement reported for comparable tests.

One double line monotonic test was performed with a sustained load applied to an orthogonal line as a second line was loaded monotonically to failure. With the equivalent of 50% of the peak load resistance sustained on the orthogonal line, ultimate load resistance (failure) in the second line was reduced by 4%. If the total resultant peak resistance is considered, (combined effect of sustained orthogonal load and monotonic load), resultant peak load resistance was greater than the reference single line monotonic by 31%. Line displacement at peak resistance in the direction of the failure load was the same as in the single line monotonic test. Double line loading resulted in larger percentage reduction of the internal pore pressure, thus an increased development of suction.

6.2.2. First Cyclic Loading Series: Low Mean Low Amplitude

The first series of single line cyclic, double line cyclic-sustained and double line cyclic-cyclic tests was performed with low cyclic mean load and low cyclic load amplitude (LMLA). For all cyclic tests, post-cyclic monotonic P-δ behavior consisted of two adjoining linear segments, where the first slope was steeper, indicating a stiff response, and the following slope was milder indicating a softened response. The first post-cyclic P-δ slope was 141% to 188% of the initial (pre-cyclic), whereas the second post-cyclic P-δ slope was 61%- 81% of the initial (pre-cyclic) slope. The intersection of first and second post-cyclic P-δ slopes occurred at 150% $P_{cy,max}$.

Cycling in both perpendicular directions (cyclic-cyclic) resulted in increased initial rate of displacement accumulation, compared to the effect of a perpendicular sustained load combined with cyclic loading (sustained-cyclic). After a higher number of load cycles the rate of displacement accumulation of the cyclic-cyclic test was reduced to less than that of the sustained-cyclic test). For all LMLA tests, displacement accumulated during cyclic loading contributed less than 10% of the displacement at failure. Rotational displacement during cyclic loading was greater in cyclic-cyclic tests than in cyclic sustained tests.

For LMLA tests, post-cyclic monotonic load resistances on the lines loaded to failure were greater than the reference monotonic-only load resistance by 18 – 26%. The greatest increase was observed in the single line cyclic tests. If the total resultant load (vector summation of loads from both lines) is considered, the increase in peak load resistance for post-cyclic monotonic loading compared to monotonic-only loading is 52 – 53%. The angle ‘swept’ by the changing orientation of the resultant load during the cyclic loading due to phase offset of the two sinusoidal loads appears to have a direct relationship to the post-cyclic monotonic load resistance where the greater the angle of sweep (ω_{sweep}), the greater the increase in post-cyclic peak monotonic load resistance.

During the monotonic load components of the cyclic tests (load to initial for line 1/line 2 and load to failure), pore pressure response is similar to response observed in baseline monotonic

tests. During cyclic loading, as the cyclic load magnitude follows a symmetric sinusoidal waveform about a constant mean, pore pressure response correlates well to caisson displacement.

Based on visual observations at the completion of the tests, there was visible gapping on the backside of all three tests. As there was a notable difference in the appearance of the sample surface in the region of failure between tests, there is potential that the gapping observed may have been caused by different mechanisms.

6.2.3. Effect of Cyclic Load Amplitude

A second series of single line cyclic, double line cyclic-sustained and double line cyclic-cyclic tests were performed with low mean high amplitude (HMLA) to observe the effects of increased cyclic load amplitude.

Steepness of the first post cyclic P-δ slope (M_{pc1}) relative to initial (M_{in}) was 58% to 112% greater in LMHA tests than in LMLA tests. The point of changeover between first and second linear components of P-δ slope occurred at 116% - 141% $P_{cy,max}$, slightly lower than in low amplitude tests. Steepness of the second linear component of post-cyclic P-δ slope (M_{pc2}) was similar between LMHA and LMLA tests at 63 - 84% M_{in}.

Cyclic at a higher amplitude resulted in initial displacement accumulation rate which was a maximum of six times the displacement accumulation rate at lower cyclic amplitude. After a greater number of cycles, the relative effect of high amplitude versus low amplitude cyclic loading was reversed. The displacement accumulation rate over the last 100 cycles of the high amplitude test was 91% of the displacement rate of the corresponding low amplitude tests. Total permanent cyclic displacement (δ_{cyc}) of higher amplitude tests was 203% δ_{cyc} of corresponding low amplitude test. Relative contribution of permanent cyclic displacement to total displacement at peak load resistance does not appear to have a clear relationship to cyclic load amplitude. Permanent caisson rotation occurring during cyclic loading was similar in higher load amplitude and lower cyclic load amplitude tests.

Cyclic pre-loading with high cyclic amplitude resulted in significant increases in (post-cyclic) monotonic inclined load resistance of 9 – 29% over the corresponding low cyclic amplitude tests. Consideration of the total resultant load resistance indicates increases of total peak monotonic inclined load resistance of 18 – 19% over the corresponding low cyclic amplitude tests. These increases in post-cyclic monotonic load resistance support the suggestion that post-cyclic load resistance increases with sweep angle, where in the high amplitude tests, sweep angles were 64% and 92% larger than in the corresponding low amplitude tests.

6.2.4. Effect of Cyclic Mean Load

A third series of single line cyclic, double line cyclic-sustained and double line cyclic-cyclic tests were performed with high mean low amplitude (HMLA) cyclic loads to observe the effect of cyclic loading about a higher mean load.

Steepness of the first post cyclic P-δ slope (M_{pc1}) relative to initial (M_{in}) was 74% to 174% greater in high mean tests than in low mean tests, indicating a stiffer responses. Changeover points from first to second linear component of P-δ slope (P_x) were 129% - 141%$P_{cy,max,}$ in high mean tests, slightly higher than in the low mean tests. Reduction in second post-cyclic P-δ slope (M_{pc2}) relative to M_{in} was similar between high mean and low mean tests.

Cycling about a higher mean load resulted in a higher initial displacement accumulation rate, 280% of the corresponding rate at low mean load. At a high number of cycles, the displacement accumulation rate of the high mean tests was reduced to 73% of the rate of displacement accumulation for corresponding low mean tests. Greater total cyclic displacement is accumulated in tests with higher cyclic mean load.

Based on results of cyclic-sustained double line tests, permanent caisson rotation occurring during cyclic loading was greater in higher mean load tests than in lower cyclic mean load tests. Rotational displacement in high mean tests was 275 - 750% of rotation in corresponding LMLA tests.

Post-cyclic peak monotonic load resistance (relative to reference monotonic-only peak load resistance) for tests with high cyclic mean pre-loading were marginally different than post-cyclic peak monotonic load resistance for tests with low cyclic mean pre-loading. The difference in post-cyclic peak monotonic load resistance in high mean tests, considering only peak load resistance on the line subjected to monotonic load, ranged from 13% of $P_{mn,peak}$ less, to 2%of $P_{mn,peak}$ greater than the corresponding low mean test. Consideration of the total resultant load resistance also resulted in slight differences in peak monotonic load resistance in comparison to tests with lower amplitude cyclic pre-loading. Slight decreases of 1% of $P_{mn,peak}$ to slight increases of 2% of $P_{mn,peak}$ in total resultant load resistance were observed in HMLA tests compared to corresponding LMLA tests. Resultant load resistances correlated well with angle of sweep of resultant load vectors.

The general trend of pore pressure response in tests with higher cyclic mean load was different than the response in lower cyclic mean load. For both higher cyclic mean load double line tests, mean pore pressure level remained stable during the cyclic load progression compared to the decreasing trend in the lower cyclic mean load tests. The range of pore pressure induced during cyclic loading was similar between tests of higher and lower cyclic mean load.

Gapping was observed on the backside of the caisson in both double line high mean tests but not in the single line test. Contrastingly to previous tests sets, in all three HMLA tests a tension crack appeared, set back from the soil-structure interface at the backside of the suction caisson.

6.3. Applicability of Existing Design Standards/Recommended Practices

DNV RP-E303 (DNV 2005) identifies the limiting equilibrium method (LEM) as the most commonly used method for estimating capacity. The LEM mechanism is aligned with the projected area of the caisson and the direction of loading. During cyclic loading in multiple directions (with cyclic phase offset), direction of loading is not constant, therefore different

'areas' of soil would constitute the resistance mechanism at different times throughout the cyclic load cycle. To appropriately apply the LEM, a modified definition of the soil volume contributing to the resistance mechanism would likely be necessary.

Not only does the 'plan view' direction of the load resultant (for multi-directionally loaded suction caissons) change, but the load angle also varies throughout a load cycle. DNV RP-E303 (DNV 2005) indicates there is an optimum pad eye depth for a given load inclination and soil strength profile that results in the 'optimal' translational failure. Therefore, as the resultant load inclination varies during multi-direction cyclic loading, the optimum depth of the pad eye also varies. The physical limitation of a fixed pad eye may result in periods of rotational and translational displacement, which does not follow the assumption for use of the LEM.

A key difference between offshore oil and gas platform design and offshore wind turbine platform design is the critical load condition. For oil and gas platforms, dead load and live loads corresponding with the 'design storm' (typically 3-hour storm with 1000 year return period conditions) are the critical load conditions (DNV 2005; API 2000). Whereas critical load condition for offshore floating wind turbine platforms is long-term operational condition (Goupee 2010). Where soil parameters are load-dependent (affected by parameters such as load rate, cyclic load parameters, loading time, etc.), design soil parameters are affected by difference in critical load condition. The undrained cyclic shear strength ($\tau_{f,cy}$) associated with the oil and gas critical load condition is the applied shear stress that causes failure *at the number of cycles defined by the design storm*, and is a function of average shear stress, cyclic shear stress amplitude and load frequency (Andersen 2009). A more appropriate definition of $\tau_{f,cy}$ for the critical operational condition for wind turbine platform anchors might be the 'critical level of repeated loading (CLRL)' (Chaney & Fang 1986), below which continued cycling does not progressively increase strain or pore pressure accumulations.

6.4. Further Research

This program modeled only the following conditions: normally consolidated kaolin clay, smooth surface suction caisson with L/D=2 and 4 pad eyes symmetrically placed, load applied at 4/9 L from the tip of the caisson, load angle of 45° from the horizontal (taut line), 0.15 Hz model scale frequency cyclic loading, 0.1 mm / s monotonic loading rate. As only a limited number of tests with limited load configurations, a limited load progression were completed. There are a number of advancements that could be made to the testing program to more thoroughly define the behavior of suction caissons loaded in this manner and further extensions to the investigation that would clarify the applicability of this proposed foundation concept.

More testing would be beneficial to confirm the results and to expand on the scope of the investigation to better understand the mechanisms, performance and potential for application.

6.4.1. Suggestions for Confirmation Testing

Only single tests were performed for each selection of controlled conditions. To establish repeatability and gain an understanding of the consistency of the results, multiple tests of each condition should be performed. Cyclic load magnitudes applied in the different tests within a single load category (e.g. LMLA) varied due to a combination of equipment error and lack of data processing during the test progression. Better precision of cyclic load magnitudes (equipment controlled). Processing of data during the testing would contribute to more precise load selection and improved load control, and cause of variability in results would be more easily identified during analysis. The small model size allowed for a greater number of tests to be performed in a given sample, however, this benefit may be offset by physical configuration limits of a small model. In order for a better understanding of displacement and rotation behavior, sufficient instrumentation should be used such that the x, y, and z displacements and inclination can be measured without the need for assumptions and derivations. For this to occur the size of the model caisson needs to be large enough for sufficient instrumentation.

The pore pressure monitored was limited to the internal underside of the cap of the caisson. To have a more complete understanding of the resistance mechanism and the contribution of the pressure differential to the uplift resistance of the caisson additional locations of pore pressure measurements along the external sides of the model caisson would be beneficial. Pore pressure measurements in the sample in the region around the model caisson would contribute to the understanding of the zone of influence of the caisson loading. Although the evaluation of the line load resistance is determined in terms of undrained shear strength, the monitoring of the extent of pore pressure change would allow for a better understanding of the extent of influence of the multi-directional loading.

In the tests conducted in this program, the caisson was installed by jacking instead of suction. It would be beneficial to test multi-directional line loaded caissons that are installed with suction to gauge more accurately what the performance of the anchor under more representative conditions.

Similarly, since the capacity and behavior of the suction caisson is determined by the soil-structure interaction, more representative results would be obtained if actual samples of the natural soil from the project site were used for model testing.

Additional tests that would be beneficial to the analysis of the test results include investigation of creep effects occurring as a result of simple sustained loads. For both single and double line tests, tests with a sustained load for a period equal to the cyclic loading would aid in isolating the effect of individual cyclic loading parameters (mean load/load amplitude) from the effect of creep.

Additional tests with varied load combinations would provide a larger database for comparison and distinction of the trend in the effects of parameter effect on the behavior and capacity of the caisson. Performing tests with cyclic load amplitude / mean cyclic load resulting in failure would be beneficial for identifying the difference between the critical level of repeated

loading for single line loads versus multiple line loads. Frequency of cyclic loading is another important consideration for further testing .

6.4.2. Extension of Investigation Topics

The multi-directional loading of suction anchors is in its infancy of development. There is minimal information available and the results collected in this testing program are not exhaustive. Investigation of multi-directional line loaded suction anchors could be developed in numerous areas. Some key areas that would be particularly beneficial for the application of multi-directional line loaded suction anchors for offshore wind turbine platforms are:

- Investigation of the true resistance mechanism: consideration of the effect of cyclic load parameters, variation of resultant load direction.
- Location of the optimum pad eye position with consideration of variant resultant load direction, magnitudes and angles.
- Investigation of horizontal-vertical resistance interactions with changing resultant load angles.
- Additional loading orientations: circumferential distribution/offset of pad eyes where load resultants might result in two way loading.
- Non-similar cyclic load magnitudes on different lines: effect of cyclic load parameters that are substantially different for each line.

REFERENCES

Abdel-Rahman, K. and Achmus, M. (2007). "Three dimensional numerical modelling of foundation systems for offshore wind energy plants." *Proc. Abaqus User Conference*, Paris, France.

Achmus, M., Kuo, Y.S. and Abdel-Rahman, K. (2009). "Behaviour of monopile foundations under cyclic lateral load." *Computers and Geotechnics*, 36, 725-735.

Acosta-Martinez, H.E. and Gourvenec, S.M. (2008). "Response of skirted foundations for buoyant facilities subjected to cyclic uplift loading." *Proc. 18th Int. Offshore and Polar Engineering Conference*, Vancouver, Canada, July 6-11. ISOPE.

Allersma, H.G.B. (1998). "Using small geotechnical centrifuge in offshore engineering." *17th Int. Conf. on Offshore Mechanics and Arctic Engineering*, Lisbon, Portugal. OMAE98-3097.

Allersma, H.G.B. (2004). "Centrifuge tests on monotonic and cyclic loaded caissons." *Proc. Int. Conference on Cyclic Behaviour of Soils and Liquefaction Phenomena*, Bochum, Germany. Ruhr University, Bochum, 335-340.

Allersma, H.G.B. (2004). "Physical modeling of offshore foundation systems in a centrifuge." *Actes du Colloque International de Geotechnique*, May 19-22, Beyrouth.

Allersma, H.G.B., Kirstein, A.A., Brinkgreve, R.B.J. and Simon, T. (1999). "Centrifuge and numerical modelling of horizontally loaded suction piles." *Proc. 9th Int. Offshore and Polar Engineering Conference*, 711-717, Brest, France, May 30-June 4. ISOPE, 711-717.

Allersma, H.G.B., Kirstein, A.A. and Maes, D. (2000). "Centrifuge modelling on suction piles under cyclic and long term vertical loading." *Proc. 10th Int. Offshore and Polar Engineering Conference*, Seattle, WA, May 27 – June 2. ISOPE, 334-341.

American Petroleum Institute. (2005). Design and Analysis of Stationkeeping Systems for Floating Structures, API Recommended Practice 2SK, 3rd ed. Washington, D.C.: API Publishing Services.

Andersen, K.H. (1976). "Behaviour of off-shore structures." *Proceedings of the 1st International Conference: BOSS* '76, Trondheim, Norway.

Andersen, K.H. (1988). "Properties of soft clay under static and cyclic loading." *Proc. Int. Conf. on Engineering Problems of Regional Soils*. Beijing, China.

Anderson, K., et al. (2008). ``Deep Water Geotechnical Engineering``. *Proceedings of the 24th National Conference of the Mexican Society of Soil Mechanics*, Aguascalientes, Mexico, November 26-29.

Andersen, K.H. (2009). "Bearing capacity under cyclic loading – offshore, along the coast and on land. The 21st Bjerrum Lecture presented in Oslo, 23 Novermber 2007." *Canadian Geotechnical Journal*, 46, 513-535.

Andersen, K.H., Dvyvik, R., Kikuchi, Y. and Skomedal, E. (1992). "Clay Behavior Under Irregular cyclic loading.

Andersen, K.H., Dyvik, R., Schroder, K., Hansteen, O.E. and Steinar, B. (1993). "Field tests of anchors in clay II: predictions and interpretations." *Journal of Geotechnical Engineering*, 119(10), 1532-1549.

Andersen, K. H., Hansteen, O.E., Hoeg, K. and Prevost, J.H. (1978). "Soil deformations due to cyclic loads on offshore structures." *Numerical Methods in Offshore Engineering*, ed: Zienkiewicz, O.c., Lewis, R.W. and Stagg, J. Chichester: J.Wiley & Sons.

Andersen, K.H. and Jostad, H.P. (1999). "Foundation design of skirted foundations and anchors in clay." *Proc. 31st Annual Offshore Technology*, Houston, TX. OTC 10824.

Andersen, K.H. and Jostad, H.P. (2002). "Shear strength along outside wall of suction anchors in clay after installation." *Proc. 12th Int. Offshore and Polar Engineering Conference*, Kitakyushu, Japan, May 25-31. ISOPE, 785-794.

Andersen, K., Murff, J.D., and Randolph, M. (2004). "Deepwater anchor design practice – Phase II report to API/Deepstar – Volume II-4 Suction caisson anchors – Findings and recommendations." Report submitted to API/Deepstar.

Andersen,K.H., Murff, J.D., Randolph, M.F., Clukey, E.C., Erbrich, C., Jostad, H.P., Hansen, B., Aubery, C., Sharma, P. And Supachawarote, C. (2005). "Suction anchors for deepwater applications." *Proc. International Symposium on Frontiers in Offshore Geotechnics*, Perth, Australia, Sep 19-21. Taylor &Francis.

Anderson, D.G. and Richart, F.E. (1976). "Effects of straining on shear modulus of clays." *Journal of the Geotechnical Engineering Division.* 102(9), 975-987.

Ansal, A.M. and Erken, A. (1989). "Undrained behaviour of clay under cyclic shear stresses." *ASCE Journal of the Geotechnical Engineering Division*, 115, 968-983.

Aubeny, C., Han, S. and Murff, J. (2003). "Inclined load capacity of suction caissons." *International Journal of Numerical and Analytical Methods in Geomechanics,* 27, 1235-1254.

Aubeny, C. and Murff, D. (2005). Final Report on the Suction Caissons & Vertically Loaded Anchors: Design Analysis Methods for the Project Suction Caissons and Vertically Loaded Anchors. Texas A&M University.

Aubeny, C. and Murff, J.D. (2005). "Simplified limit solutions for undrained capacity of suction anchors." *Ocean Engineering*, 32, 864-877.

AWS Truewind, LLC. (2009). *Offshore Wind Technology Overview*. Albany, New York.

Azzouz, A.S., Malek, A.M., Baligh, M.M. (1989). ``Cyclic behaviour of clays in undrained simple shear." *ASCE Journal of Geotechnical Engineering*, 115(5), 637-657.

Aubeny, C. and Murff, D. (2005). *Suction Caissons and Vertically Loaded Anchors: Design Analysis Methods*. Minerals Management Service/Offshore Technology Research Center.

Bang, S., Jones, K., Kim, Y.S., Kim, K.O. and Cho, Y. (2008). "Verical pullout capacity of embedded suction anchors in clay." *Proc. United States – Korea Conference on Science, Technology and Entrepreneurship*, San Diego, CA, Aug 14-17. CEE-1.6.

Bang, S., Jones, K., Kim, Y.S. and Cho, Y. (2011). "Horizontal capacity of embedded suction anchors in clay." *Journal of Offshore Mechanics and Arctic Engineering*, 133, ASME.

Bang, S. (2001). "Calibration of suction pile installation design with centrifuge model tests." *Proc. 20th Int. Conf. on Offshore Mechanics and Arctic Engineering*, Rio de Janeiro, Brazil, June 3-8. ASME, 5, 121-125.

Belknap, D., Kelley, J.T and Kelley, A. R. (2011). Report on Geophysical Studies Conducted June through October 2010: University of Maine Deepwater Offshore Wind Test Site: Offshore Monhegan Island, Maine. University of Maine, Orono.

Bienen, B., Byrne, B., Houlsby, G., and Cassidy, M. (2006). "Investigating six-degree-of-freedom loading of shallow foundations on sand." *Geotechnique*, 56 (6), 367-379.

Bilgili, M., Yasar, A. And Simsek, E. (2011). "Offshore wind power development in Europe and its comparison with onshore counterpart." *Renewable and Sustainable Energy Reviews*, 15, 905-915.

Black, Veatch. Percent wind energy penetration in the united states: a technical analysis of the energy resource; 2007. Technical Report for the American Wind Energy Association.

Bogard, D. and Matlock, H. (1979). A model study of axially loaded piles including pore pressure measurements: Report to the American Petroleum Institute. The University of Texas, Austin.

Boulanger,R.W. and Idriss, I.M. (2007). "Evaluation of cyclic softening in silts and clays." *Journal of Geotechnical and Geoenvironmental Engineering*, 133(6), 641-652.

Bransby M.F. and Randolph, M.F. (1998). "The effect of skirted foundation shape on response to combined V-M-H loadings." *International Journal of Offshore and Polar Engineering*, 9(3), 214-218.

Briaud, J-L. And Felio, G.Y. (1986). "Cyclic axial loads on piles: analysis of existing data." *Canadian Geotechnical Journal*, 23, 362-371.

Brown, S.F., Andersen, K.H. and McElvaney, J. (1977). "The effect of cyclic loading of clays." *Proc. 9th Int.Conf. on Soil Mechanics and Foundation Engineering*, Tokyo, Japan. ICSMFE, 2,195-200.

Butterfield, S., Musial, W., Jonkman, J. and Sclavounos, P. (2007). "Engineering challenges for floating offshore wind turbines." *Copenhagen Offshore Wind Conference*, Copenhagen, Denmark, October 26-28.

Byrne, B.W. and Cassidy, M.J. (2002). "Investigating the response of offshore foundations in soft clay." *Proc. 21st Int. Conf. on Offshore Mechanics and Arctic Engineering*, Oslo, Norway, June 23-28. ASME, V(4), 263-275.

Byrne, B.W. and Houlsby, G.T. (2002). "Experimental investigations of response of suction caissons to transient vertical loading." *Journal of Geotechnical and Geoenvironmental Engineering,* 128(11), 926-939.

Byrne, B.W. and Houlsby, G.T. (2004). "Experimental investigations of the response of suction caissons to transient combined loading." *ASCE Journal of Geotechnical and Geoenvironmental Engineering*, 130(3), 240-253.

Byrne, B.W. and Houlsby, G.T. (2006). "Assessing novel foundation options for offshore wind turbines." *World Maritime Technology Conference*, London, UK, March 6. IMarEST.

Cao, J. (2003). *Centrifuge Modeling and Numerical Analysis of the Behaviour of Suction Caissons in Clay*. PhD Thesis. Memorial University of Newfoundland, St. John's, Canada.

Cassidy, M.J., Byrne, B.W. and Randolph, M.F. (2004). "A comparison of the combined load behaviour of spudcan and caisson foundations on soft normally consolidated clay." *Geotechnique*, 54(2), 91-106.

Castro, G. and Christian, J.G. (1976). "Shear strength of soils and cyclic loading." *ASCE Journal of the Geotechnical Engineering Division*, 102(9), 887-894.

Cermelli, C. Aubault, A., Roddier, D. And McCoy, T. (2010). "Qualification of a semi-submersible floating foundation for multi-megawatt wind turbines." *Proc. Offshore Technology Conference*, Houston, TX, May 3-6. OTC 20674.

Chakrabarti, S. (2005). *Handbook of Offshore Engineering*. Netherlands: Elsevier.

Chaney, R.C. and Fang, H.Y. (1986). "Static and dynamic properties of marine sediments." *Marine Geotechnology and Nearshore/Offshore Structures*, ASTM STP 923, 74-111.

Chen, W.F. (1975). *Limit analysis and soil plasticity*. Amsterdam, Netherlands: Elsevier.

Chen, W. and Randolph, M.F. (2005). "Centrifuge tests on axial capacity of suction caissons in clay." *Proc. Int. Sym. Frontiers in Offshore Geotechnics*, Perth, Australia, Sep 19-21. Taylor & Francis, 243-249.

Chen, W. and Randolph, M.F. (2006). "Measuring radial total stresses on model suction caisson in clay." *Geotechnical Testing Journal*, 30 (2).

Chen, W. and Randolph, M. F. (2007). "Uplift capacity of suction caissons under sustained and cyclic loading in soft clay." *ASCE Journal of Geotechnical and Geoenvironmental Engineering,*133(11), 1352-1363.

Chen, W., Zhou, H. and Randolph, M.F. (2009). "Effect of installation method on external shaft friction of caissons in soft clay." *Journal of Geotechnical and Geoenvironmental Engineering*, 135(5), ASCE.

Chen, W.F. and Randolph, M.F. (2007). "Uplift capacity of suction caissons under sustained and cyclic loading in soft clay." *ASCE Journal of Geotechnical and Geoenvironmental Engineering*, 133(11), 1352-1363.

Cho, Y. and Bang, S. (2002) "Inclined loading capacity of suction piles." *Proc. 12th Int. Offshore and Polar Engineering Conference*, Kitakyushu, Japan, May 26-31, 827-832. ISOPE.

Clukey, E.C., Aubeny, C.P. and Murff, J.D. (2004). "Comparison of analytical and centrifuge model tests for suction caissons subjected to combined loads." *Journal of Offshore Mechanics and Arctic Engineering*, 126, 364-367, ASME.

Clukey, E.C. and Morrison, M.J. (1993). "A centrifuge and analytical study to evaluate suction caissons for TLP applications in the Gulf of Mexico." *ASCE Geotechnical Special Publication No. 38*, 141-156.

Clukey, E.C., Morrison, M.J., and Corte, J.F. (1995). "The response of suction caissons in normally consolidated clays to cyclic TLP loading conditions." *Proc. Offshore Technology Conference*, Houston, TX, May 1-4. OTC 7796.

Coffman, R.A., El-Sherbiny, R.M., Rauch, A.F. and Olson, R.E. (2004). "Measured horizontal capacity of suction caissons." *Proc. Offshore Technology Conference*, Houston, TX, May 3-6. OTC 16161.

Colliat, J-L. (2002). "Anchors for deepwater to ultradeepwater moorings." *Proc. 2002 Offshore Technology Conference*, Houston, TX, May 6-9. OTC 14306.

Dahlberg, R., Ronold, K.O., Strom, P.J., Andersen, K.H. and Jostad, H.P. (2005). *Project Summary, Joint Industry Project on Reliability-Based Calibration of Design Code for Suction Anchors*, DNV Report No. 2005-0150. Hovik, Norway.

Deng, W. and Carter, J.P. (2006). *Uplift capacity of suction caissons in uniform soil.* University of Sydney, Australia.

Det Norske Veritas. (2000). Recommended Practice RP-E301: Design and Installation of Fluke Anchors in Clay. Norway: Norway: Det Norske Veritas.

Det Norske Veritas. (2008). *Offshore Standard DNV-OS-E301 Position Mooring*. Norway: Det Norske Veritas.

Det Norske Veritas. (2002). Recommended Practice RP-E302: Design and Installation of Plate Anchors in Clay. Norway: Det Norske Veritas.

Det Norske Veritas. (2005). Recommended Practice RP-E303: Geotechnical Design and Installation of Suction Anchors in Clay. Norway: Det Norske Veritas.

Dicorato, M., Forte, G., Pisani, M. and Trovato, M. (2011). "Guidelines for assessment of investment cost for offshore wind generation." *Renewable Energy*, 36, 2043-2051.

DONGenergy. (2009). "The monopod bucket foundations." *European Offshore Wind Conference and Exhibition*, Stockholm, Sweden, Sep 14-16. EWEA.

Doyle, E.H., Sharma, J.S., Bolton, M.D., Balsangkar, A.J. and Newlin, J.A. (2004). "Centrifuge model tests on anchor piles for tension leg platforms." *Proc. Offshore Technology Conference,* Houston, TX, May 3-6, OTC 16845.

Dutt, R.N., Doyle, E.H., and Ladd, R.S. (1992) "Cyclic behavior of a deepwater normally consolidated clay." *Proceedings of Civil Engineering in the Oceans V*, College Station, Texas, November 2-5, ASCE, 546-559.

Dzwilewski, P.T. and Richards, A.F. (1974). "Consolidation properties of Wilkinson Basin soils." Journal of the Geotechnical Engineering Division, 100(10), 1175-1179.

El Hosri, M.S., Biarez, H. and Hicher, P.Y. (1986). "Liquefaction characteristics of silty clay." *Proc. 8th World Conf. on Earthquake Engineering*. Prentice Hall, New Jersey, 277-284.

El-Gharbawy, S.L., and Olson, R.E. (1999). "The cyclic pullout capacity of suction caisson foundations." *Proc. 9th Int. Offshore and Polar Engineering,* Brest, France, May 30-June 4. ISOPE, Vol. 2, 660-667.

Eltaher, A., Rajapaksa, Y., and Chang, K-T. (2003). "Industry trends for design of anchoring systems for deepwater offshore structures." *Proc. Offshore Technology Conference*, Houston, TX, May 5-8. OTC 15265.

Erken, A. and Ansal, A.M. (1994). "Liquefaction characteristics of undisturbed sands." *Performance of Ground and Soil Structures: 13th Int. Conf. on Soil Mechanics and Foundation Engineering*, New Delhi, India. 165-170.

Erken, A. and Can Ulker, B.M. (2006). "Effect of cyclic loading on monotonic shear strength of fine-grained soils." *Engineering Geology*, 89, 243-257.

Esteban, M.D., Diez, J.J., Lopez, J.S. and Negro, V. (2011). "Why offshore wind energy?". *Renewable Energy*, 36, 444-450.

European Environment Agency. (2009). "Europe's onshore and offshore wind energy potential: an assessment of environmental and economic constraints." *EEA Technical Report No. 6/2009*. Copenhagen: European Environment Agency.

Fines, S., Stove, O. And Guldberg, F. (1991). "Snore TLP tethers and foundation." *Proc. Offshore Technology Conference*, Houston, TX, May 6-9. OTC 6623.

Fulsang, L.D. and Steensen-Bach, J.O. (1991). "Breakout resistance of suction piles in clay." *Proc. Int. Conf. Centrifuge*, 153-159. Boulder, CO.

Gottardi, G. Houlsby, G.T. and Butterfield, R. (1999). "Plastic response of circular footings on sand under general planar loading." *Geotechnique*, 49 (4), 453-469.

Goupee, A. (2010). *Mooring Loads for the NREL Floating Turbines*. (Confidential document). University of Maine, Orono.

Green, R. and Vasilakos, N. (2011). "The economics of offshore wind." *Energy Policy*, 39, 496-502.

Grosh, J.J. and Reese, L.C. (1980). "Field tests of small scale pile segments in soft clay deposit under repeated axial loading." *Proc. Offshore Technology Conference*, Houston, TX, May 5-8. OTC 3869 .

Houlsby, G.T. and Byrne, B.W. (2000). "Suction caisson foundations for offshore wind turbines and anemometer masts." *Wind Engineering*, 24(4), 249-255.

Houlsby, G.T., Ibsen, L.B., and Byrne, B.W. (2005). "Suction caissons for wind turbines." *Proc. International Symposium on Frontiers in Offshore Geotechnics*, Perth, Australia, 75-93.

Hyde, A.F.L. and Brown, S.F. (1976). "The plastic deformation of a silty clay under creep and repeated loading." *Geotechnique*, 26(1), 173-184.

Hyde, A. F. and Ward, S. J. (1985). "A pore pressure and stability model for a silty clay under repeated loading." *Geotechnique*, 35(2), 113-125.

Ibsen, L.B. (2008). "Implementation of a new foundations concept for offshore wind farms." *Proc. 15th Nordic Geotechnical Meeting*, Sandefjord, Norway.

Ibsen, L.G. and Brincker, R. (2005). "Design of a new foundation for offshore wind turbines." *Proc. International Symposium on Frontiers in Offshore Geotechnics*, Perth, Australia, Sep 19-21. Taylor & Francis.

Ibsen, L.B, Liingaard, M. and Nielsen, S.A. (2005). "Bucket Foundation, a status." *Proc. Copenhagen Offshore Wind Conference*, Copenhagen, Denmark.

International Society for Soil Mechanics and Geotechnical Engineering Technical Committee TC2 Physical Modelling in Geotechnics. (2007). *Catalogue of Scaling Laws and Similitude Questions in Centrifuge Modelling.*

International Society for Soil Mechanics and Geotechnical Engineering. (2005). *Geotechnical & Geophysical Investigations for Offshore and Nearshore Developments.* ISSMGE.
Iskander, M., El-Gharbawy, S., and Olson, R. (2002). "Performance of suction caissons in sand and clay." *Canadian Geotechnical Journal*, 39(3), 576-584. NRC Research Press.

Jiao, B., Lu, X., Zhao, J., Wang, A., Shi, A., and Zeng, X. H. (2009). "Experimental study on the bearing capacity of suction caissons in saturated sand." *Proc. 19th International Offshore and Polar Engineering Conference*, Osaka, Japan, June 21-26, 2009. ISOPE.

Jitno, H. *Stress-strain and strength characteristics of clay during post-cyclic monotonic loading*. M.A.Sc. Thesis. University of British Columbia, Vancouver, Canada.

Jeanjean, P., Znidarcic, D., Phillips, R., Ko, H.Y., Pfister, S., Ciniciolglu, O., Bogazici, U. And Schroeder, K. (2006). "Centrifuge testing of suction anchors: double-wall, over-consolidated clay and layered soil profile. " *Proc. Offshore Technology Conference*, Houston, TX, May 2-5. OTC 18007.

Jonkman, J.H. (2007). Dynamic Modelling and Loads Analysis of an Offshore Floating Wind Turbine, NREL Technical Report 500-41958.

Kelly, R.B., Houlsby, G.T. and Byrne, B.W. (2006). "A comparison of field and laboratory tests of caisson foundations in sand and clay." *Geotechnique*, 56(9), 617-626.

Kim,Y.S., Kim, K.O., Cho, Y., Bang, S. and Jones, K.D. (2009). "Inclined loading capacity of embedded suction anchors in clay." *Proc. Int. Conf. on Ocean, Offshore and Arctic Engineering*, 35-39, Honolulu, HI, May 31-Jun 5. OMAE2009-79035.

Kirstein, A.A., Allersma, H.G.B., Brinkgreve, R.B.J. and Simon, T. (1999). "Comparison study on analytical, centrifugal and numerical modeling of quasi-horizontal loaded suction piles." *Beyond 2000 in Computational Geotechnics – 10 years of Plaxis International*, 227-235.

Kirstein, A., Allersma, H., Brinkgreve, R. and Simon, T. (2000). "Comparison study on analytical, centrifugal and numerical modeling of quasi-horizontal loaded suction piles." *Beyond 2000 in Computational Geomechanics – 10 years of Plaxis International*. Balkema, Rotterdam.

Koutsoftas, D.C. (1978). "Effect of cyclic loads on undrained strength of two marine clays." *ASCE Journal of the Geotechnical Engineering Division*, 104(5), 609-620.

Kumar, N. Darga, and Rao, S. Narashima. (2010). "Earth pressures on caissons in marine clay under lateral loads – a laboratory study." *Applied Ocean Research*, 32, 58-70.

Kwag, D. J., Cho, I.H., Bang, S. and Cho, Y. (2010). "Embedded suction anchors for mooring of a floating breakwater." *Journal of Offshore Mechanics and Arctic Engineering*, 132, ASCE.

Landon Maynard, M. and Chung, J. (2011). *Preliminary Geotechnical Site Investigation, for the University of Maine Deepwater Offshore Test Site.* Orono, ME: University of Maine.

Larew, H.G. and Leonards, G.A. (1962). "A repeated load strength criterion." *Proc. Hwy. Res. Bd.*, 41, 529.

LeBlanc, C. (2004). *Design of Offshore Wind Turbine Support Structures*, Ph. D. Thesis, Aalborg University, Denmark.

Lee, S.H., Cho, Y., Kim, K.O., Kim, Y.S., Lee, T.H. and Kwag, D.J. (2003). "Centrifuge model tests on embedded suction anchor loading capacities." *Proc. 13th Int. Symposium on Offshore and Polar Engineering Conference*, 788-792, Honolulu, HI, May 25-30. ISOPE.

Lefebvre, G. and LeBoeuf, D. (1989). "Stability threshold for cyclic loading of saturated clay." *Canadian Geotechnical Journal*, 26, 122-131.

Lee, S.H., Cho, Y., Kim, K.O, Kim, Y.S., Lee, T.H. and Kwag, D.J. (2003). "Centrifuge model tests on embedded suction anchor loading capacities." *Proc. 13th Int. Offshore and Polar Engineering Conference*, Honolulu, HI, Jun 19-24. ISOPE, 788-792.

Levy, N.H., Gaudin, C. and Einav, I. (2007). "The behaviour of piles undergoing a change in lateral loading direction." *International Journal of Physical Modelling in Geotechnics*, 1, 13-23.

Liingaard, M. (2006). *Dynamic behaviour of suction caissons*. PhD Thesis. Aalborg University.

Lu, X., Wu, Y., Jiao, B. And Wang, S. (2007). "Centrifugal experimental study of suction bucket foundations under dynamic loading." *Acta Mech Sin*, 23, 689-698.

Luke, A.M., Rauch, A.F., Olson, R.E. and Mecham, E.C. (2003). "Components of suction caisson capacity measured in axial pullout tests." *Proc. 22nd International Conference on Offshore Mechanics and Arctic Engineering*, Cancun, Mexico, June 8-13. OMAE.

Luke, A.M., Rauch, A.F., Olson, R.E. and Mecham, E.C. (2005). "Components of suction caisson capacity measure in axial pullout tests. " *Ocean Engineering*, 32, 878-891.

Lunne, T., Berre, T., Andersen, K.H., Strandvik, S. and Sjursen, M. (2006). "Effects of sample disturbance and consolidation procedures on measured shear strength of soft marine Norwegian clays." *Canadian Geotech. J.*, 43(7), 726-750.

Malhotra, S. (2009). "Design & construction considerations for offshore wind turbine foundations in North America." *Civil Engineering Practice*, Spring/Summer, 7-42.

Manwell, J.F., Elkinton, C.N., Rogers, A.L., McGowan, J.G. (2007). "Review of design conditions applicable to offshore wind energy systems in the United States." *Renew. Sustain. Energy Rev.*, 11, 210-234.

Matha, D., Schlipf, M., Cordle, A., Pereira, R. and Jonkman, J. (2011). "Challenges in simulation of aerodynamics, hydrodynamics and mooring-line dynamics of floating offshore wind turbines." *Proc. 21st Int. Offshore and Polar Engineering Conference*, Maui, HI, May 25-30. ISOPE.

Matlock H. and Holmquist, D.V. (1976). A model study of axially loaded piles in soft clay: Report to the American Petroleum Institute. The University of Texas, Austin.

Matsui, T. and Abe, N. (1981). "Behaviour of clay on cyclic stress-strain history." *Proc. 10th ICSMFE*, V(3), 261-264. Stockholm.

Matsui, T., Bahr, M.A. and Abe, N. (1992). "Estimation of shear characteristics degradation and stress-strain relationship of saturated clays after cyclic loading." *Soils and Foundations*, 32(1), 161-172. Japanese Society of Soil Mechanics and Foundation Engineering.

Matsui, T., Ohara, H. And Ito, T. (1980). "Cyclic stress-strain history and shear characteristics of clay." *Journal of the Geotechnical Engineering Division.* 106(10), 1101-1120.

Maynard, M. and Chung, J. (2011). Preliminary Geotechnical Engineering Site Investigation for the University of Maine Deepwater Offshore Wind Test Site. University of Maine DeepCwind Consortium.

Mercier, R. (-). "Technology issues with deepwater wind energy systems."

Monajemi, H. and Razak, H.A. (2009). "Finite element modeling of suction anchors under combined loading." *Marine Structures*, 22, 660-669.

Moon, W. L. and Nordstrom, C.J. (2010). "Tension leg platform turbine: a unique integration of mature technologies." *Proc. 16th Offshore Symposium*, Houston, TX.

Moses, G.G. and Narasimha Rao, S. (2007). "Behavior of marine clay subjected to cyclic loading with sustained shear stress." *Marine Georesources & Geotechnology*, 25 (2), 81-96.

Murff, J.D. (1996). "The geotechnical centrifuge in offshore engineering." *Proc. Offshore Technology Conference*, Houston, TX, May 3-6. OTC 8265.

Murff, J.D and Hamilton, J.M. (1993). "P-Ultimate for undrained analysis of laterally loaded piles." *Journal of Geotechnical Engeineering*, ASCE, 119(1), 91-107.

Musial W. And Butterfield, S. (2004). "Future for Offshore Wind Energy in the United States". *Ocean Energy* Proceedings, Florida. National Renewable Energy Laboratory.

Musial, W. and Butterfield, S. (2006). "Energy from Offshore Wind." *Proceedings of the Offshore Technology Conference*, Houston, TX, May 1-4.

Musial, W. and Ram, B. (2010). *Large Sclae Offshore Wind Power in the United States: Assessment of Opportunities and Barriers.* NREL TP-500-40745.

Narasimha Rao, S., Hema Latha, K., Pallavi, B. and Surendran, S. (2006). "Studies on pullout capacity of anchors in marine clays for mooring systems." *Applied Ocean Research*, 28, 103-111.

Narasimha Rao, S., Ravi, R. and Prasad, B. Siva. (1997). "Pullout behaviour of suction anchors in soft marine clays." *Marine Georesources & Geotechnology*, 15(2), 95-114.

Narasimha Rao, S. and Darga Kumar, N. (2007). "Earth pressure on caissons in marine clay under cyclic loading." *Marine Georesources and Geotechnology,* 25, 15-35.

National Renewable Energy Laboratory (NREL), *Wind Energy Resources for the United States.* Technical Report NREL/TP-500-45889.

Norwegian Geotechnical Institute. (1997). "Skirted foundations and anchors in clay; state-of-the-art report." *NGI Report 524071-1*. NGI Joint Industry Project.

Pillai, R.J., Robinson, R.G. and Boominathan, A. (2011). "Effect of microfabric on undrained static and cyclic behaviour of kaolin clay." *ASCE Journal of Geotechnical and Geoenvironmental Engineering*, 137(4), 421-429.

Ponniah, D.A. and Finlay, T.W. (1988). "Cyclic behaviour of plate anchors." *Canadian Geotechnical Journal*, 25, 374-381.

Poulos, H.G. (1981). "Cyclic axial response of single piles". *ASCE Journal of the Geotechnical Engineering Division*, 107(1), 41-58.

Poulos, H.G. (1988). *Marine Geotechnics*. Unwin Hyman, London, England.

Prakasha, K.S., Joer, H.A. and Randolph, M.F. (2005). "Establishing a model testing capability for deep water foundation systems." *Proc. Int. Sym. Frontiers in Offshore Engineering*, Perth, Australia, 309-315.

Raines, R.D. and Garnier, J. (2004). "Physical modeling of suction piles in clay." *Proc. 23rd Int. Conf. on Offshore Mechanics and Arctic Engineering*, 621-631, OMAE2004-51343. Vancouver, Canada.

Randolph, M.F., Gaudin, C., Gourvenec, S.M., White, D.J., Boylan, N. and Cassidy, M.J. (2011). "Recent advances in offshore geotechnics for deep water oil and gas developments." *Ocean Engineering*, 38, 818-834.

Randolph, M. and Gourvenec, S. (2011). *Offshore Geotechnical Engineering*. New York, USA: Spon Press.

Randolph, M.F. and Hope, S. (2004). "Effect of cone velocity on cone resistance and excess pore pressures." *Proc. Engineering Practice and Performance of Soft Deposits IS-OSAKA 2004*, Osaka, Japan, 147-152.

Randolph, M.F. and Houlsby, G.T. (1984). "The limiting pressure on a circular pile loaded laterally in cohesive soil." *Geotechnique,* 34(4), 613,623. London, England.

Randolph, M.F. and House, A.R. (2002). "Analysis of suction caisson capacity in clay." *Proc. Offshore Technology Conference*, Houston, TX, May 6-9. OTC 14236.

Randolph, M.F., Jewell, R.J., Stone, K.J.L. and Brown, T.A. (1991). "Establishing a new centrifuge facility." *Proc. Int. Conf. Centrifuge*. Boulder, CO.

Renzi, R., Maggiono, W. and Smith, F. (1991). "A centrifugal study on the behaviour of suction piles." *Proc. Int. Conf. Centrifuge,* 169-176. Boulder, CO.

Royal Haskoning. (2011). Galloper Wind Farm Project: Preliminary Environmental Report.

Saigal, R.K., Dolan, D., Kiureghian, A.D., Cam, T. and Smith, C. (2007). "Comparison of design guidelines for offshore wind energy systems." *Proc. Offshore Technology Conference*, Houston, TX, Apr 30 – May 3. OTC 18984.

Sangrey, D.A. (1968). *The behaviour of soils subjected to repeated loading*. PhD thesis. Ithica, NY: Cornell University.

Sangrey, D. A., Castro, G., Poulos, S.J. and Grance, J.W. (1978). "Cyclic loading of sands, silts, clays." *Proceedings of Specialty Conference on Earthquake Engineering and Soil Dynamics,* ASCE, California.

Sangrey, D.A., Henkel, D.J., Esrig, M.I. (1969). "The effective stress response of a saturated clay soil to repeated loading." *Canadian Geotechnical Journal*, 6, 241-252.

Schofield, A.N. (1980). "Cambridge geotechnical centrifuge operations." *Geotechnique*, 30(3), 227-268.

Schneider, J.A. and Senders, M. (2010). "Foundation design: a comparison of oil and gas platforms with offshore wind turbines." *Marine Technology Society Journal*, 44(1), 32-51.

Schwartz, M., Heimiller, D., Haymes, S., and Musial, W. (2010). "Assessment of offshore wind energy resources for the United States." *Technical Report NREL/TP-500-45889*. National Renewable Energy Laboratory (NREL).

Senders, M. (2005). "Tripods with suction caissons as foundations for offshore wind turbines on sand." *Proceedings of the International Symposium on Frontiers in Offshore Geotechnic*. Taylor & Francis, London, 397-403.

Senpere D. And Auvergne, G.A. (1982). "Suction anchor piles: a proven alternative to driving or drilling." *Proc. Offshore Technology Conference*, Houston, TX, May 3-6. OTC 4206.

Singh, B., Mistri, G. and Patel, R. (2004). Comparison of Foundation Systems for Offshore Wind Turbine Installation.

Sukamaran, B. (1998). "Suction caisson anchors – a better option for deep water applications." *Proc. Society for Women Engineers Conference*, Houston, Texas.

Stewart, D.P. (1992). Lateral loading of piled bridge abutments due to embankment construction. Ph.D. Thesis, University of Western Australia.

Stewart, D.P. and Randolph, M.F. (1994). "T-bar penetration testing in soft clay." *ASCE Journal of Geotechnical Engineering*, 120(12), 2230-2235.

Taylor, R.N. (1995). *Geotechnical Centrifuge Technology*. Blackie Academic and Professional.

Theirs, G.R., and Seed, H.B. (1968). "Cyclic stress-strain characteristics of clay." *Soil Mech Found. Eng.*, 94(SM2), 555-569.

Thorel, L., Garnier, J., Rault, G. and Bisson, A. (2005). "Vertical uplift capacity of suction caisson in clay." *Proc. Int. Symposium on Frontiers in Offshore Geotechnics*, Perth, Australia, Sep 19-25. Taylor & Francis Group, London.

Tjelta, T. (1994). "Geotechnical aspects of bucket foundations replacing piles for the Europipe 16/11-E jacket." *Proc. Offshore Technology Conference*, Houston, TX, May 2-5. OTC 7397.

Tjelta, T. (1995). "Geotechnical experience from the installation of the Europipe jacket with bucket foundations." *Proc. Offshore Technology Conference*, Houston, TX, May 1-4. OTC 7795.

Tjelta, T. (2001). "Suction pile: their position and application today." *Proc. 11th International Symposium of Offshore and Polar Engineering*, Stavanger, Norway, Jun 17-22. ISOPE, 1-6.

Tjelta, T., Guttormsen, T. and Hermstad, J. (1986). "Large-scale penetration test at a deepwater site." *Proc. Offshore Technology Conference*, Houston, TX, May. OTC 5103.

Ue, S., Yasuhara, K. and Fujiwara, H. (1991). "Influence of consolidation period on undrained strength of clays." *Ground and Constr.*, 9(1), 51-62. Tokyo, Japan.

United States Geological Survey / Woods Hole Field Center. (2010). *Map of the Gulf of Maine Region.* Retrieved April 10, 2010, from http://www.gulfofmaine.org/gommi/imagelibrary.php

University of Maine and James W. Sewall Company (2011). *Maine Deepwater Offshore Wind Report.* Orono, ME: University of Maine.

Utsunomiya, T., Nishida, E. and Sato, I. (2009). "Wave response experiment on SPAR-type floating bodies for offshore wind turbines." *Proc. 19th International Symposium of Offshore and Polar Engineering*, Osaka, Japan, Jun 21-26. ISOPE, 378-384.

Vattenfall. (2011). *Vattenfall's Power Plants: Thanet*. Retrieved August 29, 2011. Available: http://powerplants.vattenfall.com/powerplant/thanet

Villalobos, F.A., Byrne, B.W. and Houlsby, G.T. (2010). "Model testing of suction caissons in clay subjected to vertical loading." *Applied Ocean Research*, 32, 414-424.

Vucetic, M. (1988). "Normalized behaviour of offshore clay under uniform cyclic loading." *Canadian Geotechnical Journal*, 25, 33-41.

Vucetic, M. (1990). "Normalized behaviour of offshore clay under irregular cyclic loading." *Canadian Geotechnical Journal,* 27, 29-46.

Vryhof Anchors. (2010). *Anchor Manual 2010: Guide to Anchoring*. Netherlands: Vryhof Anchors.

Watson, P.G. and Randolph, M.F. (2006). "A centrifuge study into cyclic loading of caisson foundations." *Proc. 6th Int. Conf. on Physical Modelling in Geotechnics*, Hong Kong, Aug 4-6, 1, 693-699.

Wang, J. and Yao, M. (1996). "Elasto-plastic simulation of undrained cyclic properties in clay." *Chinese Journal of Geotechnical Engineering*, 18(3), 12-18.

Wang, Y., Lu, X., Wang, S. and Shi, A. (2006). "The response of bucket foundation under horizontal dynamic loading. *Ocean Engineering*, 33, 964-973.

Whitehouse, R.J.S., Harris, J.M., Sutherland, J. and Rees, J. (2011). "The nature of scour development and scour protection at offshore windfarm foundations." *Marine Pollution Bulletin*, 62, 73-88.

Wilson, N. E. And Greenwood, J.R. (1974). "Pore pressure and strains after repeated loading of saturated clay." *Canadian Geotechnical Journal*, 11, 269-277.

Wood, D.M. (1990). *Soil Behaviour and Critical State Soil Mechanics*. Cambridge University Press, New York.

Yao, M. and Nie, S. (1994). "A model of the calculation of soil dynamic deformation on saturated clay." *Journal of Water Conservancy*, 7, 51-55.

Yasuhara, K. (1995). "Postcyclic undrained strength for cohesive soils." *Journal of Geotechnical Engineering*, 120(11), 1961-1979.

Yasuhara, K., Hirao, K. and Hyde, A.F.L. (1992). "Effects of cyclic loading on undrained strength and compressibility of clay." *Soils and Foundations*, 132(1), 100-116. Japanese Society of Soil Mechanics and Foundation Engineering.

Zergoun, M. and Vaid, Y.P. (1994). "Effective stress response of clay to undrained cyclic loading." *Canadian Geotechnical Journal*, 31, 714-727.

Zaaijer, M.B. (2002). Dutch offshore wind energy converter. TU Delft

Zaaijer, M.B. (2003). "Comparison of monopile, tripod, suction bucket and gravity base design for a 6MW turbine." *Offshore wind energy in Mediterranean and other European Seas (OWEMES conference)*. Naples, Italy.

Zhang, J.H., Zhang, L.M. and Lu, X.B (2007) "Centrifuge modeling of suction bucket foundations for platforms under ice-sheet-induced cyclic lateral loadings." *Ocean Engineering*, 34, 1069-1079.

Zhou, J. and Gong, X. (2001). "Strain degradation of saturated clay under cyclic loading." *Canadian Geotechnical Journal*, 38, 208-212.

Zhu, R. and Law, K.T. (1988). "Liquefaction potential of silt." *Proc. 9th Int. Conf. on Earthquake Engineering*, Tokyo, Japan, 237-242.

Estimated peak monotonic inclined load capacity of model scale suction caisson.

Soil Description			
Total density		1.59	Mg/m3
Total Unit Wt.	γ	15.6	kN/m3
Buoy. Unit Wt.	γ'	5.8	kN/m3
s_u/z		0.96	kPa/m
$s_u/\sigma'v_0$		0.17	

Caisson Description			
Diameter	d	3.75	m
Total Length	L	7.5	m
Thickness	t	0.15	m
Base Area	A	11.04466	m2
Equiv. Side Width	s	3.323351	m
Caisson Volume	V	14.91029	m3
Total Weight	W	394.2282	kN
Buoyant Weight	W'	248.2564	kN

Upper Zone Description			
Upper Limit	z	6.1	m
	$s_{u,upp}$	2.928	kPa
API 2A ext.	α_{API}	1.229626	
DNV max lim.	α	0.614813	
3D shear	α_{ss}	0.6	rad
3D shear rad	R	5.034547	m
3D area 1	A_1	8.670294	m2
3D area 2	A_2	2.349613	m2
3D area 3	A_3	12.67333	m3

*** manually enter value so "Total Horz Resistance of Upper > Resistance of Lower***

Lower Zone Description			
DNV max lim.	α	0.614813	
	Δ	0.662149	rads
	ψ	0.454324	
	$s_{u,low}$	6.528	kPa

Blue fill indicates required parameter entry

UPPER SECTION - Classical Earth Pressure Theory with 3D modifications

Vertical convention (up -, down +) Horizontal convention (load direction - , against load +)

Resistance Calculations (Pressure / Stress Units)

Active Stress			
Peak Active	SPA	29.5606	kPa
Peak Vert Active	SAV	1.800172	kPa
Peak Horz Active	SAH	-29.5057	kPa

Passive Stress			
Peak Passive	SPP	41.2726	kPa
Peak Vert Passive	SPV	1.800172	kPa
Peak Horz Passive	SPH	41.23332	kPa

Side Shear Stress			
Peak Vert Sd Shear	TV	3.600344	kPa
Peak Horz Sd Shear	TH	3.600344	kPa

Resistance Calculations (Force Units)

Active Force			
Total Active Force	PA	250.0896	kN
Vert Active Force	PAV	30.45975	kN
Norm. Active Force	PAN	-248.228	kN

Passive Force			
Total Force	PP	477.7059	kN
Vert Pass.	PPV	-36.4939	kN
Norm. Passive	PPN	476.3099	kN

3D Shear Effects			
3D Area Total	A_{ss}	23.69324	m2
Passive Side Shear		110.9981	kN

Side Shear Effects			
Caisson Area per side	A_{cais}	20.27244	m2
Vert Shear	T_{cais}	72.98776	kN
Horz Shear	H_{cais}	72.98776	kN

RESULTING TOTAL RESISTANCE

UPPER SECTION - Earth Pressure Theory

Lateral Resistance FRUH 412.068 kN

LOWER SECTION - Classical Plasticity Theory

Resistaince Pressure SR 72.63214 kPa

Lateral Resist Force FRLH 381.3188 kN

CAISSON TIP - Shear on base area

Horizontal Resistance FRTH 79.52156 kN

TOTAL RESISTANCE

Horizontal Resistance FRH 872.9083 kN

45 deg Load Resistance 1234.479 kN

CENTRIFUGE SCALE RESISTANCE

Total Resistance CFRT 0.054866 kN

Normilization factor 0.00575 kN

Normalized Resistance **9.541865** kN

** NOTE ** Assuming the TRANSLATIONAL failure we are interested in the Limiting LATERAL RESISTANCE only

BIOGRAPHY OF THE AUTHOR

Jade Chung was born in Calgary, Alberta, Canada on June 29, 1984. She was raised in Calgary and graduated from Sir Winston High School in 2002. She moved to Wolfville, Nova Scotia, Canada and attended Acadia University, graduating in 2004 with a Diploma in Applied Science. She then moved to Halifax, Nova Scotia, and attended the civil engineering program at Dalhousie University and graduated in 2007 with a Bachelor of Engineering. Jade began her career as a geotechnical engineer with BGC Engineering in 2007 and obtained her Professional Engineering designation at the end of 2009. She then entered the Civil Engineering graduate program at the University of Maine in the spring semester of 2010. Jade is a candidate for the Masters of Science degree in Civil Engineering from The University in Maine in August 2012.